The Dissertation Committee for Menal Gupta Certifies that this is the approved version of the following dissertation:

Using Direct S-wave Seismic Modes for Reservoir Characterization in Wellington Field, Kansas

Committee:

Bob A. Hardage, Supervisor

Kyle T. Spikes

Robert H. Tatham

Stephen P. Grand

Don E. Wagner

Using Direct S-wave Seismic Modes for Reservoir Characterization in Wellington Field, Kansas

by

Menal Gupta, B.S.; M.S. Exploration Geophysics

Dissertation

Presented to the Faculty of the Graduate School of

The University of Texas at Austin

in Partial Fulfillment

of the Requirements

for the Degree of

Doctor of Philosophy

The University of Texas at Austin

May 2017

Acknowledgements

I would like to express the deepest appreciation to my advisor, Bob Hardage, for believing in me and my research ideas and encouraging and supporting me to outreach and work with the best in scientific community. I thank him for making sure I had the best support I needed, and mentoring me through both academic and non-academic pursuits. I also would like to thank Lesli Wood for helping me find Bob.

I also thank my other dissertation committee members, Kyle Spikes, Robert Tatham, Donald Wagoner and Steve Grand. I am grateful to Kyle for being a great mentor and always having time to discuss ideas and review my work. I thank Don for guiding me through seismic data processing and helping me process some of the seismic data for this research. I thank Steve and Bob for critically assessing my ideas and work and inspiring me.

I would also like to express my gratitude to Michael DeAngelo for helping me with SEG abstract submission and being a good friend. I also thank Diana Sava and Mehdi E. Far for their help in rock physics modeling. I am thankful to Alexander Klokov for his help in seismic data processing and to Junzhe Sun and Sergey Fomel for brainstorming discussions and software help.

I would also like to thank SEG, Anadarko, Statoil and ExxonMobil and the Jackson School of Geosciences for providing scholarships and grants, without which conducting and presenting my research would have been very difficult. I also thank EGL consortium members for their valuable feedback; Kevin Wright, Adrian Chen, and Bruce Karr from Fairfield Nodal for their seismic data processing; and Lynn Watney and Jason Rush from the Kansas Geological Survey for providing data and feedback on my results.

A very special thanks to Khushboo, a partner who sat beside me through this whole rollercoaster ride and was my pillar of strength. Without her persistent help and brainstorming sessions, this dissertation would have not been possible. I would like to thank my mom and dad for believing in me and my aspirations. Last but not the least, this acknowledgement will be incomplete without thanking my brother Kunal, for taking care of everything back home in my absence.

Using Direct S-wave Seismic Modes for Reservoir Characterization in Wellington Field, Kansas

Menal Gupta, PhD

The University of Texas at Austin, 2017

Supervisor: Bob A. Hardage

S-waves exhibit birefringence, provide independent measurements of subsurface elastic properties and play a vital role in reservoir characterization. Despite obvious advantages, direct S-wave data (S-S and SV-P) remain under-utilized for characterization of fractured reservoirs, partly due to limited understanding of seismic attributes quantitatively estimate fracture properties, and because of the high-cost associated with direct S-wave data acquisition. This dissertation offers solutions to these challenges by creating S-S AVO attributes that can estimate fracture properties, and demonstrating use of low-cost, mode-converted P-wave data (SV-P) generated by conventional P-wave sources, for reservoir characterization.

Multicomponent seismic data and well data from Wellington Field, Kansas are analyzed to understand reservoir facies and fractures characteristics in the Arbuckle Group, which is being considered for CO_2 injection. Results from multicomponent seismic interpretation suggest a mechanically stratified Arbuckle interval with varying lithofacies, and presence of seismic anisotropy caused by fractures. Rock physics modeling and S-wave AVO analysis demonstrate that the Intercept Anisotropy (IA) attribute and Gradient Anisotropy (GA) attribute proposed in this dissertation can be used to estimate fracture-density and fluid-fill in fractures, respectively. Results show that

amplitude-based anisotropy analysis, in conjunction with travel-time-based analysis for seismic anisotropy, helps reduce ambiguity and provides high-resolution fracture characterization. Finally, a series of comparisons between the inversion results of P-P, P-SV and SV-P seismic data show that vertical-vibrator SV-P data from vertical geophones work as good as P-SV seismic data from horizontal geophones to estimate reservoir properties, and provide better subsurface resolution than do SV-P data generated by a horizontal vibrator. These results validate that direct S-wave data generated by conventional P-wave sources are a low-cost, yet highly-effective, alternative to data generated by more expensive S-wave sources. Overall, this dissertation advances our understanding of S-wave AVO attributes, and offers novel workflows to characterize naturally fractured reservoirs using direct S-wave data that do not require expensive seismic data acquisition.

Table of Contents

List of Figures xi

Chapter 1: Introduction 1

1.1 Motivation 1

1.2 Organization of Chapters 4

Chapter 2: Interpretation of Direct P- and S-waves for Reservoir Characterization: A Case Study from the Arbuckle Interval in Wellington Field, Kansas 8

2.1 Abstract 8

2.2 Introduction 9

2.3 Methods 11

2.3.1 Multicomponent seismic interpretation 11

2.3.2 Well-log interpretation for seismic anisotropy 12

2.4 Results 13

2.4.1 P-P and S-S seismic data analyses 13

2.4.2 Well-log analyses for seismic anisotropy 15

2.5 Discussion 16

2.5.1 Integration of multicomponent seismic data and well-log analysis 16

2.5.1 Challenges in multicomponent seismic interpretation 17

2.6 Conclusions 19

Chapter 3: Statistical Rock Physics and Amplitude Variation with Offset Modeling of Direct P-and S-waves in Wellington Field, Kansas 29

3.1 Abstract 29

3.2 Introduction 30

3.3 Methods 31

3.3.1 Rock physics study of Upper Arbuckle formation 32

3.3.2 AVO modeling and intercept-gradient analysis 32

3.3.3 Uncertainty 33

3.4 Results 33

3.5 Conclusions 36

3.6 Appendix A 38
3.6.1 Hudson's model for HTI media 38
3.6.2 Linear slip model for HTI media 38
3.7 Appendix B 41
3.7.1 Approximations to P-wave and S-wave AVO equations (Ruger, 2001) 41

Chapter 4: Characterization of Naturally Fractured Arbuckle Group in Wellington Field, Kansas, Using S-wave Amplitude Variation with Offset 52
4.1 Abstract 52
4.2 Introduction 53
4.3 Study Area and Data Set 57
4.3.1 Seismic data 58
4.3.2 Well data 59
4.4 Methods 60
4.4.1 Rock physics modeling 61
4.4.2 S-wave AVO attributes for fracture characterization 62
4.5 Results 64
4.5.1 Rock physics and AVO modeling of the Arbuckle Group 64
4.5.2 Fracture characterization of Arbuckle Group in Wellington Field 67
4.6 Discussion 69
4.7 Conclusions 72
4.8 Appendix A 73
4.8.1 S-wave AVO intercept gradient attributes 73

Chapter 5: SV-P: A Viable Alternative to Mode-converted P-SV Seismic Data for Reservoir Characterization 87
5.1 Abstract 87
5.2 Introduction 88
5.3 Data Set 91
5.3.1 Seismic data 92
5.3.2 Well data 93

5.4 Methods 94
5.4.1 Pre-stack conditioning of multi-component seismic data 94
5.4.2 Post-stack interpretation of P-P, P-SV and SV-P wave modes 94
5.4.3 Seismic inversion for subsurface elastic properties 95
5.5 Results 97
5.5.1 P-P and P-SV data analyses 97
5.5.2 Analyses of SV-P seismic data 100
5.6 Discussion 102
5.7 Conclusions 104
Chapter 6: Conclusions and Future Work 116
6.1 Conclusions 116
6.2 Future work 118
References 120

List of Figures

Figure 2.1: General stratigraphic column for Kansas (Carr et al. 2005). The Wellington Field produces hydrocarbons from Mississippian aged reservoirs. The Ordovician-aged Arbuckle Group is a part of the Ozark Plateau Aquifer System and is being considered for CO_2 storage. ...20

Figure 2.2: Sketch showing different facies types and fracturing present in the Arbuckle formation (Franseen et al., 2003). A) reservoirs with abundant fractures in which litho-facies control porosity and fractures control overall permeability, B) reservoirs with karst overprinting on litho-facies and fractures, resulting in complex porosity and permeability, and C) reservoirs where litho-facies control porosity and permeability.....21

Figure 2.3: Base map of Wellington Field (shaded blue area) showing the 9C-2D seismic data (blue lines), 3D P-wave seismic data (green area) and different wells with at least some log data available. 2D-9C Line-1 was used for the multicomponent seismic interpretation presented in this chapter. Wells 1-32 and 1-28 had a full suite of well logs and cores acquired and are used as calibration wells. 22

Figure 2.4: (a) Rose diagram of 132 drilling-induced fractures identified on the image logs that yielded a maximum horizontal stress direction of 75°E. (b) Rose diagram depicting the azimuthal orientation of 485 partially closed fractures. These partial fractures have no particular orientation and are distributed randomly throughout the azimuthal space. 23

Figure 2.5: P-P well-to-seismic tie for well 1-32. The correlation coefficient was more than 76%. The top of Arbuckle (pink) is an increase in P-impedance and is represented by a peak (positive) on seismic.....24

Figure 2.6: S-S well-to-seismic tie for well 1-32. The correlation coefficient was more than 82%. The top of the Arbuckle (pink) is an increase in S-impedance and is represented by a trough (negative) on seismic data due to the negative reflection coefficient.....25

Figure 2.7: P-P and slow S-S seismic modes (wiggle plot) in P-P travel time after event correlation. The inserted curve is gamma ray with grey color representing shaly intervals. Inserted color at well location is the Vp/Vs determined from borehole data. Color plot in the seismic background is the Vp/Vs obtained from event correlation. Note Vp/Vs from event matching is consistent with Vp/Vs recorded in the wells. Marker 1 represents a high Vp/Vs unit in the middle Arbuckle, which might indicate a tight or baffle zone.....26

Figure 2.8: P-P, S-S slow and S-S fast seismic modes in their respective time domain with interpreted horizons. The inserted curve is gamma ray with grey color representing shaly intervals. Note the relative up shift in the fast S-wave section. Marker-1 shows updip pinch-out on Oread horizon and Marker-2 shows a channel type feature that can be found on all wave modes, which aids event correlation. 27

Figure 2.9: (a) Seismic anisotropy measurements made in wells 1-28 and 1-32 for the Mississippian interval. Based on the anisotropy estimates, the Mississippian interval is divided into 4 zones, M1 through M4, with zones M1 and M3 showing low seismic anisotropy and zones M2 and M4 showing high seismic anisotropy. (b) Seismic anisotropy measurements made in wells 1-28 and 1-32 for the Arbuckle interval. Arbuckle interval is also divided into 4 zones, A1 through A4, with zones A1 and A3 showing low seismic anisotropy and zones A2 and A4 showing high seismic anisotropy. The vertical dotted line drawn at a percentage anisotropy value of 2 is the threshold value used to calculate the rose diagrams of fast S-wave polarization. 28

Figure 3.1: Data set comes from Wellington field, situated in south central Kansas, United States 43

Figure 3.2: Porosity histograms and distributions of the upper Arbuckle formation obtained from well logs (green) and the background porosity distribution used in the model (red). Assumed porosity distribution is kept close to the porosity indicated by well data to keep model input parameters as realistic as possible. 44

Figure 3.3: Histograms and distributions of crack density (a) and crack aspect ratio (b) assumed for rock physics modeling. These distributions depict realistic variability in crack densities and crack aspect ratios for the upper Arbuckle layer and are in agreement with observations made on core and thin sections. 45

Figure 3.4: Porosity dependence of elastic parameters color coded with crack density (a, b and c) and fracture fill (d, e and f). Both P- and S-wave velocities show some degree of change with changing crack density. This change is probably not enough to deduce fracture density information from these velocities. However, modeled γ, which is the relative difference in fast- and slow- S-wave velocities, is directly correlated to crack density. Figures d, e and f show how anisotropic parameters are affected by change in fracture-fluid. δv is relatively insensitive to fluid-fill in fractures. εv on the other hand, shows some shift due to change in fluid-fill. $\Delta\varepsilon v$-$\Delta\delta v$ is very sensitive to the fluid-fill, showing good separation between dry (black) and brine (blue) filled fractures.....46

Figure 3.5: Porosity dependence of elastic parameters color coded with aspect ratio for brine-saturated rock. Note that εv (e) and $\Delta\varepsilon v$-$\Delta\delta v$ (f) show a small systematic decrease with increasing aspect ratio. However, that systematic variation still lies below the uncertainty threshold, making prediction of aspect-ratio extremely difficult from seismic amplitude measurements alone. 47

Figure 3.6: Reflectivity vs. incident-angle plot for brine-saturated rock in isotropy (solid) and symmetry (dashed) planes for P-waves (a), fast S-wave (b), and slow S-wave (c). For P-waves, reflectivities parallel and perpendicular to fractures show significant overlap. Fast S-waves have two different gradients corresponding to polarization in isotropy plane (SV) and the symmetry plane (SH). Similarly, slow S-waves have gradients corresponding to polarization in the isotropy plane (SH) and the symmetry plane (SV). A difference between the AVO intercepts of fast- and slow- S-waves, and AVO gradients of fast- and slow- SV waves caused by presence of fractures can be seen, underscoring the value of S-waves in fracture identification. 48

Figure 3.7: AVO intercept-gradient cross plot for brine-saturated rock in isotropy (filled circles) and symmetry (open circles) planes for P-waves (a and d), fast S-wave (b and e), and slow S-wave (c and f). Figures a, b and c are color coded with crack-density parameter, and figures d, e and f are color-coded with crack-aspect ratio parameter. Two clusters with different gradients are observed for fast S-waves, which correspond to polarization in the isotropy plane (SV) and the symmetry plane (SH). Similarly, slow S-waves show clusters corresponding to polarization in the isotropy plane (SH) and the symmetry plane (SV). A systematic change is seen on slow S-wave AVO intercepts and gradient with changing crack density, underscoring the value of S-waves in fracture identification. 49

Figure 3.8: Reflectivity vs. incident-angle plot in symmetry planes for dry (black) and brine (blue) saturated rock. A difference in P-wave reflectivity can be seen for different fluid-fill (a). A small change in slow S-wave AVO gradient is also observed for different fluid-fills (c). It was observed that change in P-wave reflectivity was primarily caused by change of fluid in the pores whereas; slow S-wave reflectivity was affected by change of fluid in the fractures. 50

Figure 3.9: AVO intercept-gradient cross plots for P-wave (a and d), fast S-wave (b and e) and slow S-wave (c and f) in symmetry planes for dry and brine saturated rock. Figures a, b and c are color coded with crack-density parameter, and figures d, e and f are color-coded with crack-aspect ratio parameter. A difference in P-wave AVO intercept distribution can be seen for different fluid-fill (a and d). Systematic changes in slow S-wave AVO intercept and gradient are observed with changing crack density (c). However, change in S-wave AVO intercepts and gradient due to change in fluid is not apparent. Advanced attribute extraction might be necessary to observe fluid change in S-wave attributes.....51

Figure 4.1: Wellington field (red star) is located in Sumner County (red square), Kansas. It is a sub-crop play of Mississippian age carbonate reservoirs within the Sedgwick Basin, a Precambrian structure formed by the Nemaha uplift, The Nemaha ridge separates the Sedgwick Basin from the Cherokee Basin to the east. Black arrows show the direction of crustal extension resulting from the Nemaha uplift, and contours represent the regional Precambrian basement. The Sedgwick Basin is bounded by the Central Kansas Uplift to the west, the Salina Basin to the north, and the Anadarko Basin to the south (not shown). Figure modified after Merriam (1963) and Baars and Watney (1991).....74

Figure 4.2: Base map of Wellington Field (shaded blue area) showing the 9C-2D seismic data (blue lines), 3D P-wave seismic data (green area) and different wells with at least some log data available. 2D-9C Line-1 was used for the S-wave AVO analysis presented in this paper. Wells 1-32 and 1-28 had a full suite of well logs and cores acquired and are used as calibration wells.....75

Figure 4.3: Well log suite acquired in well 1-32. The area shaded yellow in the GR track corresponds to the carbonate intervals in the well. Shaly intervals are shaded gray. Wellington Field produces from the Mississippian interval, and the Arbuckle Group is being considered for CO_2 storage. Seismic velocity measurements (Vp and Vs curves in red) were made in the wells. Backus averages of seismic velocities ($\bar{V}p$ and $\bar{V}s$ curves in blue) were used to calibrate the rock physics model. Dipole sonic measurements were taken in this well to estimate the percentage of S-wave anisotropy, which is shown in the Aniso track.....76

Figure 4.4: Slow and fast P-wave velocities (a and b) and S-wave velocities (c and d) obtained from rock physics model plotted against total porosity. Black and blue open circles correspond to modeled seismic velocities for the Upper Arbuckle with dry and brine-saturated fractures, respectively. Green points are seismic velocities obtained from the well logs in well 1-32. Note that the modeled S-waves and fast P-wave velocities are consistent with borehole measurements.....77

Figure 4.5: Porosity dependence of Thomsen style anisotropic parameters derived from the rock physics model. (a) Variation of γ with total porosity, color coded with crack density parameter. Modeled γ (open circles) is consistent with the well measurements (filled black circles). Also note that gamma is directly correlated to the crack density parameter. (b) Variation of $\Delta\delta v$-$\Delta\varepsilon v$ with total porosity, color coded with fluid fill, respectively. $\Delta\delta v$-$\Delta\varepsilon v$is sensitive to the fluid fill and is able to discriminate between dry (black) and brine (blue) filled fractures...78

Figure 4.6: (a) Modeled SV and SH wave AVO intercept cross plots for dry, brine and CO_2 filled fractures in symmetry plane, color-coded with crack density parameter. Since fluid fill does not affect AVO intercepts, no separation is seen between different fluid fills. Increasing offset between SV and SH AVO intercepts suggests increase in fracture density, as indicated by the color shift towards yellow end of the spectrum. (b) Modeled SV and SH wave AVO gradient cross plot in symmetry plane for different fluid fill in fractures. Black open circles are modeled gradients for dry fractures. Blue and magenta open circles represent AVO gradients for brine and CO_2 filled fractures, respectively. Note that S-wave AVO gradients can be used to discriminate between different fracture fluids. 79

Figure 4.7: Crossplots between Gradient Anisotropy (GA) and Intercept Anisotropy (IA) attributes modeled in the symmetry plane. (a) IA-GA cross plot for dry, brine-filled and CO_2-filled fractures, color-coded with crack density parameter. Each cluster in the cross plot corresponds to a different fracture-fill. These clusters can be identified using Figure 4.7b. Irrespective of the fluid fill, the IA increases with increasing crack density, demonstrating its viability as a fracture density attribute. (b) IA-GA crossplot for dry (black), brine-filled (blue), and CO_2-filled (magenta) fractures. Separation between clusters of different fluids along y-axis indicate applicability of GA as a proxy for fluid fill in fractures. Note that the separation between different fluid fill increases with increasing fracture density, as depicted by IA. 80

Figure 4.8: AVO intercepts for different S-S wave modes acquired on Line-1 in Wellington field. For this study, CDPs on the SW half of Line-1 are interpreted because they show reliable amplitudes. The NE part of the seismic line shows low discontinuous seismic amplitudes, which is probably due to S-static issues and poor seismic illumination of targets. (a) Slow S-S AVO intercepts on Line-1. Bright colors showing the AVO intercept anomalies are primarily located at Well 1-32 and towards the SW end of the line. (b) Fast S-S AVO intercepts on Line-1. Bright colors showing the AVO intercept anomalies are primarily located above the Oread reflector, at Well 1-32 and towards the SW end of the line. Difference in AVO intercepts of slow and fast S-waves is an indicator of fracture-induced seismic anisotropy. 81

Figure 4.9: (a) IA attribute calculated using the difference between the AVO intercepts of fast and slow S-wave modes for Line-1 in Wellington field depicting fracture-induced seismic anisotropy. (b) Seismic velocity anisotropy estimated from the percentage difference in S-wave interval velocities obtained from stacking velocities after Dix conversion and lateral and vertical smoothing. Note that the high-frequency estimates of fracture density obtained from S-S AVO qualitatively agree with the low-frequency anisotropy estimates obtained from seismic velocities. High fracture density is observed above the Oread reflector, near the location of well 1-32 and towards SW end of the Line 1. Higher fracture density near well 1-32 is due to presence of fracture swarms associated with a regional fault, which runs sub-parallel to the strike of the seismic line. High anisotropy observed above the Oread towards the NE on seismic velocities are not present on the IA attribute. This difference is caused by the poor S/N ratio in this area. 82

Figure 4.10: S-S AVO Intercepts crossplot for slow and fast S-waves color coded by the Intercept Anisotropy (IA) attribute for Line-1. Data points on and near the Y=X line correspond to low values of the IA attribute and indicate low fracture density. Departure from the Y=X line corresponds to increasing value of the IA attribute and higher fracture density...83

Figure 4.11: S-S Intercept Anisotropy (IA) attribute depicting lateral and depth variation in fracture density in the Arbuckle Group. Well log information inserted at the well locations is anisotropy measured from dipole sonic logs, which is in qualitative agreement with the high magnitude of the IA attribute as seen near well 1-32. Attribute quality at and east of well 1-28 is sub-optimal due to poor data quality. The dotted horizon describes the interpreted top of the High Permeability Zone (HPZ) in the Arbuckle Group. Fracture density seems to vary laterally within the HPZ with higher values near Well 1-32 possibly due to the presence of a fault. Above the HPZ, a low fracture-density zone can be seen that thickens SW of the well. This zone might be responsible for reduced vertical hydraulic connectivity between the Upper and Lower Arbuckle and may act as a baffle zone. 84

Figure 4.12: AVO gradients for different S-S wave modes acquired on Line-1 in Wellington field. The NE part of the seismic line is excluded from the interpretation because of its poor image quality. (a) Slow S-S AVO gradients on Line-1. Bright colors showing the AVO gradient anomalies are primarily located above the Kansas City, Mississippi, and Arbuckle reflectors. Within the Arbuckle such anomalies are near well 1-32 and towards the SW end of the line. (b) Fast S-S AVO gradients on Line-1. AVO gradient anomalies for fast S-wave mode are higher than for the slow S-waves. These anomalies are primarily located above the Kansas City, Mississippi, and Arbuckle reflector. Within the Arbuckle such anomalies are seen near well 1-32 and in the Middle and Lower Arbuckle. AVO gradients of slow and fast S-waves are further used to understand fluid fill in fractures.....85

Figure 4.13: GA attribute calculated using S-wave AVO gradients on Line 1 in Wellington field. Most of the GA anomalies in the Arbuckle either lie in the HPZ or close to well 1-32 where fracture swarms associated with the regional faults have been identified. High values of GA that coincide with high values of IA suggest that these fractures are predominantly brine filled, except for the oil producing Mississippian interval that shows lower values of GA in the upper interval. Data were acquired prior to CO_2 injection in the Lower Arbuckle, so all fractures were assumed to be brine saturated. A time-lapse version of the GA attribute might help in monitoring the movement of CO_2 in the Arbuckle Group. 86

Figure 5.1: Well log suite acquired in well 1-32. The area shaded yellow in the Gamma Ray (GR) track corresponds to the carbonate intervals in the well. Shaly intervals are shaded gray. Wellington Field produces from the Mississippian interval, and the Arbuckle Group is being considered for CO_2 storage. Seismic velocity measurements (Vp and Vs curves in red) were made in the wells. Backus averages of seismic velocities (Vp and Vs) are overlain in blue. Dipole sonic measurements were taken in this well to estimate the percentage of S-wave anisotropy, which is shown in the Aniso track. Rate of Penetration (ROP) and lithology estimates for the Arbuckle group are digitized from the mud-log of well 1-32. Middle Arbuckle (between markers A and B) shows a higher GR and slower ROP compared to the Lower Arbuckle (below marker B), suggesting the Middle Arbuckle is a tighter formation. This variation is not captured by the seismic velocities measurements made at well-log scale.....106

Figure 5.2: Conditioned P-P (a) and P-SV gathers (b) for CDPs near well 1-32 on Line-1. Original gathers for both P-P and P-SV modes underwent a series of gather-conditioning steps to suppress noise and enhance signal. P-P and P-SV conditioned gathers have been depth registered and polarity matched, and are shown in P-P time. The zone of interest is the Arbuckle group between 710 ms and 810 ms. High positive amplitude at 740 ms in both P-P and P-SV gathers marks the top of Middle Arbuckle (horizon A) that has been interpreted as the baffle zone. High negative amplitude at 775 ms marks the top of Lower Arbuckle (horizon B), which is being considered for CO_2 injection. The proposed injection zone has been highlighted in green. 107

Figure 5.3: P-P (a) and P-SV (b) stacked seismic section showing the key interpreted seismic horizons on Line-1. P-P seismic has better signal-to-noise ratio compared to the P-SV seismic section. Both P-P and P-SV images have been depth registered and are shown in P-P time. Polarity on the P-SV seismic section has been matched to the P-P seismic data to see event correspondence. Within the Arbuckle Group, high amplitude reflectors in the Lower Arbuckle injection zone (green highlighted zone) are observed on both seismic sections. Image quality of the P-SV mode towards NE side of well 1-32 is sub-standard due to S-wave static related issues. 108

Figure 5.4: (a) P-impedance (IP) obtained from AVO inversion of P-P gathers for Line-1 compared to IP computed from well-logs (vertical colored strips below well labels). Middle Arbuckle interval (between A and B) shows high IP values, suggesting a possible lithology change, consistent with presence of muddy crystalline dolomite observed in core. This high impedance layer coincides with the baffle zone known to be present in the Middle Arbuckle (Watney and Rush, 2012). Lower Arbuckle injection zone (below horizon B) shows lower values of IP which coincides with the presence of fractured dolomitic limestone. (b) S-impedance (IS) obtained from AVO inversion of P-P gathers compared to IS computed from well-logs. Middle Arbuckle interval (between A and B) shows high values of IS. Change in IS values from Middle to Lower Arbuckle is considerably less compared to what was observed on IP section. Lower Arbuckle injection zone is not clearly visible on IS image.....109

Figure 5.5: (a) P-impedance (IP) obtained from a joint-inversion performed on P-P gathers and P-SV stacked seismic section for Line-1 compared to IP computed from well-logs (vertical colored strips below well labels). This IP image is consistent with IP obtained from P-P AVO inversion, capturing all the detained in Arbuckle Group. (b) S-impedance (IS) obtained from P-P and P-SV joint inversion compared to IS computed from well-logs. Middle Arbuckle interval shows IS (between A and B) indicating a change in lithology. Lower Arbuckle injection zone (below B) show low values of IS, suggesting some variation in lithology and possibly presence of fractures, which are not observed on well-logs. Low IS values in the injection zone are consistent with the observations made on IP images. Use of an independent shear-wave measurement (P-SV seismic) helps constrain the inversion result of IS, making it more reliable compare to IS obtained from P-P data alone. 110

Figure 5.6: (a) P-SV seismic section along Line-1 showing the key interpreted seismic horizons. A bandpass filter with corner frequencies (10, 15, 65, 90) has been applied to the P-SV image to match its frequency spectrum with the SV-P image. (b) SV-P seismic section generated from a vertical vibrator on Line-1 with the P-SV horizons overlain. This SV-P image generated from a conventional P-wave source provides a low-cost alternative to a P-SV seismic image. Seismic reflections corresponding to Kansas City, Mississippi, Arbuckle and Precambrian can be seen on both converted-wave modes. In the Arbuckle group, geological events like top of Middle Arbuckle (A) and top of Lower Arbuckle (B) are also visible on both images. Lower Arbuckle injection zone is highlighted in green on both images. Seismic image quality NE of well 1-32 is sub-standard on the P-SV image. Degradation of the SV-P image NE of well 1-32 is less obvious. 111

Figure 5.7: A comparison of the SV-P image obtained from a horizontal vibrator (a) with the SV-P image obtained from a vertical vibrator (b). Seismic reflections corresponding to Kansas City, Mississippi, Arbuckle and Precambrian are shown on both converted-wave modes. Within the Arbuckle Group, top of the Middle Arbuckle reflection (A) and top of the Lower Arbuckle injection zone (highlighted in green) are consistent in both seismic sections, demonstrating the efficacy of using a vertical vibrator to generate down-going S-waves. However, seismic image quality NE of well 1-32 is sub-standard due on both images due to S-wave static-related issues. 112

Figure 5.8: A comparison of the frequency spectra of SV-P seismic mode generated by P-wave source (red) and S-wave source (blue). A window from 0-900 ms in P-P time was used to calculate these spectra. The SV-P mode generated by a vertical vibrator contains more high frequency energy from 57 Hz to approximately 67 Hz. This increase in frequency content is a result of using a P-wave source which generates sweeps with broader frequency spectrum compared to an S-wave source. These additional high frequencies help generate higher resolution image of the subsurface enabling more reliable interpretation. The vertical vibrator sweep parameters were not optimal for low frequencies (non-linear sweep with a slope of +3 db/octave and starting frequency 6 Hz). If the data were acquired using a lower starting frequency and linear sweep, SV-P mode could also provide the valuable low-frequency energy needed for broad-band applications. 113

Figure 5.9: (a) P-impedance (IP) obtained from joint-inversion of P-P gathers and SV-P stacks (from vertical vibrator) for Line-1 compared to IP computed from well-logs (vertical colored strips below well labels). High IP in Middle Arbuckle (between A and B), and low IP in Lower Arbuckle injection zone are consistent with the observations made on IP obtained from P-P AVO inversion, and P-P and P-SV joint inversion in Figures 5.4a and 5.5a. (b) S-impedance (IS) obtained from joint-inversion of P-P gathers and SV-P stacks (from vertical vibrator) for Line-1 compared to IS computed from well-logs. This IS is consistent with the IS estimated from P-P and P-SV joint inversion as shown in Figure 5.5b. Moreover, IS estimated from P-P and SV-P joint inversion better resolves lithology variation in Kansas City and Mississippi horizons, and within Arbuckle Group, compared to IS estimated from P-P inversion (Figure 5.4b). Lower Arbuckle injection zone (below B) shows low values of IS, suggesting lithology variation not as evident on P-P inversion results. 114

Figure 5.10: Well log panel showing permeability (track 1) and T_2 relaxation times (track 3) in Arbuckle interval, alongside I_P and I_S obtained from Sv-P and P-P joint inversion. Upper Arbuckle (zone between Top Arbuckle and marker A) and Lower Arbuckle injection zone (below marker B) show low I_P and I_S values, indicating presence of larger vugs and fractures. This interpretation is corroborated by higher permeability and T_2 relaxation times calculated from NMR measurements. Similarly, Middle Arbuckle (zone between marker A and B) shows smaller T_2 relaxation times, low permeability and higher I_P and I_S values, suggesting presence of a baffle zone. 115

Chapter 1: Introduction

1.1 MOTIVATION

Multi-component seismic technology is based on energizing the Earth with longitudinal (P) and transverse (S) seismic waves, recording the various reflected wave modes, and then meaningfully interpreting them to infer the subsurface geology. When P- and S-waves are incident on an elastic boundary, the energy of these waves is redistributed into reflected and transmitted waves and gives rise to P-P, P-S (P-SV), S-P (SV-P), and S-S (SV-SV and SH-SH) wave modes. Because particle-displacement vectors for each of these modes are oriented in different directions, they sense a different earth fabric along their propagation paths and carry direction-dependent information about elastic constants, grain cementation, pore geometry, anisotropy, and lateral variations in rock and fluid (Hardage et al., 2011). Tatham and McCormack (1991) provide a detailed account on historical development and applications of multi-component seismology.

P-waves do provide some information about fracture properties like orientation and spatial density, but these estimates can have a high degree of uncertainty associated with them and often require wide azimuth P-wave seismic data acquisition (Corrigan et al., 1996; Liu and Martinez, 2013; Lynn, 2007; Mallick et al., 1996; Ruger, 2001; Jenner, 2001; and Roche et al., 2005). Moreover, some properties like fluid fill and aperture of fractures are challenging to determine from P-wave data due to theoretical restrictions and non-uniqueness in determining these parameters (Sava and Mavko, 2004, Shen et al., 2002).

S-wave modes on the other hand have proven to be very effective in detecting azimuthal anisotropy (Martin and Davis, 1987; Mueller, 1991; DeVault et al., 2002; Lynn and Thomsen, 1990; and Li, 1997). S-waves provide a set of subsurface measurements independent of P-waves that can help characterize fluids and heterogeneities in the subsurface (Sinha et al., 2012). In anisotropic media, S-waves (P-S, S-S and S-P) split into fast and slow wave modes; the velocities and amplitudes of which contain information about causes of anisotropy such as aligned fractures and micro-cracks or presence of layered rocks or anisotropic subsurface stresses. Especially important in this thesis investigation is the fact that S-waves play a vital role in improving understanding of carbonate reservoirs where fracture-induced seismic anisotropy is observed (Anselmetti and Eberli, 1993; Assefa et al., 2003). However, identifying fracture properties for subsurface fracture characterization using surface S-wave seismic attributes is still an area of active research and needs attention.

Even though S-waves are more reliable for understanding reservoir properties and subsurface anisotropy, S waves account for only 5% of current total seismic processing and have made minimal contributions to exploration and production (Bansal and Gaiser, 2013). Among the few S-wave studies that there are, more focus is given to P-S wave data compared to direct shear-wave data (S-S and S-P), which makes direct shear wave data even more under-utilized for reservoir characterization applications. The simplest of all direct S-wave modes is the S-S mode where S-waves can be generated directly at the source (vertical- or horizontal-force source) and recorded by a 3-component (3C) geophone. S-S wave data are relatively easier to process, as principles of CMP domain processing developed for P-P wave modes can be directly extended to S-S. Moreover, S-S data often have a higher signal-to-noise ratio compared to mode-converted P-S data. Another direct S-wave mode that needs attention is the SV-P mode, which is a mode that

is emphasized in this thesis. Frasier and Winterstein (1990) show that SV-P data have higher signal-to-noise ratio as compare to P-SV data, resulting in a better seismic image. Also, studies done by the Exploration Geophysics Laboratory (EGL) at the University of Texas at Austin, show that SV-P data provide better seismic resolution than P-SV data. These EGL reports are private unpublished reports done for EGL sponsors that are now being openly shared. Copies and supporting digital data, have been given to seven university research groups and will be shared with anyone who requests that material. Interested parties can obtain this information by contacting Dr Bob A. Hardage (bob.hardage@beg.utexas.edu). Despite obvious advantages of direct S-waves, economics of seismic data acquisition and processing have so far discouraged S-S and SV-P data as choices of seismic data used in geophysical workflows.

Underdevelopment and underutilization of direct S-wave data have been attributed to the cost of direct S-wave acquisition (Perez et al., 1999). Studies show that direct and converted S-waves can be produced in the immediate vicinity of a compressional-wave source (Miller and Pursey, 1954; Fertig, 1984). Modeling of elastic wave-fields suggests that vertical-force sources produce SV-waves of relatively good strength to produce a down-going S-wave illumination for imaging subsurface targets. Field experiments done by EGL corroborate modeling results that direct S-waves are produced by conventional vertical-force sources as well as the horizontal-force sources (Alkan and Hardage, 2013). Technological advances in extracting direct S-waves generated from P-wave sources have posed a unique opportunity to obtain shear wave surface seismic data at more affordable costs than ever before (Gaiser and Verm, 2012; and Hardage and Wagner, 2014a, b). This development requires that we revisit S-wave surface seismic analysis methods that can be used for subsurface reservoir characterization.

This dissertation utilizes direct S-wave seismic data (S-S and SV-P) acquired in Wellington Field, Kansas, to create workflows for fracture-property estimation and reservoir characterization. First, P-P and S-S seismic data are interpreted to identify key geological boundaries, and well log data are analyzed to understand the cause of seismic anisotropy observed in the seismic data. Then, rock physics and AVO modeling are performed on the Arbuckle interval to understand the dependence of elastic parameters on fracture properties. Once the elastic parameters sensitive to fractures are determined, S-S AVO attributes are designed and extracted to understand lateral variations in fracture-density and fluid-fill in the fractures for the Arbuckle interval. These attributes delineate high permeability zones required for CO_2 injection, and baffle zones that cap the injection intervals. S-S AVO attributes described in this dissertation provide a useful tool to identify sweet spots for drilling in tight reservoirs, and monitor fluid-flow within natural fractures. Lastly, to understand the lateral heterogeneities within injection and baffle zones, P-P and mode-converted SV-P data (generated by vertical vibrator) are inverted and analyzed. Comparisons made between SV-P data generated by vertical and horizontal vibrators demonstrate that direct S-waves data generated by vertical vibrators provide geological details with better seismic resolution. This work offers a novel workflow of utilizing low-cost mode-converted data for reservoir characterization.

1.2 ORGANIZATION OF CHAPTERS

Chapter 2 acts as an introduction to the detailed fracture characterization study (Chapter 4) presented in this dissertation. It discusses interpretation of multicomponent seismic data (P-P and S-S) and well log data to identify seismic reflections corresponding to the regional geological markers and intervals of interest. It also establishes seismic

velocity models through depth registration of identified seismic reflectors. Seismic velocity ratios estimated from the depth registration process are used to characterize spatial variability in lithofacies and fracture-related seismic anisotropy in the subsurface. Dipole-sonic logs and borehole image logs are used to understand plausible causes of seismic anisotropy observed on well logs and fast and slow S-wave seismic data. This chapter also discusses challenges involved in 9C2D seismic interpretation and ways in which these challenges can be mitigated. Results of this analysis help map the lateral heterogeneities present in the Arbuckle interval, which is the primary target for CO_2 injection in Wellington Field.

Chapter 3 discusses the details of rock physics and AVO modeling for P- and S-waves that are necessary to understand the observed seismic responses. A statistical rock physics model is constructed for Ordovician age carbonates of the Arbuckle Formation encountered in wells drilled in the Wellington Field, Kansas. This statistical model is then used to understand which P-wave and S-wave AVO attributes would be optimal for observing variations in elastic constants caused by spatial density, and fluid-fill of fractures. AVO modeling shows that azimuthal variations in the S-S mode AVO gradient can be used to determine the fracture properties in the subsurface. Azimuthal variations in P-P mode AVO attributes are often masked by the uncertainty of lithology and fracture-density, which limits the ability of P-waves to determine fracture properties. Results of this study demonstrate that in angle and azimuth space, S-wave AVO intercepts can quantitatively estimate the γ (crack density) parameter of a rock formation, and AVO gradients of slow S-wave in a direction normal to fracture-orientation can be used for discriminating fluid fill in fractures.

In Chapter 4, two S-wave AVO attributes are designed to identify fracture-density and fluid-fill in fractures, respectively. These AVO attributes can be derived from any S-

S surface seismic measurement made using a P- or S-wave source. Application of these attributes is demonstrated on the S-S seismic data acquired in Wellington Field and results are corroborated with other geological measurements made in the wells. Results show that the Intercept Anisotropy (IA) attribute obtained from AVO intercepts of shear waves provides fracture-density estimates within the Arbuckle Group. The Gradient Anisotropy (GA) attribute obtained from the AVO gradient of shear waves suggests that most fractures in the Arbuckle are brine saturated. This GA attribute has a potential application in monitoring the movement of CO_2 plumes in the Arbuckle Group when time-lapse data are available.

In Chapter 5, I investigate SV-P (converted-P) data generated by P-wave sources (e.g. a vertical vibrator) and recorded by vertical geophones, as a cost-effective alternative to traditional P-SV data. To evaluate the efficacy of the SV-P mode relative to P-P and P-SV modes, Three sets of inversions are performed and results compared. P-P AVO trace gathers and stacked SV-P seismic data are jointly inverted to estimate subsurface elastic properties. Resulting P- and S-impedances were compared with the estimates obtained from joint-inversion of P-P AVO trace gathers and stacked P-SV seismic data, and inversion of P-P AVO trace gathers data. Results show that a significant improvement in S-impedance estimates is observed when P-wave and converted wave (SV-P or P-SV) data are inverted jointly, compared to inversion results of P-P data alone. No major difference in the inversion results is seen when SV-P data are used instead of P-SV data, in conjunction with P-P seismic mode. Additionally, comparisons are made between SV-P seismic images obtained from the vertical vibrator and SV-P images obtained from the horizontal vibrator to establish that both modes are essentially equivalent, except that the former contains valuable higher frequencies than the latter. Such a comparison has never been demonstrated before and is unique to this dissertation.

Chapter 6 integrates the individual research projects described in previous chapters and highlights the contribution of each part towards characterization of reservoirs using direct S-wave data (S-S and SV-P). Limitations of this research are also discussed, to set the stage for potential future work.

Chapter 2: Interpretation of Direct P- and S-waves for Reservoir Characterization: A Case Study from the Arbuckle Interval in Wellington Field, Kansas[1]

2.1 ABSTRACT

Reservoir characterization requires integration of different geological and geophysical data to infer reservoir architecture and rock properties. This study utilizes multicomponent seismic data and well-log data that were acquired in Wellington field, Kansas, to understand reservoir characteristics of Ordovician-aged, fractured-carbonates called the Arbuckle Group. I demonstrate here how P-P and S-S seismic wave modes can be employed in conjunction with dipole sonic measurements to characterize spatial variability in lithofacies and fracture-related seismic anisotropy. This study also discusses challenges involved in multicomponent seismic interpretation and ways in which these challenges can be mitigated. Details of the 9C2D seismic interpretation workflow are discussed and include well-to-seismic ties, data polarity, seismic velocity models, event correlation, and seismic velocity ratio (Vp/Vs). Factors contributing to seismic anisotropy are investigated using dipole sonic logs and borehole-image logs along with S-S data to understand the role of fractures in causing anisotropy. Analysis of direct P- and S-wave data in the Arbuckle reservoir indicate high Vp/Vs values in the Middle Arbuckle reservoir, implying that interval is a possible baffle zone. Differential travel-time shifts

[1]A part of this chapter was previously published in Gupta, M., M.V. DeAngelo, and B., Hardage, 2015, December. PP and SS Wave Interpretation of a Carbonate Formation: A Case Study from the Arbuckle Interval in the Wellington Field, Kansas. In 2015 SEG Annual Meeting. Society of Exploration Geophysicists; M. Gupta conceptualized and performed the research. M. Gupta wrote the manuscript with assistance from co-authors.

observed between top and base of the Arbuckle reservoir in slow and fast S-S data, imply variations in fracture-density. Well-based measurements suggest that seismic anisotropy might be linked to presence of fractures in the Mississippian and Arbuckle intervals that remained open in response to subsurface stress. Presence of fractures and low Vp/Vs values suggest the presence of possible high permeability zones in the Lower Arbuckle. Results of this analysis help understand lateral heterogeneities and fracture-presence in the Arbuckle interval and their potential effects on the movement of CO_2 in the subsurface.

2.2 INTRODUCTION

Multicomponent seismic data can provide information about the subsurface that P-wave data alone cannot provide. S-wave modes can play a vital role in improving understanding of carbonate reservoirs where fracture-induced seismic anisotropy is observed (Anselmetti and Eberli, 1993; Assefa et al., 2003). S-waves, on encountering an anisotropic media, split into fast and slow wave modes, and the seismic velocities and amplitudes of these modes contain information about the causes of anisotropy. Even in formations that can be considered practically isotropic, independent measurements from S-wave seismic waves can help characterize fluids and heterogeneities in the subsurface (Sinha, et al., 2012). The simplest of all direct S-wave data are the S-S data where S-waves can be generated directly at the source by either a horizontal or a vertical force source (Alkan, 2012; Hardage and Wagner, 2014b) and recorded by a 3-component (3C) geophone. S-S wave data are relatively easier to process compared to P-SV data, as principles of CMP-domain processing developed for P-P wave data can be directly

extended to S-S (Miller and Pursey, 1954; Hardage and Wagner, 2014a). S-S and P-P wave data are being used in this study.

A 9C2D seismic survey has been acquired in Wellington Field, which is part of a sub-crop play of Mississippian cherty, dolomitic reservoirs located in Sumner County, Kansas. The stratigraphic units that are of immediate interest to this study are Ordovician age carbonates in the Arbuckle reservoir as shown in Figure 2.1. The Arbuckle reservoir has been described in detail and is understood to have multiple reservoir types ranging from lithofacies dominated, to fracture dominated and karst dominated, resulting in large variabilities in porosity and permeability (Figure 2.2). The Lower Arbuckle is believed to be predominantly fractured and is being considered for CO_2 storage (Watney and Rush, 2012). For efficient disposal of CO_2 in the Arbuckle reservoir, it is important to understand spatial distribution of heterogeneities and fractures within the formation. P-P and S-S wave modes recorded in the Wellington Field provide a unique opportunity to extract shear-wave information like Vp/Vs ratio and seismic anisotropy in Arbuckle reservoirs, which will result in better characterization of these reservoirs.

In this study, I use P-P and S-S data in addition to well log data to identify geological intervals of interest and perform depth registration of seismic images so that P-wave and S-wave data can be correlated with accuracy. As a result of the depth registration process, seismic velocity ratios are determined that help quantify the variation in reservoir characteristics. Dipole-sonic and borehole image logs are used to determine the presence of fracture-related seismic anisotropy in the Mississippian and Arbuckle intervals and help explain time-shifts observed between fast and slow S-wave data. This study lays out a simple, yet effective, workflow for multi-component seismic interpretation that can be applied prior to a detailed fracture characterization.

2.3 METHODS

As a part of the multicomponent seismic acquisition program, a 9-component 2D seismic survey was acquired in Wellington field as shown in Figure 2.3. This survey consisted of two seismic lines, 7 miles (11 km) in length, with 9-component seismic data collected using 3-component geophones and vertical and horizontal vibrators. Line-1 and Line-2 were orientated at 55°E and 135°E, respectively. This study uses P-P and S-S wave data from Line 1 for multicomponent seismic interpretation. The radial and transverse S-S seismic data were processed at a commercial data-processing shop where they were rotated to the best-known estimates of fast (90°E) and slow (0°) directions obtained from velocity analysis and dipole sonic measurements in the calibration wells. Line 1 intersects two wells, 1-32 and 1-28, that have a full suite of well logs including spectral gamma ray, neutron density, resistivity, cross-dipole sonic, Nuclear Magnetic Resonance (NMR) and micro-resistivity imaging. P- and S-wave velocity measurements made in the well along with other geological information (e.g., core, thin sections, pressure measurements) are used to interpret and calibrate seismic-based observations.

2.3.1 Multicomponent seismic interpretation

Well-to-seismic ties were performed on both wells for P-P and S-S data. P-P and S-S seismic data showed opposite polarity, which is consistent with the fact that an increase in P-impedance across a reflector creates a positive reflection of the P-P mode; whereas, an increase in S-impedance creates a negative reflection (Gupta et al., 2014 and Ruger, 2001). After establishing well-to-seismic ties for P-wave and S-wave, time-depth relationships from wells 1-28 and 1-32 were used to create P- and S-wave velocity models for Line 1. Using the velocity models as a guide, depth registration was performed on P-P and S-S seismic sections for all of the five interpreted seismic horizons. Depth registration is a technique used to correlate seismic events in P-P and S-S

seismic sections in their respective time domains away from calibration wells. As a result of this event correlation, a Vp/Vs section was created using horizon travel times (Gaiser, 1996 and Tatham and McCormack, 1991). This Vp/Vs ratio section, after being checked for consistency with the well observations, was used to update the S-wave velocity model. Estimates of Vp/Vs ratio obtained from depth registration were also used to understand the lateral variation in lithology. Next, slow and fast S-wave data were cross-correlated to obtain travel-time shifts that act as a measure of seismic anisotropy in the Arbuckle interval.

2.3.2 Well-log interpretation for seismic anisotropy

Well-logs acquired in well 1-28 and 1-32 were analyzed to understand the rock characteristics and to calibrate lateral variation in lithofacies obtained from surface seismic measurements. The borehole image logs gathered in both wells were used to estimate the direction of maximum horizontal stress. This was done by measuring the orientations of drilling-induced fractures that tend to open-up in the direction parallel to maximum horizontal stress. Figure 2.4a shows a rose diagram of 132 drilling-induced fractures identified on the image logs that yielded a maximum horizontal stress direction of 75^{o}E. These subsurface stresses can cause measurable seismic anisotropy. A very small population of open- and mineralized-fractures was also observed on the image logs, but the data for such fractures were statistically insignificant to be used in this study. In addition to open- and mineralized-factures, several partially closed fractures were observed on the image logs. Figure 2.4b shows the rose diagram depicting the azimuthal orientation of 485 such fractures. These partial fractures have no particular orientation and are distributed randomly throughout the azimuthal space.

To understand the impact of subsurface stresses and presence of fractures on seismic anisotropy in Mississippian and Arbuckle intervals, data from cross-dipole sonic logs were analyzed. Shear velocity measurements recorded in the field coordinates were rotated to obtain seismic velocities for fast and slow S-waves. All depth samples with anisotropy above a specified threshold (2%) were used to calculate polarization of the fast S-wave, which was plotted on a rose diagram to understand the orientation of seismic anisotropy in the subsurface. Fast S-wave orientations were analyzed along with the image log measurements to understand the link between observed fractures and anisotropy measured at well-log and seismic scales.

2.4 RESULTS

2.4.1 P-P and S-S seismic data analyses

The signal-to-noise ratio (S/N) of 9C2D seismic data acquired on Line 1 ranges from moderate to high, resulting in an excellent well-to-seismic ties on well 1-32 for both P- and S-wave modes. Figure 2.5 shows a subset of the well-logs that were acquired and interpreted in well 1-32. The area shaded yellow in the GR track corresponds to the various carbonate intervals in the well. Shaly intervals are shaded gray. The Vp and Vs log represent the Backus averages of seismic velocities. Seismic velocity ratio Vp/Vs is derived from these Backus averages. Dipole sonic measurements were also taken in this well to estimate the percentage of S-wave anisotropy, which is shown in the Aniso track. In the last track of the panel in Figure 2.5, repeated synthetic seismogram traces (blue), repeated composite traces calculated by averaging seismic traces near the well location (red), and the actual P-wave seismic (black) traces are also shown. The correlation coefficient between the synthetic and composite P-P traces is 77%.

Similar to the P-P data, a synthetic seismogram was obtained for the S-S seismic data (Figure 2.6), which had a correlation coefficient of 82% when compared to the composite S-S traces. Following well-to-seismic tie analysis and wavelet extraction on P-P and S-S mode, polarity of the 9C2D data were identified. The top of Arbuckle Group (increase in impedance) on P-wave data is represented by a peak (positive); whereas, on S-wave data, is represented by a trough (negative) as shown in Figures 2.5 and 2.6. This change in reflectivity sign was also observed from rock physics and AVO modeling of the Arbuckle reservoir (Gupta et al., 2014). In addition to the Arbuckle reservoir top, four other regionally extensive horizons were interpreted to create a robust structural framework for reservoir characterization. Those key horizons are Oread, Kansas City, Mississippian and Precambrian (Figures 2.5 and 2.6).

After the structural framework was built, well-calibrated time-depth relationships from wells 1-28 and 1-32 were used to create P-wave and S-wave velocity models for Line 1. Depth registration was performed on P-P and S-S seismic sections and the Vp/Vs was determined. Figure 2.7 shows the Vp/Vs ratio (colored background) obtained after event matching the seismic horizons interpreted on P-P and S-S seismic section (wiggle-trace overlays). Vp/Vs values throughout the section are consistent with the respective lithology between the interpreted horizons. A Vp/Vs of 1.8–1.9 is observed in the Upper and Lower Arbuckle, whereas the Middle Arbuckle unit appears to have a higher Vp/Vs ratio (2–2.1), indicating a possible change in lithofacies.

In addition to Vp/Vs, seismic anisotropy is estimated from the multicomponent seismic data acquired in the Wellington Field. Figure 2.8 shows the comparison of P-P seismic data with the fast and slow S-wave seismic data. The well-log curve overlain on the seismic sections is gamma ray, with highlighting the shaly intervals (gray color). An up-shift in the fast S-wave data compared to the slow S-wave data can be seen in Figure

2.8. An up-dip pinch-out on Oread horizon (label 1), and a channel type feature found in the Lower Mississippian (label 2), also show a time shift in the fast S-wave seismic data, again suggesting presence of anisotropy. The difference in time thicknesses of different intervals between the fast and slow mode was calculated to estimate amount of anisotropy in these intervals. For the Arbuckle Group, this time shift was estimated to be around 6-8 ms (Figure 2.8), indicating an average seismic anisotropy of approximately ~5%.

2.4.2 Well-log analyses for seismic anisotropy

To understand the cause of seismic anisotropy observed on the S-S seismic data, dipole sonic log data from well 1-28 and well 1-32 were analyzed. Figure 2.9 shows the magnitude and orientation of seismic anisotropy in the Mississippian and Arbuckle intervals. Figure 2.9a shows that seismic anisotropy in the Mississippian interval varies from one well location to the other at similar depths. Based on the anisotropy estimates, the Mississippian interval is divided into 4 zones, M1 through M4. Zones M1 and M3 have low anisotropy whereas zones M2 and M4 show anisotropy varying from 2–10%. The vertical dotted line drawn as a percentage anisotropy value of 2% is the threshold value used to calculate the rose diagram shown in Figure 2.9a. This rose diagram depicts orientation of the fast S-wave polarization observed in the Mississippian interval. A unimodal distribution of the fast S-wave polarization with an 85^{o}E orientation is seen on the rose diagram.

A similar interpretation of cross-dipole sonic data done for the Arbuckle Group is shown in Figure 2.9b. Data from both wells shows that the majority of anisotropy in the Arbuckle Group is in zones A2 and A4 with values varying from 2–20%. Zone A1 that coincides with the Upper Arbuckle shows moderate anisotropy (2–10%). Zone A3 shows

less anisotropy often <5%, except for a thin interval close to a depth of 4820 ft. This zone forms the lower part of the Middle Arbuckle, which is interpreted to act as a baffle zone. The fast S-wave polarization direction for all the zones, A1 through A4, for both wells, is found to have an E-W orientation and is shown on the rose diagram in Figure 2.9b.

2.5 DISCUSSION

2.5.1 Integration of multicomponent seismic data and well-log analysis

As a result of depth registration of P-P and S-S data, an estimate of Vp/Vs is obtained for Line 1 in Wellington Field. Vp/Vs acts as a proxy to lithology (Tatham, 1982), and its variation in the subsurface can be used to understand variations in lithofacies. The Mississippian interval, which is the major hydrocarbon producing zone in Wellington Field, shows a Vp/Vs ratio varying from 1.7–1.9, which is consistent with oil-saturated dolomitic limestone. Based on Vp/Vs values, the Arbuckle group can be divided into three zones: the Upper Arbuckle (Vp/Vs = 1.9), the Middle Arbuckle (Vp/Vs = 2.1), and the lower Arbuckle (Vp/Vs = 1.8). Vp/Vs values of 1.8–1.9 in the Upper and the Lower Arbuckle are consistent with the presence of vuggy and fractured dolomite, as reported from the drill cuttings of well 1-28 and well 1-32 and core analysis. Higher Vp/Vs (2–2.1) in the Middle Arbuckle indicates a change in lithofacies from vuggy dolomite to cherty and muddy dolomitic facies, which is also reported from various thin-section and core analysis studies (Watney and Rush, 2012). This result is also corroborated by seismic-inversion studies that showed high P-impedance in the Middle Arbuckle, which led researchers to conclude it is a baffle zone (Watney and Rush, 2012).

Measurements made at both well-log and surface-seismic scales show seismic anisotropy in the subsurface. A dipole-sonic log provides a higher vertical resolution for

seismic anisotropy compared to the S-wave seismic data estimates. Well logs suggest that anisotropy varies from 2–10% in the Mississippian interval and up to 20% in certain zones of the Arbuckle Group (zones A2 and A4). These estimates agree with the low-resolution anisotropy estimate from time-shift analysis of fast and slow S-waves that suggest an average anisotropy of 5% in the Arbuckle Group. E-W orientation of seismic anisotropy obtained from dipole-sonic logs is sub-parallel to the maximum horizontal stress orientation (75^{o}E) estimated from orientation of drilling induced fractures (Figure 2.4a). Based on the analysis of image log data, it is hypothesized that the anisotropy observed on well log and seismic observations could be a result of preferential closing of randomly oriented fractures (Figure 2.4b) in response to the stress field. Micro-cracks and fractures in the direction of maximum horizontal stress remain open, causing the observed anisotropy. Similar observations and conclusions have been reported in Kay County, OK (Queen and Rizer, 1990) and Carter County, OK (Beckham, 1996), which are 50 mi and 250 mi respectively, from the Wellington Field, and at the San Andreas Fault Observatory at Depth (SAFOD) pilot-hole study (Boness and Zoback, 2004) done in Parkfield, California.

2.5.1 Challenges in multicomponent seismic interpretation

Interpretation of multicomponent seismic data has its own set of challenges. Identification and correlation of reflection events on P-P and S-S sections can be challenging (DeAngelo, et al., 2003). This might be due to a difference in frequency content and low Signal-to-noise (S/N) ratio of seismic data sets. S/N east of well 1-28 was relatively lower in S-S data due to challenging S-wave static corrections. For this reason, all of my analysis has been restricted to seismic data west of well 1-28 on Line 1. Another reason for the lack of one-to-one correspondence between P- and S-wave data is

that the particle displacement vectors for each of these modes are oriented orthogonal to each other. Those two waves thus sense a different earth fabric along a common propagation paths and carry this direction-dependent information about elastic constants, grain cementation, pore geometry, anisotropy, and lateral variations in rock and fluid (Hardage et al., 2011), which causes P and S reflection signatures to differ. In such cases, identification of specific stratigraphic signatures such as channel cuts and pinch-outs can aid interpretation (see Figure 2.8). Depth registration of P-P and S-S data provide a low-frequency estimate of Vp/Vs, which can be used to constrain seismic velocity models and to convert between PP-time, SS-time and depth. However, these low-frequency estimates are not suitable for reservoir characterization studies. For a high-resolution subsurface characterization, more detailed elastic properties can be obtained from amplitude-based attribute analysis (Chapter 4) and from seismic inversion of multicomponent seismic data (Chapter 5).

There are challenges in estimating anisotropy associated with different measurement scales. Well-log based anisotropic measurements are made with higher frequency waves (3–30 KHz), making them more sensitive to micro-cracks and small fractures in the vicinity of a borehole. Surface-seismic based measurements, on the other hand, are made using low frequency seismic waves (2–200 Hz), which respond to large scale, laterally extensive fractures and discontinuities. Time-shift analysis of fast and slow S-waves provides a low-frequency estimate of seismic anisotropy. However, employing S-wave amplitude methods can give a higher-resolution insight into seismic anisotropy and its causes within intervals of interest (Tsvankin et al., 2010). An attempt to extract amplitude-based seismic attributes that can be used to understand lateral and depth variations in the density of anisotropy-causing fractures is made in subsequent chapters.

2.6 CONCLUSIONS

Interpretation of P-P and S-S wave modes carried out on Line 1 in the Arbuckle interval yielded Vp/Vs measurements from depth registration. High values of Vp/Vs in middle Arbuckle supports previous interpretations of the presence of a tight/baffle zone. Measurement and comparison of time-shifts in slow and fast S-S wave modes and dipole sonic logs show the seismic anisotropy exists in the Mississippian and Arbuckle intervals, which can be linked to the presence of fractures that remained open in response to anisotropic subsurface stress. Results of this analysis help map the lateral heterogeneities and fractures present in the Arbuckle interval, which can potentially affect the injection and movement of CO_2 in the subsurface. Valuable shear wave information obtained from S-S data demonstrates the value that multicomponent seismic brings to reservoir geophysics.

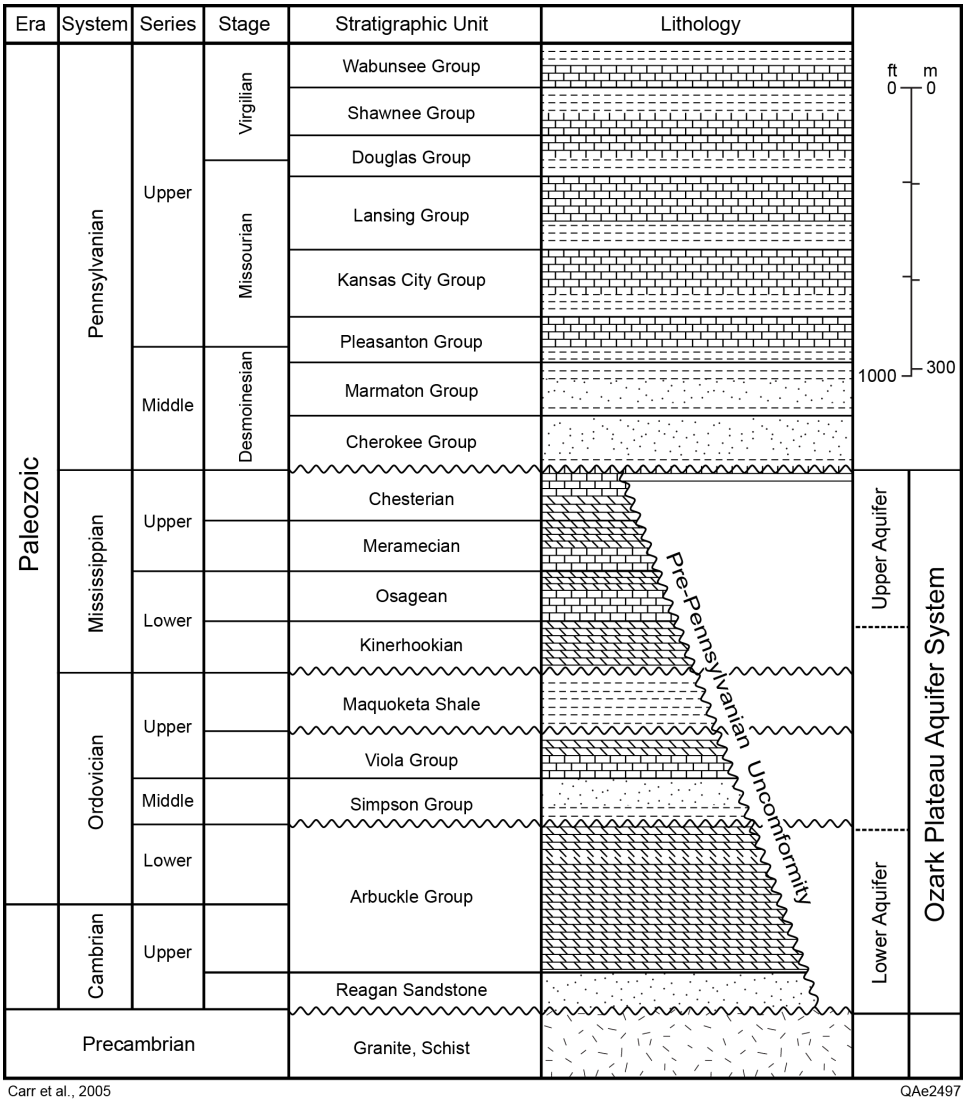

Figure 2.1: General stratigraphic column for Kansas (Carr et al. 2005). The Wellington Field produces hydrocarbons from Mississippian aged reservoirs. The Ordovician-aged Arbuckle Group is a part of the Ozark Plateau Aquifer System and is being considered for CO_2 storage.

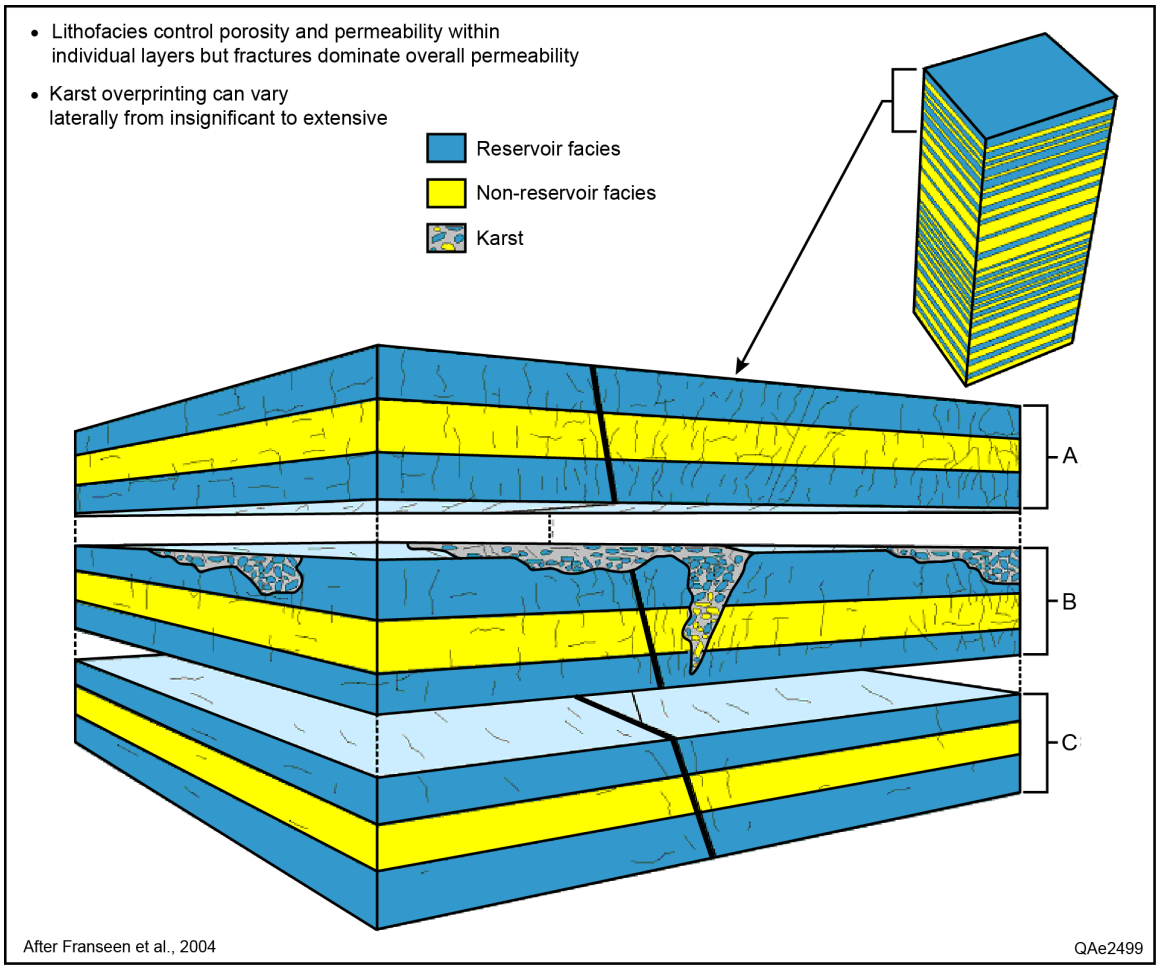

Figure 2.2: Sketch showing different facies types and fracturing present in the Arbuckle formation (Franseen et al., 2003). A) reservoirs with abundant fractures in which litho-facies control porosity and fractures control overall permeability, B) reservoirs with karst overprinting on litho-facies and fractures, resulting in complex porosity and permeability, and C) reservoirs where litho-facies control porosity and permeability.

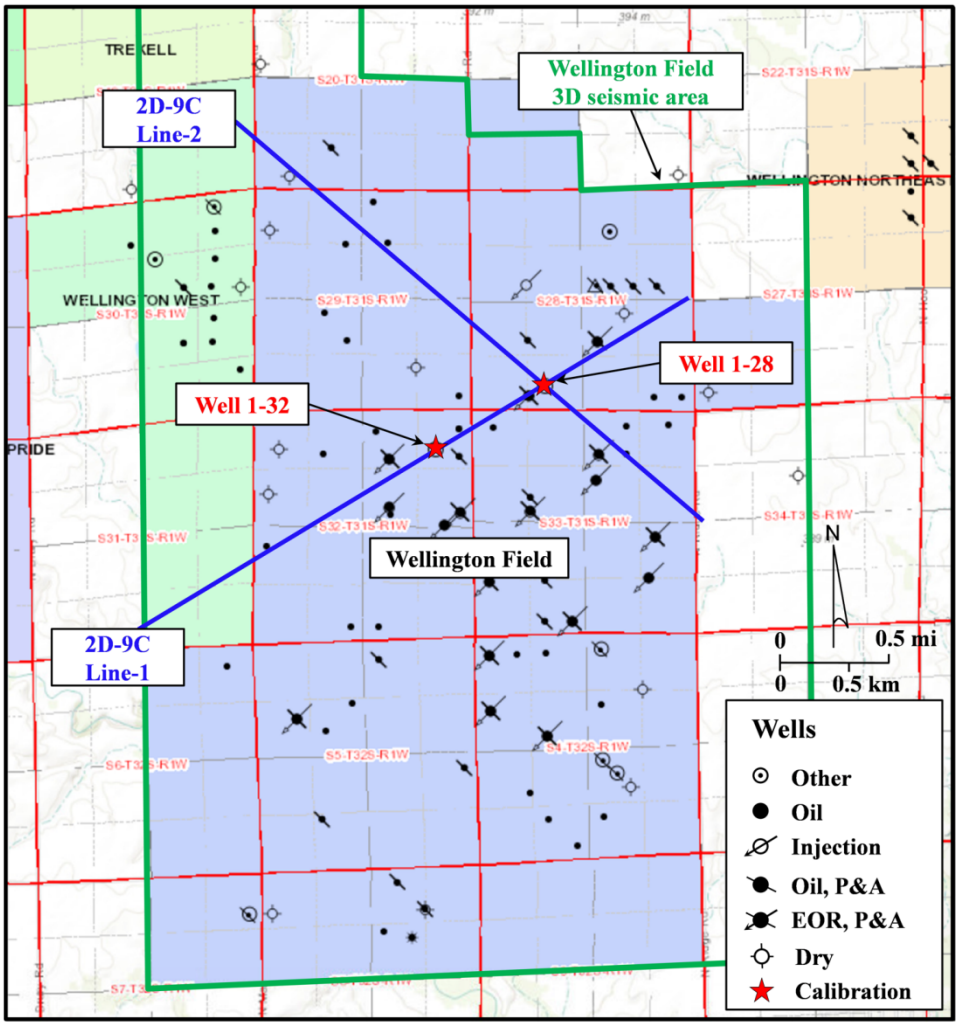

Figure 2.3: Base map of Wellington Field (shaded blue area) showing the 9C-2D seismic data (blue lines), 3D P-wave seismic data (green area) and different wells with at least some log data available. 2D-9C Line-1 was used for the multicomponent seismic interpretation presented in this chapter. Wells 1-32 and 1-28 had a full suite of well logs and cores acquired and are used as calibration wells.

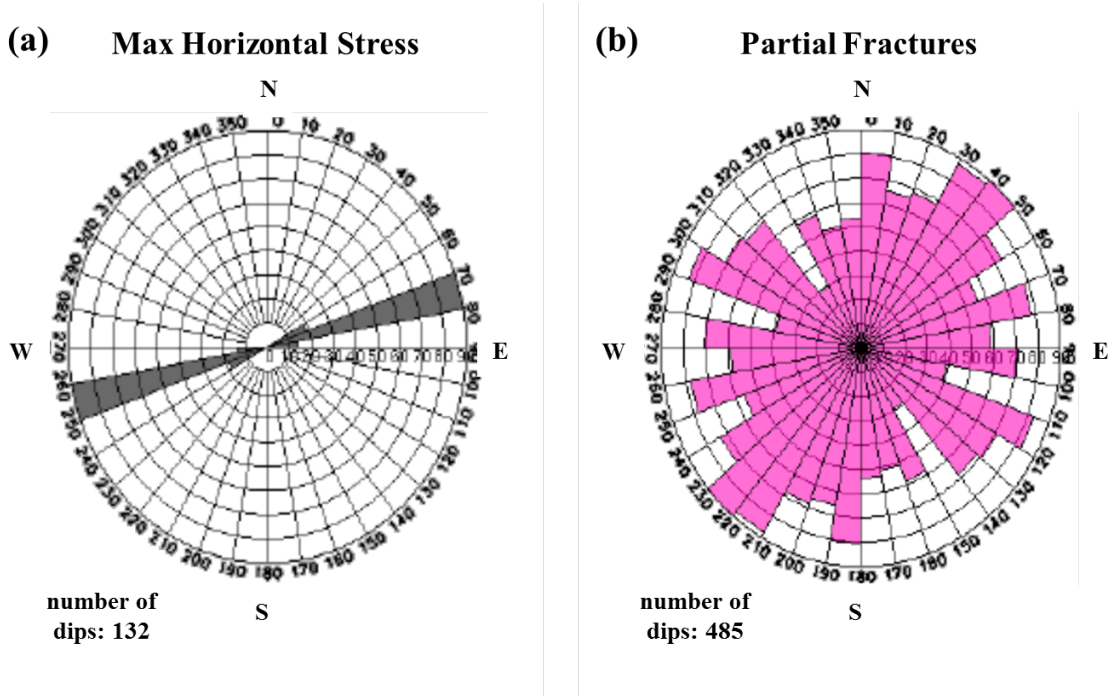

Figure 2.4: (a) Rose diagram of 132 drilling-induced fractures identified on the image logs that yielded a maximum horizontal stress direction of 75°E. (b) Rose diagram depicting the azimuthal orientation of 485 partially closed fractures. These partial fractures have no particular orientation and are distributed randomly throughout the azimuthal space.

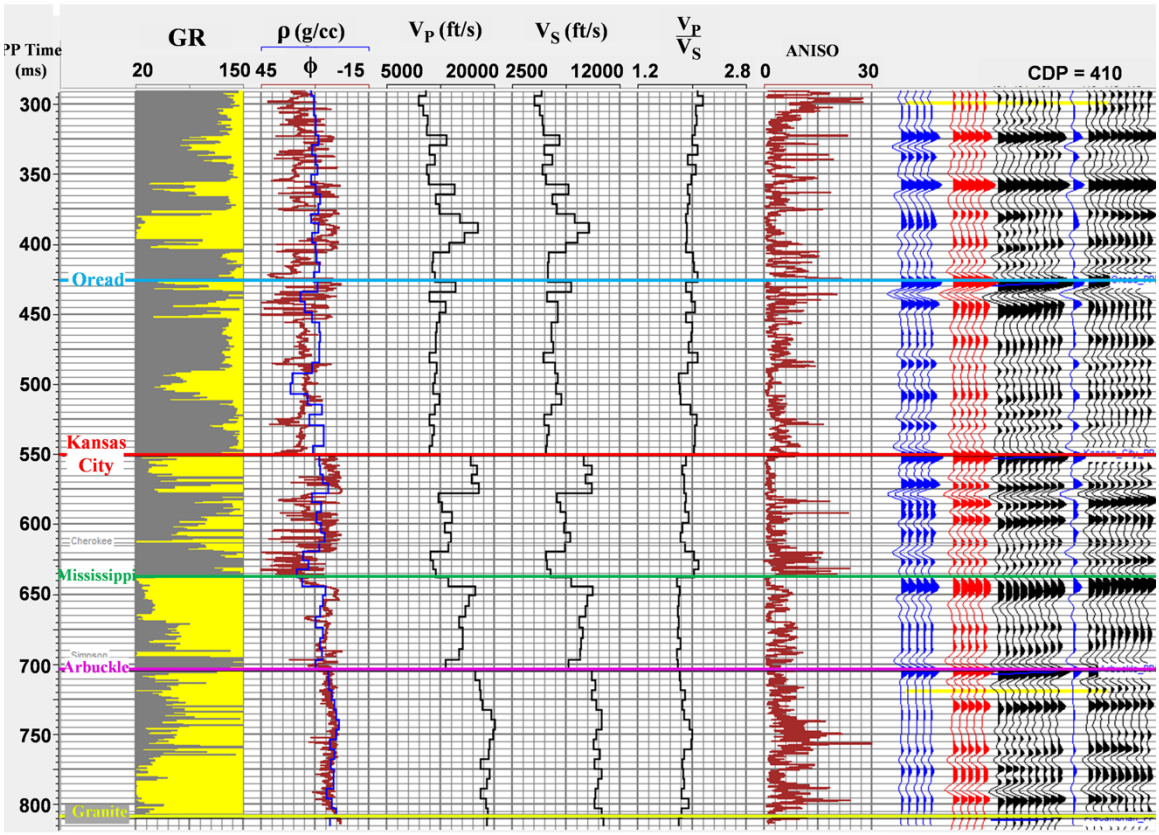

Figure 2.5: P-P well-to-seismic tie for well 1-32. The correlation coefficient was more than 76%. The top of Arbuckle (pink) is an increase in P-impedance and is represented by a peak (positive) on seismic.

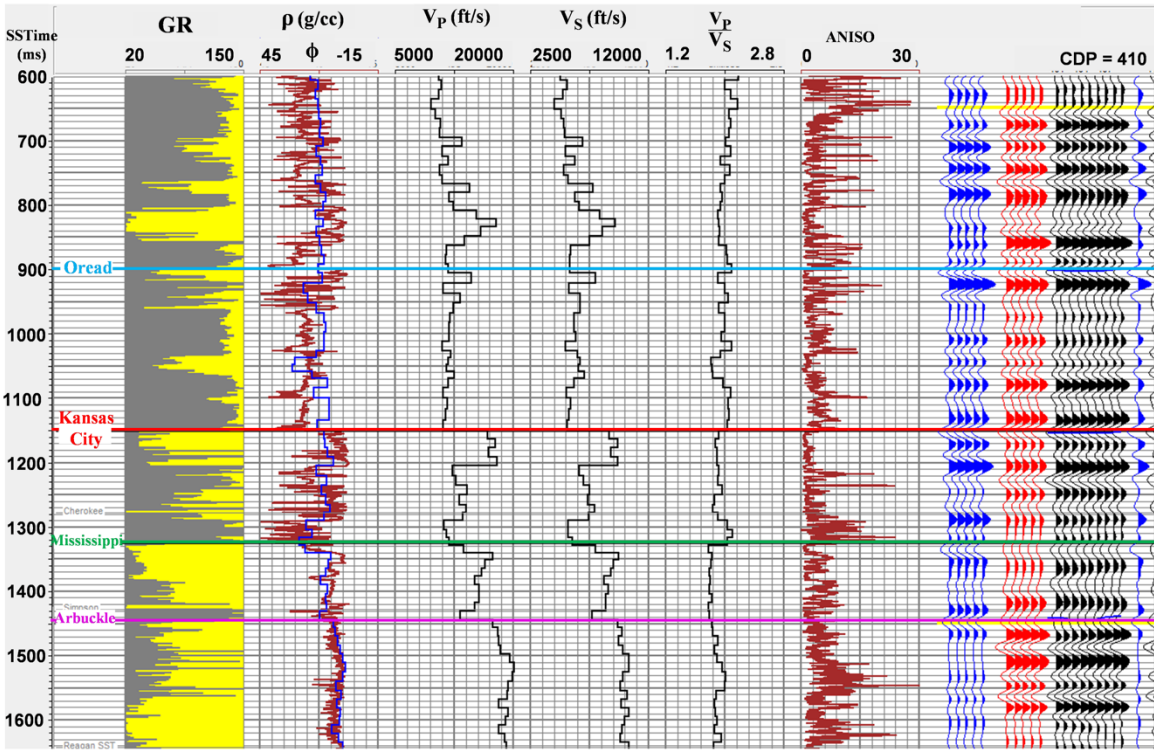

Figure 2.6: S-S well-to-seismic tie for well 1-32. The correlation coefficient was more than 82%. The top of the Arbuckle (pink) is an increase in S-impedance and is represented by a trough (negative) on seismic data due to the negative reflection coefficient.

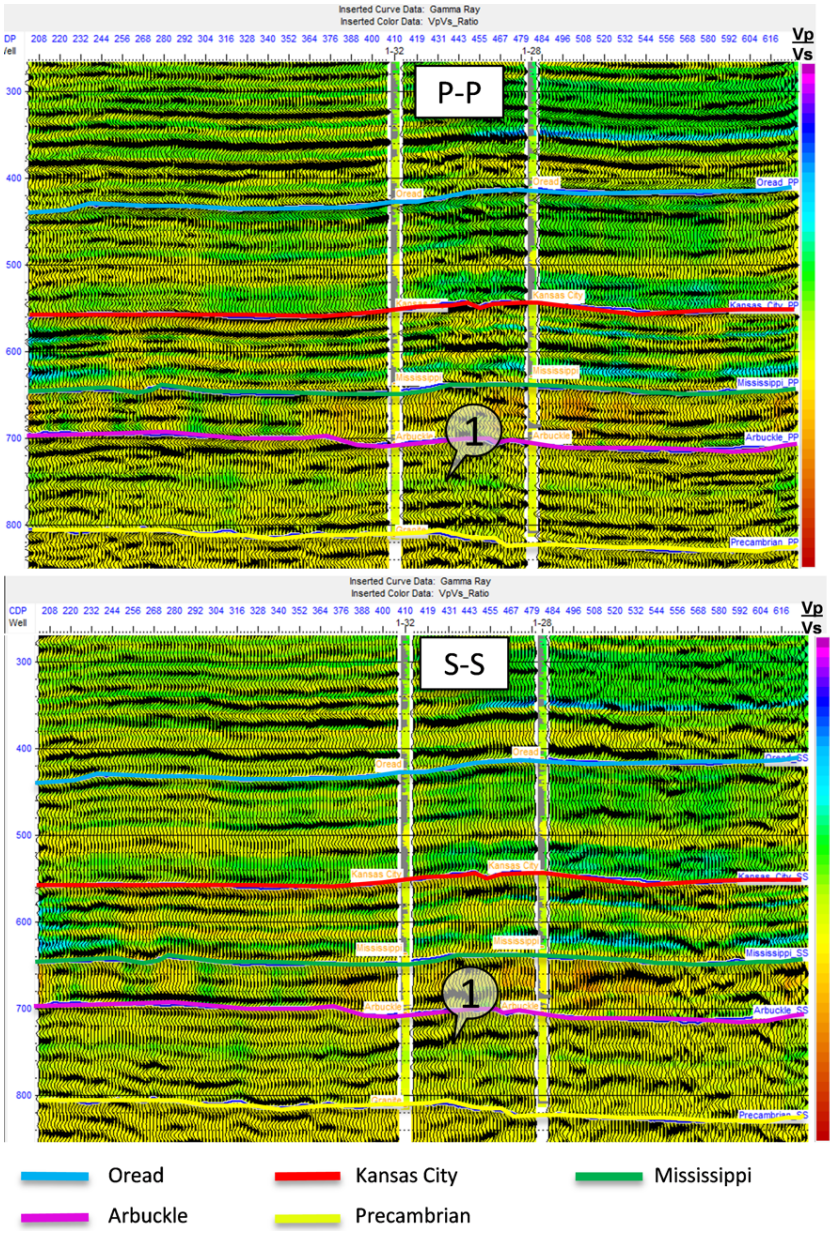

Figure 2.7: P-P and slow S-S seismic modes (wiggle plot) in P-P travel time after event correlation. The inserted curve is gamma ray with grey color representing shaly intervals. Inserted color at well location is the Vp/Vs determined from borehole data. Color plot in the seismic background is the Vp/Vs obtained from event correlation. Note Vp/Vs from event matching is consistent with Vp/Vs recorded in the wells. Marker 1 represents a high Vp/Vs unit in the middle Arbuckle, which might indicate a tight or baffle zone.

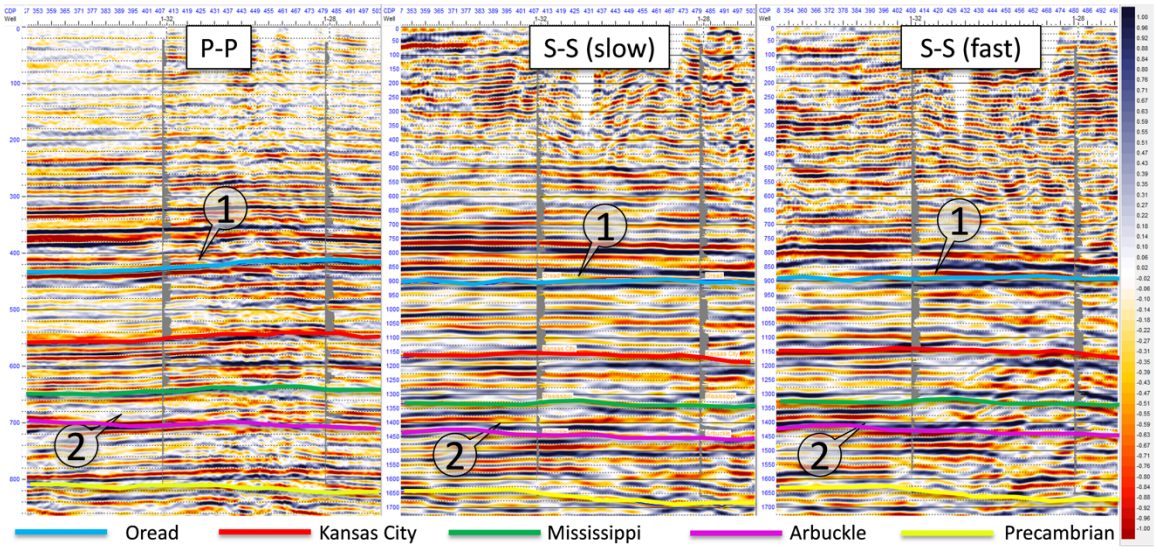

Figure 2.8: P-P, S-S slow and S-S fast seismic modes in their respective time domain with interpreted horizons. The inserted curve is gamma ray with grey color representing shaly intervals. Note the relative up shift in the fast S-wave section. Marker-1 shows updip pinch-out on Oread horizon and Marker-2 shows a channel type feature that can be found on all wave modes, which aids event correlation.

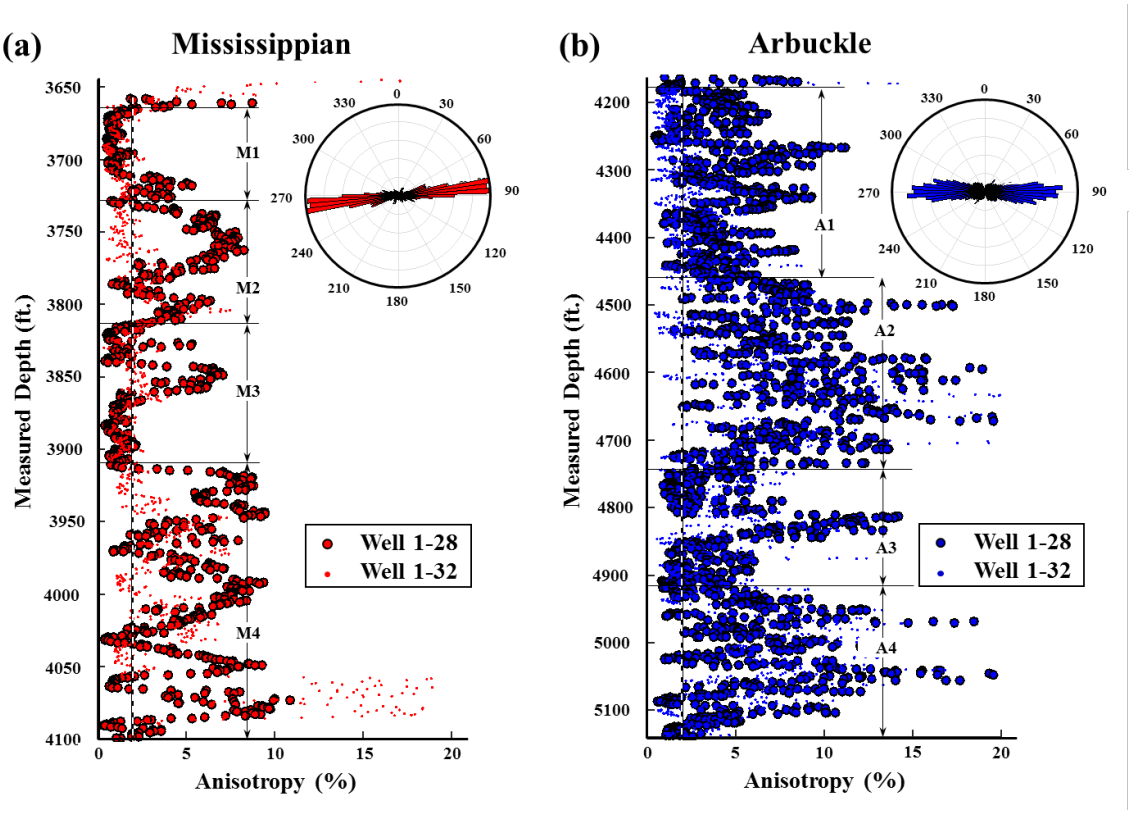

Figure 2.9: (a) Seismic anisotropy measurements made in wells 1-28 and 1-32 for the Mississippian interval. Based on the anisotropy estimates, the Mississippian interval is divided into 4 zones, M1 through M4, with zones M1 and M3 showing low seismic anisotropy and zones M2 and M4 showing high seismic anisotropy. (b) Seismic anisotropy measurements made in wells 1-28 and 1-32 for the Arbuckle interval. Arbuckle interval is also divided into 4 zones, A1 through A4, with zones A1 and A3 showing low seismic anisotropy and zones A2 and A4 showing high seismic anisotropy. The vertical dotted line drawn at a percentage anisotropy value of 2 is the threshold value used to calculate the rose diagrams of fast S-wave polarization.

Chapter 3: Statistical Rock Physics and Amplitude Variation with Offset Modeling of Direct P-and S-waves in Wellington Field, Kansas[2]

3.1 ABSTRACT

This study focuses on modeling the effects of fractures on the elastic properties of a rock and illustrates which wave modes might be helpful for quantitative interpretation of fracture properties like fracture-density and fracture-fill. A statistical rock physics model is constructed for Ordovician age carbonates of the Arbuckle Formation encountered in wells drilled in Wellington Field, Kansas. This model incorporates a priori information about matrix porosity distribution and pore shapes obtained from well logs and from analysis done on drill cores. Estimations of P-wave and S-wave seismic velocities and anisotropy parameters obtained from rock physics models are used to study AVO behaviors of P-waves and fast and slow S-waves in directions parallel to, and perpendicular to, fractures. AVO modeling shows that azimuthal variations in P-P AVO due to presence of fractures are smaller compared to the variation caused by uncertainties in lithology and fracture-density. This strong influence of unknown rock properties limits the ability of P-waves to uniquely determine fracture properties. Results of this study demonstrate that in angle-azimuth space, the AVO intercept of slow-S-wave data in the plane parallel to fracture, quantitatively estimates fracture density (γ) of a rock formation.

---

[2] This chapter was previously published in Gupta, M., K., Spikes, M. E., Far, D., Sava, and B., Hardage, 2014, October. Statistical AVO intercept-gradient analysis of direct S-waves: A methodology for quantitative fracture characterization: In 2014 SEG Annual Meeting. Society of Exploration Geophysicists; M. Gupta conceptualized and performed the research with assistance from K. Spikes and D. Sava. M. Gupta wrote the manuscript. M.E. Far and B. Hardage contributed in discussions and revisions.

In contrast, P-P azimuthal AVO attributes do not correlate well with fracture density. This study also demonstrates that the AVO gradient of slow S-wave data in a direction normal to fracture-orientation can help in discriminating fluid-fill in fractures. Conclusively, S-wave AVO attributes are less affected by subsurface uncertainty compared to P-wave attributes and hence can significantly reduce ambiguity in quantitative fracture characterization.

3.2 INTRODUCTION

P-wave velocities have been used to understand seismic anisotropy for a long time. While P-wave velocity modeling can provide important anisotropy information to create a better seismic image, it does not provide a resolution high enough to be used in reservoir characterization studies. To achieve a high-resolution anisotropy estimate, seismic amplitude-based studies have been conducted using P-waves (Corrigan et al., 1996; Liu and Martinez, 2013; Lynn, 2007; Mallick et al., 1996; Ruger, 2001; Jenner, 2001; and Roche et al., 2005), but there have been high degrees of uncertainty associated with the results. To reduce this uncertainty, there has been an increasing trend to incorporate S-waves in an anisotropy analysis.

Direct S-wave modes have proved to be effective in detecting azimuthal anisotropy (Martin and Davis, 1987). Traditionally, use of direct S-waves for fracture characterization is limited to shear-wave splitting analysis (Alford, 1986; Li, 1997; Grossman et al., 2013), travel-time analysis (Lynn et al., 1995), and post-stack amplitude analysis (Mueller, 1991; Kendall and Kendall, 1996; Lynn et al., 1995). Studies concerning pre-stack amplitude analysis for fracture characterization are rare for direct S-waves. The few S-wave AVO modeling studies (Yardley et al., 1991; Rusmanugroho and

McMechan, 2010) that have been attempted do not agree on what fracture properties can be extracted and where that information lies in offset-azimuth data space.

In this study, I establish a statistical rock physics model for elastic constants that incorporates uncertainty in lithology, porosity, shape, and spatial density of fractures. This statistical model is then used to understand what P-wave and S-wave AVO attributes would be optimal for observing variations in elastic constants caused by fracture-orientation, spatial density, and fluid-fill of fractures. The results of this modeling study show that S-wave AVO provides estimates of fracture-orientation, fracture-density and fracture-fill with significantly less ambiguity than do P-waves. I demonstrate that fracture density information lies in near-normal slow S-wave incidence angles in fracture-parallel azimuths, and fracture-fill information lies in non-normal, pre-critical slow S-wave incidence angles in fracture-perpendicular azimuths. Also, information regarding the aperture or aspect ratio of fractures is difficult to estimate from P- and S-wave amplitudes. This study also highlights the importance and advantages of S-wave AVO analysis over P-wave AVO analysis for quantitative fracture characterization and provides the necessary background and motivation to study S-wave AVO in detail.

3.3 METHODS

For this study, I use well log and core data from well 1-32 in Wellington field located in south-central Kansas shown in Figure 3.1. Wellington field is a part of sub-crop play with Mississippian cherty, dolomitic reservoirs preserved in structural blocks bounded by NE and NW trending lineaments in Sumner County, Kansas. The stratigraphic units that are of immediate interest to this study are Ordovician age

carbonates in the Arbuckle formation. The Arbuckle is fractured and heavily dolomitized and is being considered for CO_2 storage.

3.3.1 Rock physics study of Upper Arbuckle formation

First, we build an isotropic carbonate background that closely resembles the upper Arbuckle formation in terms of porosity distribution and pore-shapes. This construction is done using the isotropic Differential Effective Medium (DEM) model (Norris, 1985). This model assumes that the inclusions are dry ellipsoid pores that are randomly oriented in an isotropic and homogeneous dolomitized carbonate background. Figure 3.2 compares the actual porosity distribution in the upper Arbuckle obtained from well logs and the porosity distribution assumed for the DEM model. The background elastic constants obtained from the DEM model act as an input for the second stage, where a single set of aligned fractures are modeled using Hudson's model for HTI media (Hudson, 1981) and a linear-slip model to address any biases caused by using a particular approach. Both models are discussed in Appendix A (Section 3.6). In order to understand the effects of fluids in these cracks at seismic wavelengths, low-frequency relations given by Brown and Korringa (1975) were used to calculate the stiffness matrix of the fluid-saturated rock. This stiffness matrix is used to calculate seismic velocities and Thomsen parameters because these parameters directly affect seismic amplitudes.

3.3.2 AVO modeling and intercept-gradient analysis

P-P and S-S AVO modelling was done for the top of the Arbuckle formation in planes parallel to fractures (isotropy plane) and planes orthogonal to fractures (symmetry plane). For S-S wave modes, two polarizations have been considered corresponding to the fast and slow directions. Mathematical formulations proposed by Ruger (2001) for HTI media have been used to model these wave modes and are discussed in Appendix B

(Section 3.7). One thousand Monte-Carlo simulations were completed to model AVO responses of both S-wave mode, for varying input rock and fracture parameters. Also, AVO intercepts and gradients for all reflectivity modes were calculated and cross plotted to understand their dependence on different rock and fracture properties.

3.3.3 Uncertainty

Due to assumptions required to reduce mathematical and computational complexities and our inability to create the actual rock texture in a rock physics model, there is uncertainty in the model's prediction response. This problem can be partly solved by incorporating uncertainty in the input parameters (porosity, crack density, aspect ratio, and fluid) used by a rock physics model, propagating those uncertainties through the model, and observing the effect on the model response. This approach indicates not only the sensitivities of different rock properties, but also helps explain the observed data. Figure 3.3 shows the variation in crack density and crack aspect ratio that were used as an input into the model. Variations in the elastic parameters of the shale layer above the Arbuckle formation have also been considered in the AVO model.

3.4 RESULTS

Well log data suggest that most of the Arbuckle formation in Wellington field is fractured and saturated with brine. A rock physics model is constructed to estimate elastic stiffness for the upper Arbuckle formation. My rock physics model provides estimates of seismic velocities and anisotropic parameters like ε, δ and γ described by Thomsen (1986). Figure 3.4 shows the porosity dependence of slow P-wave and S-wave velocities and the Thomsen parameters ($\varepsilon^{(v)}$, $\delta^{(v)}$ and γ) defined with respect to vertical in an HTI media. These parameters are direct input into P-wave and S-wave AVO equations and

hence understanding their behavior with changing rock and fracture properties is important for fracture characterization. Figure 3.4 is plotted for both dry and brine-saturated Arbuckle formation. Vp, Vs and γ in Figure 3.4a, 3.4b, and 3.4c are color coded with the crack density parameter. Both P- and S-wave velocities show some degree of change with varying crack density. This change is probably not large enough to deduce fracture-density information form seismic velocities. γ shows a direct relationship with crack density i.e. a higher value of γ corresponds to high crack density and vice versa. Filled black circles shown on the γ plot are S-wave velocity anisotropy data from borehole measurements in the Upper Arbuckle formation and agree with the model. According to the model, crack density in the Upper Arbuckle formation near the well bore is less than 5-percent. $\varepsilon^{(v)}$, $\delta^{(v)}$ and $(\Delta\delta^{(v)} - \Delta\varepsilon^{(v)})$ plots in Figure 3.4d, 3.4e, and 3.4f are color coded with the fracture-content to show the modeled behavior of dry and brine-saturated Arbuckle carbonates. These plots show that $\delta^{(v)}$ is insensitive to fracture-fill, but $\varepsilon^{(v)}$ is higher for brine as compare to dry rock. Similar dependence of $\varepsilon^{(v)}$ on fracture-fill has also been discussed in Sava et al. (2001). The behavior of $(\Delta\delta^{(v)} - \Delta\varepsilon^{(v)})$ plot in Figure 3.4f shows a clear separation between two fracture-fills, implying its application as a proxy for fracture-fill.

The effect of crack aspect ratio on seismic velocities and anisotropic parameters was also studied. Figure 3.5 is plotted for brine-saturated Arbuckle formation and shows variations of all elastic parameters with respect to changing crack aspect ratio. For dry rock, none of the elastic parameters show any relationship with crack aspect ratio parameter, and as the fluid-fill in fractures gets stiffer, Vs and $\varepsilon^{(v)}$ (Figure 3.5b and 3.5e) start to show a small systematic variation with aspect ratio. All other elastic parameters like Vp, γ, and $\delta^{(v)}$ show no systematic change. The systematic variations in Vs and $\varepsilon^{(v)}$

lie below the uncertainty threshold, making prediction of aspect-ratio extremely difficult from seismic amplitude measurements alone.

To be able to extract quantitative rock and fracture information from seismic data, it is important to understand how rock and fracture properties affect AVO responses of P-waves and S-waves. Figure 3.6 shows the AVO behavior of P- waves, fast and slow S-waves in isotropy and symmetry planes when the top of the Arbuckle is saturated with brine. Ten AVO curves were randomly selected for display out of 1000 simulations done for varying crack density and crack aspect ratio. It is important to note that P-wave reflectivities parallel and perpendicular to the fractures show significant overlap, masking any anisotropic signature with the uncertainties in lithology, the aspect ratio and crack density. Fast- S-waves as shown in Figure 3.6b have two different clusters of gradients corresponding to polarization in the isotropy plane (SV) and symmetry plane (SH). Similarly, slow S-waves (Figure 3.6c) have clusters of gradients corresponding to polarization in the isotropy plane (SH) and symmetry plane (SV). There is a shift between the AVO intercepts of fast- and slow- S-waves, which is caused by the presence of fractures. Moreover, slopes of AVO curves of fast- and slow- SV waves also show a minor difference caused by presence of fractures.

Figure 3.7 is the intercept-gradient cross plot for AVO responses in Figure 3.6 color-coded with crack density and crack aspect ratio. Here, filled circles represent the isotropy plane and open circles denote the symmetry plane. It is evident that the slow- S-wave intercept (S2-S2 AVO intercept) is directly correlated to crack density. This result implies that a zone with higher fracture-densities might be seen as a dim spot on a slow-shear seismic section in the direction parallel to fracture-orientation. Also, amplitudes of S-waves for near-normal incidence angles can quantify the intensity of fracturing. These observations highlight the value of S-waves in fracture identification.

To understand the effect of different fluid fill in fractured rock, AVO behaviors of P- and S-wave modes for dry and brine-saturated rock were studied in the symmetry plane. Figure 3.8a shows a shift in the P-wave AVO intercepts for the different fluid types. According to my model, changes in the intercept for P-waves are caused by changes in the matrix porosity, not by fluid in fractures. Figure 3.8c shows changes in gradients of slow S-waves AVO curves for different fluid fill. This gradient change is a direct consequence of the dependence of the $\Delta\delta^{(v)} - \Delta\varepsilon^{(v)}$ parameter on fluids. My model suggests that the gradient of the slow S-wave in the symmetry plane gives information about the fluid present in the fractures. How this AVO information gets translated in the intercept gradient cross plots is shown in Figure 3.9. A difference in P-wave AVO intercept distribution can be seen for different fluid-fill in Figure 3.9a and 3.9d. Systematic changes in slow S-wave AVO intercept and gradient are observed with changing crack density in Figure 3.9c. However, changes in S-wave AVO intercepts and gradient due to changes in the fluid is not quite apparent. A careful decoupling process is required to extract $\Delta\delta^{(v)} - \Delta\varepsilon^{(v)}$ information from the S-wave AVO gradients to obtain fluid-fill in fractures.

3.5 CONCLUSIONS

This study suggests that S-waves are more sensitive to fractures compared to P-waves. For the P-P mode, magnitudes of azimuthal variations in AVO intercepts and gradients are less than variations due to uncertainty in lithology and fracture-density and hence will not be an optimal choice of data analysis to determine fracture properties. Crack density parameter ($\boldsymbol{\gamma}$) acts as a proxy for estimating relative changes in fracture-density in subsurface rock formations. To estimate $\boldsymbol{\gamma}$, S-S modes provide significant

advantage over a P-P mode. I demonstrate that, in angle-azimuth space, the slow-S-wave AVO intercept in the isotropy plane can estimate the $\boldsymbol{\gamma}$ (crack density) of a rock formation. Also, results suggest that $\Delta\delta^{(v)} - \Delta\varepsilon^{(v)}$ has great potential to discriminate fluids in fractures. Because $\Delta\delta^{(v)} - \Delta\varepsilon^{(v)}$ governs the AVO behavior of S-waves in the symmetry plane, I conclude that slow S-wave AVO gradient in directions normal to fracture-orientation has a potential to discriminate fluid-fill in fractures. However, obtaining quantitative information about fluids in fractures would require deriving an appropriate AVO attribute or inverting S-wave seismic data for $\Delta\delta^{(v)} - \Delta\varepsilon^{(v)}$. P-waves on the other hand are more affected by the fluid fill in pores rather than by fluid fill in aligned fractures.

Conclusively, adding S-wave AVO analysis to current fracture characterization workflows can significantly reduce ambiguity in quantitatively estimating fracture properties. Using a statistical approach is important to understand how uncertainty in rock and fracture properties affects the ability to characterize fractures. Attributes derived from S-waves are less affected by the subsurface uncertainty compared to attributes derived from P-waves and thus are more reliable for fracture characterization.

3.6 APPENDIX A

3.6.1 Hudson's model for HTI media

Hudson's model describes the stiffness matrix of an elastic solid that contains thin penny-shaped ellipsoidal cracks or inclusions (Hudson, 1981). For a single crack set with horizontally aligned crack normals, an effective medium shows transverse isotropy with a horizontal axis of symmetry. Through these preferentially aligned ellipsoidal cracks, I model a set of aligned fractures present in a rock. The effective moduli of the fractured rock C_{ij}^{eff} are given as follows

$$C_{ij}^{eff} = C_{ij}^{0} + C_{ij}^{1} + C_{ij}^{2} \qquad (A-1)$$

where C_{ij}^{0} is the isotropic background moduli, and C_{ij}^{1}, C_{ij}^{2} are first- and second-order corrections, respectively. Hudson's theory assumes isolated cracks or inclusions and simulates high-frequency wave propagation behavior. In order to understand the effects of fluids in these cracks at seismic wavelengths, low-frequency relations given by Brown and Korringa (1975) were used to calculate the stiffness matrix of the fluid-saturated rock. This stiffness matrix is used to calculate seismic velocities and Thomsen parameters.

3.6.2 Linear slip model for HTI media

The linear slip model assumes that the effective compliance of a fractured rock at seismic-scale wavelengths can be estimated by adding the compliance of the isotropic host rock and the compliance of the well-aligned fractures (Schoenberg and Sayers, 1995).

$$S_{HTI} = S_b + S_{frac} \qquad (A-2)$$

where S_b is the compliance of the isotropic background, and S_{frac} is the compliance of a single set of vertical fractures. These compliances are calculated as follows:

$$S_b = \begin{bmatrix} \frac{(\lambda+2\mu)}{\mu(3\lambda+2\mu)} & -\frac{\lambda}{2\mu(3\lambda+2\mu)} & -\frac{\lambda}{2\mu(3\lambda+2\mu)} & 0 & 0 & 0 \\ -\frac{\lambda}{2\mu(3\lambda+2\mu)} & \frac{(\lambda+2\mu)}{\mu(3\lambda+2\mu)} & -\frac{\lambda}{2\mu(3\lambda+2\mu)} & 0 & 0 & 0 \\ -\frac{\lambda}{2\mu(3\lambda+2\mu)} & -\frac{\lambda}{2\mu(3\lambda+2\mu)} & \frac{(\lambda+2\mu)}{\mu(3\lambda+2\mu)} & 0 & 0 & 0 \\ 0 & 0 & 0 & \frac{1}{\mu} & 0 & 0 \\ 0 & 0 & 0 & 0 & \frac{1}{\mu} & 0 \\ 0 & 0 & 0 & 0 & 0 & \frac{1}{\mu} \end{bmatrix} \quad (A-3)$$

$$S_{frac} = \begin{bmatrix} K_N & 0 & 0 & 0 & 0 & 0 \\ 0 & 0 & 0 & 0 & 0 & 0 \\ 0 & 0 & 0 & 0 & 0 & 0 \\ 0 & 0 & 0 & 0 & 0 & 0 \\ 0 & 0 & 0 & 0 & K_T & 0 \\ 0 & 0 & 0 & 0 & 0 & K_T \end{bmatrix} \quad (A-4)$$

λ and μ are Lame's constants for the background isotropic medium. K_N is normal fracture compliance and K_T is tangential fracture compliance. Stiffness matrix C_{HTI} of the HTI medium can be derived from equation A-2:

$$C_{HTI} = \begin{bmatrix} M(1-\Delta_N) & \lambda(1-\Delta_N) & \lambda(1-\Delta_N) & 0 & 0 & 0 \\ \lambda(1-\Delta_N) & M(1-r^2\,\Delta_N) & \lambda(1-r\,\Delta_N) & 0 & 0 & 0 \\ \lambda(1-\Delta_N) & \lambda(1-r\,\Delta_N) & M(1-r^2\,\Delta_N) & 0 & 0 & 0 \\ 0 & 0 & 0 & \mu & 0 & 0 \\ 0 & 0 & 0 & 0 & \mu(1-\Delta_T) & 0 \\ 0 & 0 & 0 & 0 & 0 & \mu(1-\Delta_T) \end{bmatrix} \quad (A-5)$$

where, $M = \lambda + 2\mu$ and $r = \lambda/(\lambda+2\mu)$. Δ_N and Δ_T are described as non-negative, dimensionless fracture parameters, with values less than 1. These parameters relate the normal and shear compliance of fractures to the total normal of shear compliance of the fractured medium, respectively.

$$\Delta_N = (\lambda + 2\mu).K_N/(1 + (\lambda + 2\mu).K_N) \qquad (A-6)$$

$$\Delta_T = \mu.K_T/(1 + \mu.K_T) \qquad (A-7)$$

3.7 APPENDIX B

3.7.1 Approximations to P-wave and S-wave AVO equations (Ruger, 2001)

The exact reflectivity equations for P and S-waves for HTI media are complex and offer little insight into the elastic properties of a rock. For this reason, many attempts have been made to simplify these reflectivity equations in a form which make more physical sense to geophysicists and at the same time are accurate enough for quantitative characterization. Ruger (2001) provides approximations to reflectivity equations for P and S-waves propagating in isotropy and symmetry planes in an HTI media. These approximations provide an intuitive insight into the AVO behavior of waves as they are derived in terms of P and S-wave velocities and Thomsen parameters for weak anisotropy.

Approximations to P-wave AVO equations for HTI media suggested by Ruger (2001) can be written as:

$$R_P^{iso} = \frac{1}{2}\frac{\Delta Z}{\overline{Z}} + \frac{1}{2}\left\{\frac{\Delta\alpha}{\overline{\alpha}} - \left(\frac{2\overline{\beta}}{\overline{\alpha}}\right)^2 \frac{\Delta G}{\overline{G}}\right\} sin^2 i + \frac{1}{2}\frac{\Delta\alpha}{\overline{\alpha}} sin^2 i.tan^2 i \quad (1)$$

$$R_P^{sym} = \frac{1}{2}\frac{\Delta Z}{\overline{Z}} + \frac{1}{2}\left\{\frac{\Delta\alpha}{\overline{\alpha}} - \left(\frac{2\overline{\beta}}{\overline{\alpha}}\right)^2 \left(\frac{\Delta G}{\overline{G}} - 2\Delta\gamma\right) + \Delta\delta^{(v)}\right\} sin^2 i + \frac{1}{2}\left(\frac{\Delta\alpha}{\overline{\alpha}} + \Delta\varepsilon^{(v)}\right) sin^2 i.tan^2 i \quad (2)$$

In these equations R_P^{iso} represents the P-wave reflectivity in the symmetry plane, R_P^{sym} represents the P-wave reflectivity in the isotropy plane; i is the angle of incidence for the P-wave, $\varepsilon^{(v)}$, $\delta^{(v)}$ and γ are Thomsen parameters for HTI media (Ruger, 2001), Z is the P-wave impedance, α and β are isotropy plane velocities of P and S-waves, respectively, and G is the shear modulus corresponding to β.

Approximations to S-wave AVO equations for HTI media suggested by Ruger (2001) can be written as:

$$R_{S_2}^{iso} = -\frac{1}{2}\left(\frac{\Delta Z^s}{\overline{Z^s}} - \Delta\gamma\right) + \frac{1}{2}\left(\frac{\Delta\beta}{\overline{\beta}} - \Delta\gamma\right) tan^2 j \quad (3)$$

$$R_{S_1}^{iso} = -\frac{1}{2}\frac{\Delta Z^s}{\overline{Z^s}} + \left(\frac{7}{2}\frac{\Delta\beta}{\overline{\beta}} + 2\frac{\Delta\rho}{\overline{\rho}}\right) sin^2 j - \frac{1}{2}\frac{\Delta\beta}{\overline{\beta}} sin^2 j . tan^2 j \quad (4)$$

$$R_{S_2}^{sym} = -\frac{1}{2}\left(\frac{\Delta Z^s}{\overline{Z^s}} - \Delta\gamma\right) + \left\{\frac{7}{2}\left(\frac{\Delta\beta}{\overline{\beta}} - \Delta\gamma\right) + 2\frac{\Delta\rho}{\overline{\rho}} + \frac{1}{2}\left(\frac{\overline{\alpha}}{\overline{\beta}}\right)^2 . \left(\Delta\varepsilon^{(v)} - \Delta\delta^{(v)}\right)\right\} sin^2 j - \frac{1}{2}\left(\frac{\Delta\beta}{\overline{\beta}} - \Delta\gamma\right) sin^2 j . tan^2 j \quad (5)$$

$$R_{S_1}^{sym} = -\frac{1}{2}\frac{\Delta Z^s}{\overline{Z^s}} + \frac{1}{2}\left(\frac{\Delta\beta}{\overline{\beta}} - \Delta\gamma\right) tan^2 j \quad (6)$$

In these equations R_S^{iso} represents the S-wave reflectivity in the symmetry plane, R_S^{iso} represents S-wave reflectivity in the isotropy plane, j is the angle of incidence for the S-wave, S2 is the slow S-wave with polarization perpendicular to fractures, and S1 is the fast S-wave with polarization parallel to fractures. $\varepsilon^{(v)}$, $\delta^{(v)}$ and γ are Thomsen parameters (Thomsen, 1986) for HTI media (Ruger, 2001), $Z^s(=\rho\beta)$ is the S-wave impedance for vertically incident fast S-wave, and α and β are isotropy plane velocities of P and S-waves, respectively.

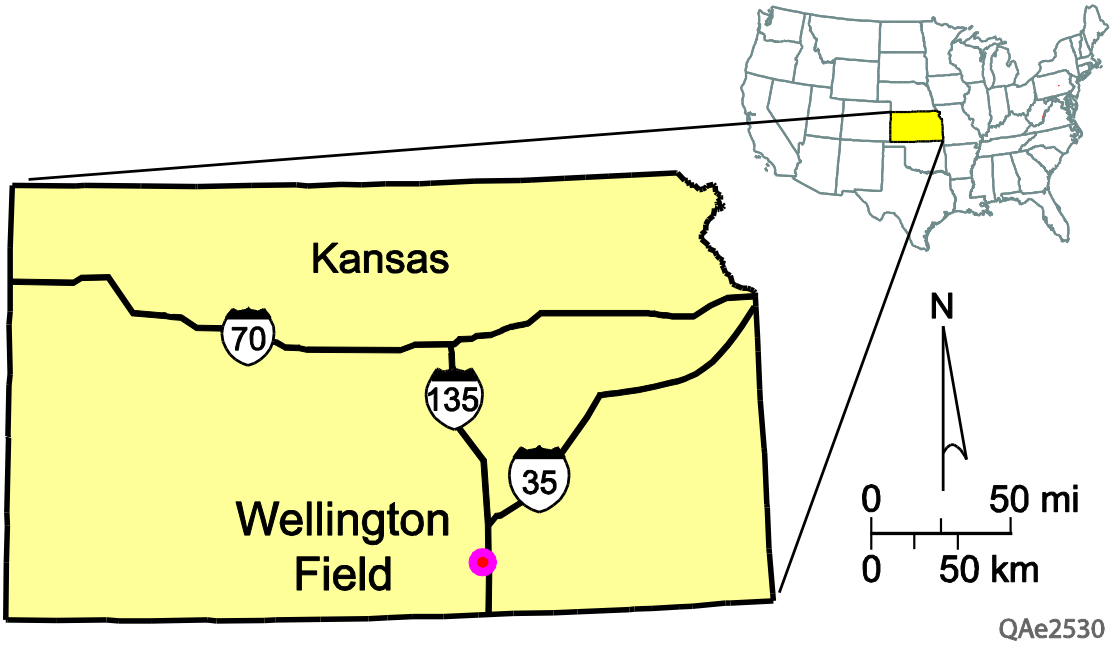

Figure 3.1: Data set comes from Wellington field, situated in south central Kansas, United States

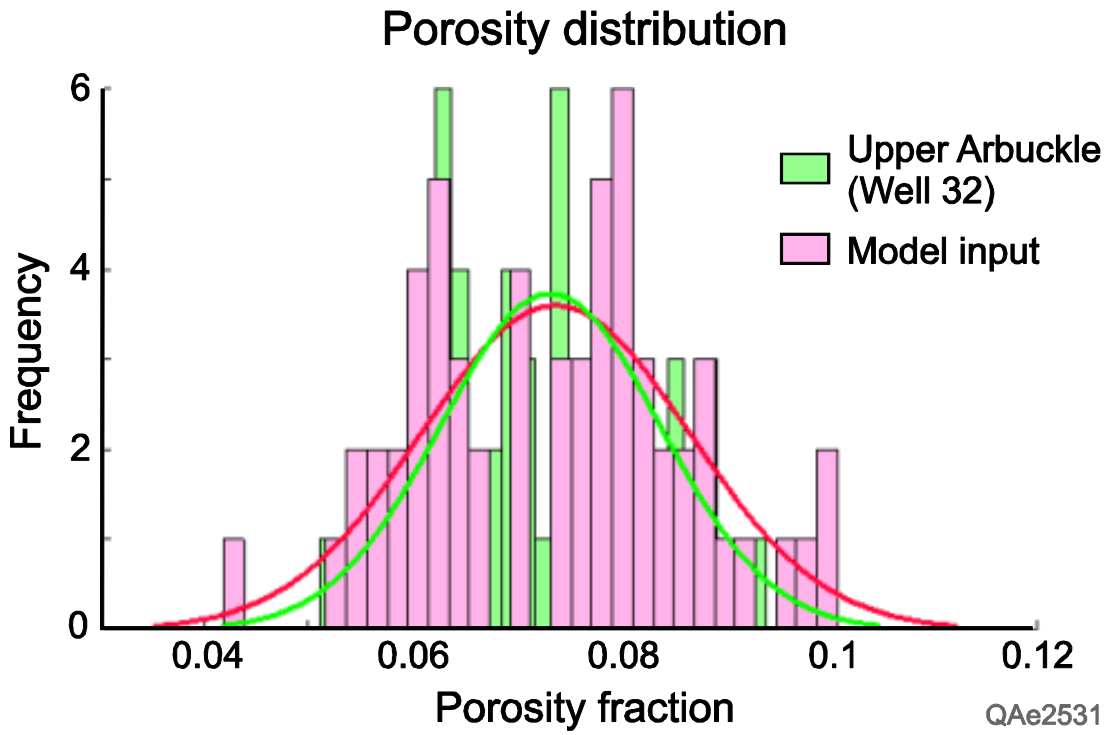

Figure 3.2: Porosity histograms and distributions of the upper Arbuckle formation obtained from well logs (green) and the background porosity distribution used in the model (red). Assumed porosity distribution is kept close to the porosity indicated by well data to keep model input parameters as realistic as possible.

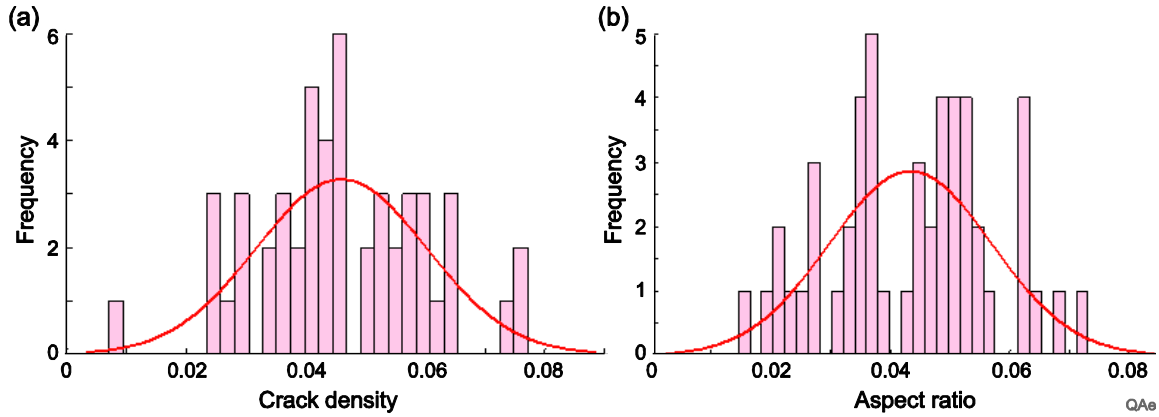

Figure 3.3: Histograms and distributions of crack density (a) and crack aspect ratio (b) assumed for rock physics modeling. These distributions depict realistic variability in crack densities and crack aspect ratios for the upper Arbuckle layer and are in agreement with observations made on core and thin sections.

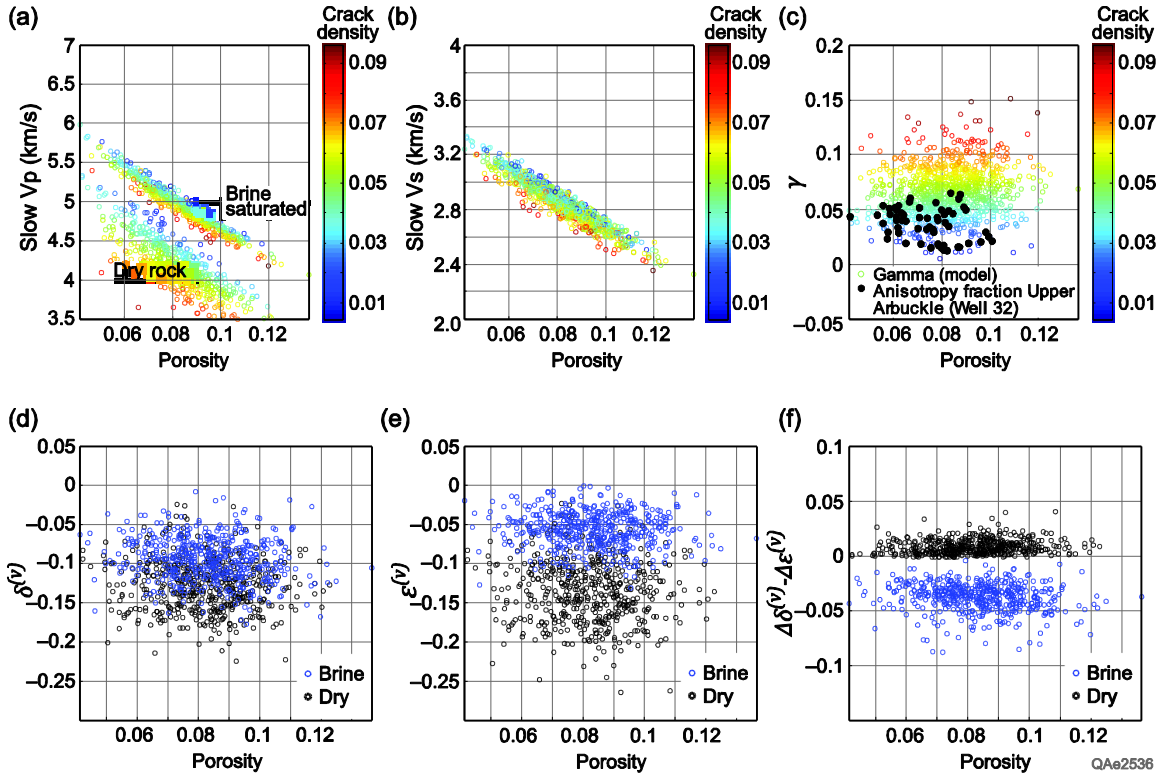

Figure 3.4: Porosity dependence of elastic parameters color coded with crack density (a, b and c) and fracture fill (d, e and f). Both P- and S-wave velocities show some degree of change with changing crack density. This change is probably not enough to deduce fracture density information from these velocities. However, modeled γ, which is the relative difference in fast- and slow- S-wave velocities, is directly correlated to crack density. Figures d, e and f show how anisotropic parameters are affected by change in fracture-fluid. $\delta^{(v)}$ is relatively insensitive to fluid-fill in fractures. $\varepsilon^{(v)}$ on the other hand, shows some shift due to change in fluid-fill. $\Delta\varepsilon^{(v)} - \Delta\delta^{(v)}$ is very sensitive to the fluid-fill, showing good separation between dry (black) and brine (blue) filled fractures.

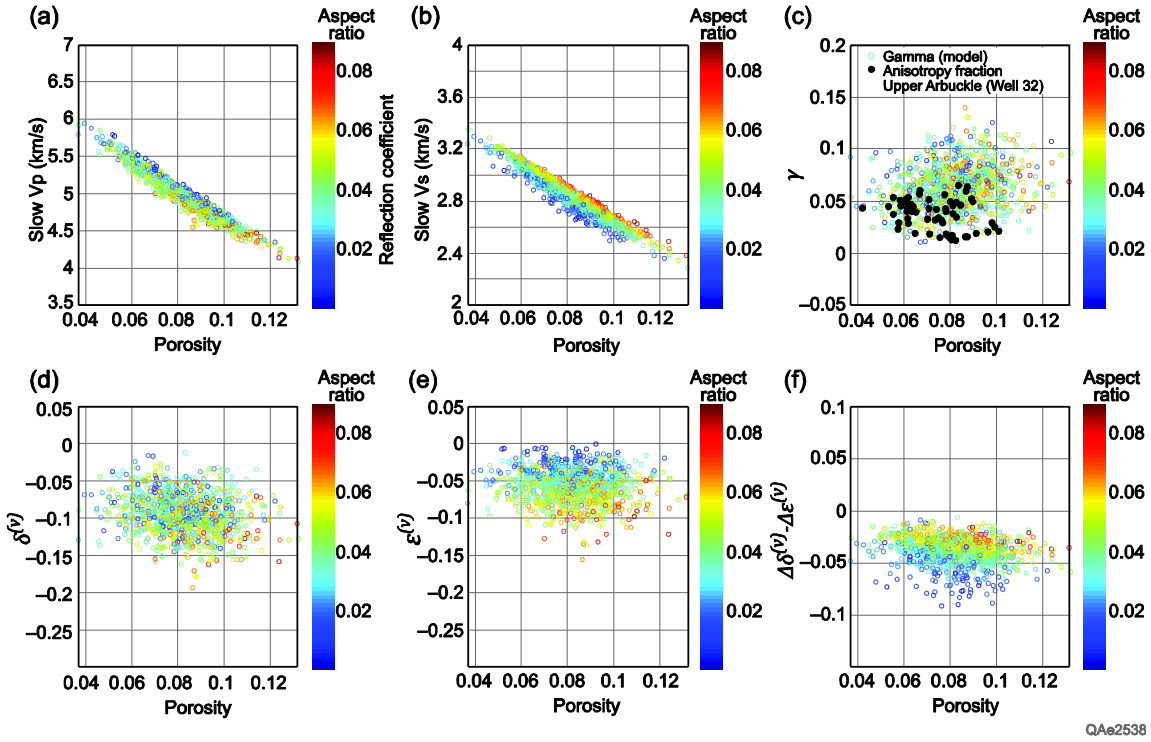

Figure 3.5: Porosity dependence of elastic parameters color coded with aspect ratio for brine-saturated rock. Note that $\varepsilon^{(v)}$ (e) and $\Delta\varepsilon^{(v)} - \Delta\delta^{(v)}$ (f) show a small systematic decrease with increasing aspect ratio. However, that systematic variation still lies below the uncertainty threshold, making prediction of aspect-ratio extremely difficult from seismic amplitude measurements alone.

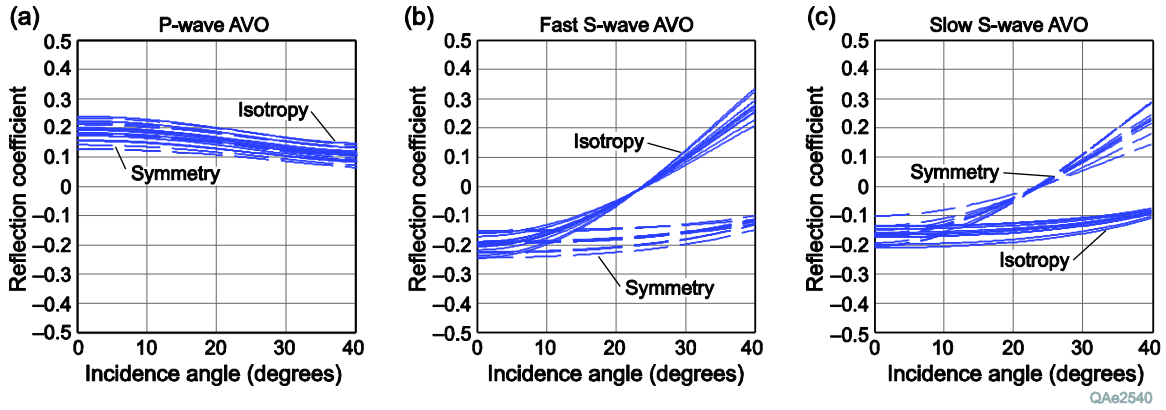

Figure 3.6: Reflectivity vs. incident-angle plot for brine-saturated rock in isotropy (solid) and symmetry (dashed) planes for P-waves (a), fast S-wave (b), and slow S-wave (c). For P-waves, reflectivities parallel and perpendicular to fractures show significant overlap. Fast S-waves have two different gradients corresponding to polarization in isotropy plane (SV) and the symmetry plane (SH). Similarly, slow S-waves have gradients corresponding to polarization in the isotropy plane (SH) and the symmetry plane (SV). A difference between the AVO intercepts of fast- and slow- S-waves, and AVO gradients of fast- and slow- SV waves caused by presence of fractures can be seen, underscoring the value of S-waves in fracture identification.

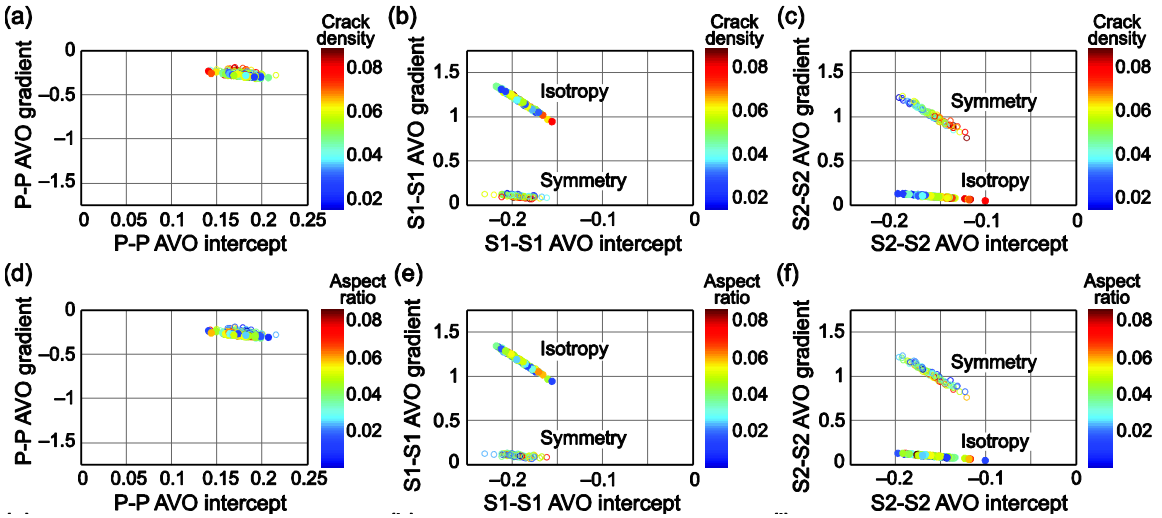

Figure 3.7: AVO intercept-gradient cross plot for brine-saturated rock in isotropy (filled circles) and symmetry (open circles) planes for P-waves (a and d), fast S-wave (b and e), and slow S-wave (c and f). Figures a, b and c are color coded with crack-density parameter, and figures d, e and f are color-coded with crack-aspect ratio parameter. Two clusters with different gradients are observed for fast S-waves, which correspond to polarization in the isotropy plane (SV) and the symmetry plane (SH). Similarly, slow S-waves show clusters corresponding to polarization in the isotropy plane (SH) and the symmetry plane (SV). A systematic change is seen on slow S-wave AVO intercepts and gradient with changing crack density, underscoring the value of S-waves in fracture identification.

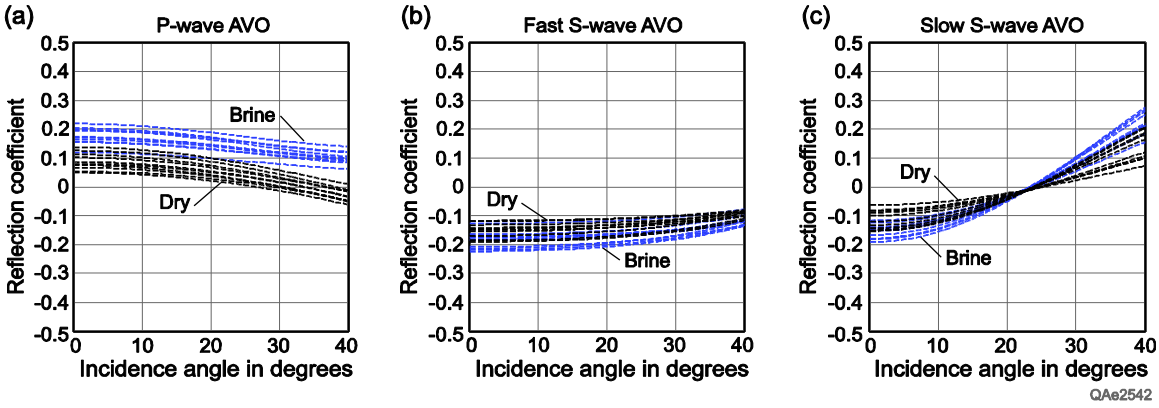

Figure 3.8: Reflectivity vs. incident-angle plot in symmetry planes for dry (black) and brine (blue) saturated rock. A difference in P-wave reflectivity can be seen for different fluid-fill (a). A small change in slow S-wave AVO gradient is also observed for different fluid-fills (c). It was observed that change in P-wave reflectivity was primarily caused by change of fluid in the pores whereas; slow S-wave reflectivity was affected by change of fluid in the fractures.

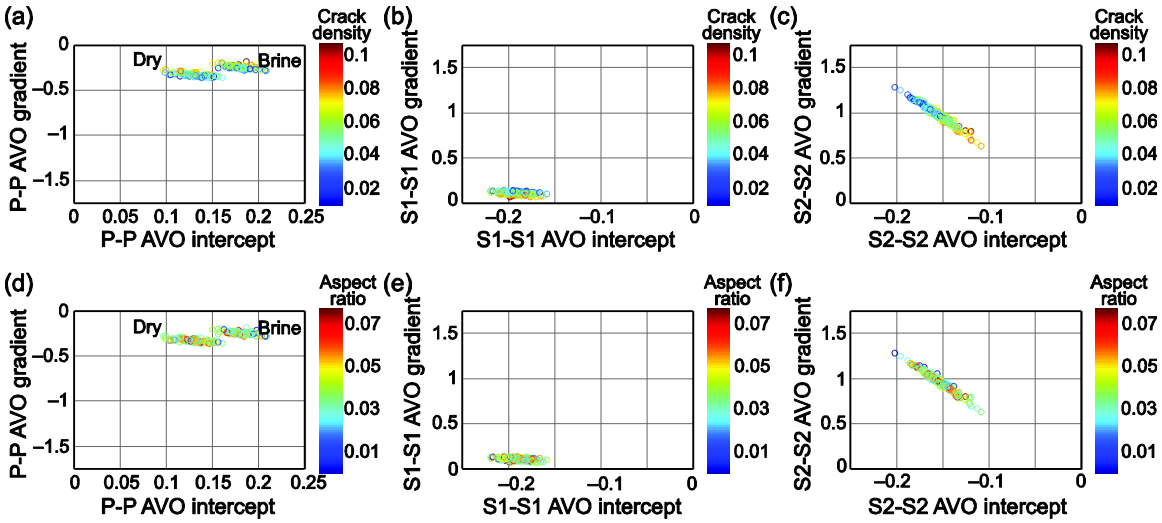

Figure 3.9: AVO intercept-gradient cross plots for P-wave (a and d), fast S-wave (b and e) and slow S-wave (c and f) in symmetry planes for dry and brine saturated rock. Figures a, b and c are color coded with crack-density parameter, and figures d, e and f are color-coded with crack-aspect ratio parameter. A difference in P-wave AVO intercept distribution can be seen for different fluid-fill (a and d). Systematic changes in slow S-wave AVO intercept and gradient are observed with changing crack density (c). However, change in S-wave AVO intercepts and gradient due to change in fluid is not apparent. Advanced attribute extraction might be necessary to observe fluid change in S-wave attributes

Chapter 4: Characterization of Naturally Fractured Arbuckle Group in Wellington Field, Kansas, Using S-wave Amplitude Variation with Offset[3]

4.1 ABSTRACT

Shear-wave amplitude variation with offset (AVO) analysis is sensitive to the presence of fractures and can provide a high-resolution seismic-based fracture characterization as compared to traditional seismic travel-time-based methods. To determine viable attributes for estimation of properties such as spatial density and fluid fill of fractures, shear-wave AVO modeling and analysis are carried out in Wellington Field, Kansas, where 9C-2D seismic data have been acquired. Analysis is performed on the Ordovician fractured-carbonate interval called the Arbuckle Group, which is being considered for CO_2 sequestration. AVO modeling of the Arbuckle interval shows that differences in AVO intercepts of different shear-wave polarizations provide an estimate of S-wave anisotropy parameter γ, which gives an estimate of fracture density. Additionally, modeling suggests that AVO gradients of SV and SH waves can be used to derive a seismic attribute to discriminate fluid fill in fractures, provided good quality shear-wave gathers are available. The Intercept Anisotropy (IA) attribute obtained from AVO intercepts of shear waves provides fracture-density estimates within the Arbuckle Group. These estimates are consistent with field-wide, low-frequency observations from

[3] This chapter was previously published in Gupta, M., K., Spikes, and B., Hardage, 2017. Characterization of naturally fractured Arbuckle Group in the Wellington Field, Kansas, using S-wave amplitude variation with offset. Interpretation, 5(1), pp. T49-T63. M. Gupta conceptualized and performed the research with assistance from K. Spikes. M. Gupta wrote the manuscript. K. Spikes and B. Hardage contributed in discussions and revisions.

seismic velocities, and from spatially limited, high-frequency estimates obtained from drill cores, sonic and borehole-image logs. The IA attribute highlights possible High Permeability Zones (HPZs) in the Upper and Lower Arbuckle suitable for CO_2 injection. The Middle Arbuckle shows low fracture density, potentially acting as a baffle to vertical flow and providing a seal for the lower Arbuckle. The Gradient Anisotropy (GA) attribute obtained from the AVO gradient of shear waves suggests that most fractures in the Arbuckle are brine saturated. This attribute has a potential application in monitoring the movement of a CO_2 plume in the Arbuckle Group when time-lapse seismic data become available. These results demonstrate that shear-wave AVO attributes can supplement P-wave derived subsurface properties and significantly reduce uncertainties in subsurface fracture characterization.

4.2 INTRODUCTION

Fracture characterization is a study of natural fractures to understand their properties and distribution in the subsurface. Natural fractures have variable characteristics. They can be open or cemented, connected or sparse, and can have a wide range of lengths and apertures. Open and connected fractures that are often associated with large apertures and long lengths, can significantly increase the in-situ permeability of reservoirs (Gale et al., 2010; Laubach, 2003; Devault et. al, 2002) as well as change their elastic properties. Such open fractures and type of fluid fill in those fractures can considerably alter seismic properties of a rock mass. When aligned, these fractures introduce measurable seismic anisotropy. Hence, understanding seismic anisotropy using seismic waves can be a useful tool in describing orientation, spatial density, and fluid fill of fractures.

To understand fracture-induced seismic anisotropy, use of direct S-waves predates use of P-waves because S-waves are more sensitive to anisotropy and show birefringence. However, when using surface seismic data for subsurface fracture analysis, geophysicists have mostly resorted to P-waves. One of the reasons for choosing P-waves over S-waves has been high cost associated with acquisition of shear-wave surface seismic data. P-waves do provide some information about fracture properties like orientation and spatial density, but these estimates can have a high degree of uncertainty associated with them and often require wide azimuth P-wave seismic data acquisition (Corrigan et al., 1996; Liu and Martinez, 2013; Lynn, 2007; Mallick et al., 1996; Ruger, 2001; Jenner, 2001; and Roche et al., 2005). Moreover, some properties like fluid fill and aperture of the fractures are challenging to determine from P-wave data due to theoretical restrictions and non-uniqueness in determining these parameters (Sava and Mavko, 2004, Shen et al., 2002). Direct S-wave modes on the other hand have proven to be very effective in detecting azimuthal anisotropy (Martin and Davis, 1987; Mueller, 1991; DeVault et al., 2002; Lynn and Thomsen, 1990; and Li, 1997). Technological advances in extracting direct S-waves generated from P-wave sources have posed a unique opportunity to obtain shear wave surface seismic data at more affordable costs than ever before (Gaiser and Verm, 2012; and Hardage and Wagner, 2014a, b). This latter development requires that we revisit S-wave surface seismic analysis methods that can be used for subsurface fracture characterization.

Relatively few studies demonstrate the use of surface-seismic measurements of S-waves to understand fracture properties. These studies can be roughly divided into two categories, shear-wave travel-time or splitting analysis and shear-wave amplitude analysis. Studies concerned with shear wave splitting analysis (Alford, 1986; Lynn et al., 1995; Li, 1997; Grossman et al., 2013) provide reliable low-frequency estimates of

subsurface seismic anisotropy but fail to give reservoir-scale descriptions of fracture-induced anisotropy. The few studies that focus on amplitude analysis (Mueller, 1991; Lynn et al., 1995; Kendall and Kendall, 1996) deal with post-stack amplitudes and provide a proxy to qualitatively estimate fracture density, a term commonly defined as number of fractures per unit volume. So far, these approaches are incapable of giving any insight into other fracture properties like fluid fill. Studies concerning pre-stack amplitude analysis for fracture characterization are even rarer for direct S-waves. Using pre-stack methods like AVO can be useful in delineating thin fractured reservoirs and can provide reservoir-scale geological information with higher vertical resolution than travel-time methods (Tsvankin et al., 2010). AVO methods have already proven useful for delineating anisotropy in P-wave and mode converted S-wave seismic data (Shen et. al, 2002; Perez et. al, 1999; Liu and Martinez, 2013; Lynn et. al, 1995) and can provide more quantitative information about fractures if applied to direct S-wave modes produced by P- or S-wave sources as well.

Under-utilization of direct S-wave AVO methods can also be attributed to limited understanding of S-S AVO attributes and their quantitative dependence on fracture properties. There is a mutual consensus in the geophysical community that S-wave AVO is sensitive to fractures, and that information about fracture density and fracture orientation can be obtained from seismic amplitudes at normal incidence in different azimuthal directions (Yardley et al., 1991, Hall and Kendall, 2000; Rusmanugroho and McMechan, 2010; Lynn and Thomsen, 1990; and Li, 1997). However, several arguable conclusions have been made about fracture properties other than fracture density and orientation. Yardley et al. (1991) concluded that information about crack fill is limited to near-critical angles of reflection, which restricts usage of S-wave AVO for crack content to cross well monitoring applications only. Hall and Kendall (2000) concluded that when

using S-wave AVO, no significant insight could be gained into fluid fill in fractures. Ruger (2001) argued and suggested that changes in S-wave AVO can provide information about crack density as well as crack fill. DeVault et al. (2002) used the theoretical framework developed by Ruger (2001) and derived crack density from S-wave AVO data and showed a correlation between crack density and field production behavior. Their work indicated a strong link between crack density and reservoir-scale permeability. However, there is not sufficient insight into which S-wave seismic attributes identify fluid fill in fractures. Other studies concerning S-wave AVO (Rusmanugroho and McMechan, 2010) do not comment on where in the offset–azimuth space fracture-property information is located and what seismic attributes would best describe them. In this study, I aim to address these gaps by deriving S-wave seismic attributes that can be used to understand fracture density and fluid fill in fractures. I demonstrate their applicability on a 2D multi-component seismic dataset acquired across Wellington Field, Kansas.

I use the rock physics model developed in Chapter 3 for Ordovician carbonates called the Arbuckle Group that are encountered in wells drilled in Wellington Field. This rock physics model is used to estimate elastic properties of the Arbuckle Group and to predict AVO behaviors of SV and SH waves in directions parallel and perpendicular to fractures present in the Arbuckle. Results show that fracture-density information lies in seismic amplitudes at near-normal angles of incidence of SV and SH waves; hence, difference in AVO intercepts of SV and SH waves can be used to estimate fracture density. This study also suggests that AVO gradients of SV and SH waves extracted from surface seismic data might be used to derive a seismic attribute that will discriminate fluid fill in fractures, subject to availability of good quality pre-stack data. A fracture-density attribute named Intercept Anisotropy (IA) is extracted from the 2D shear wave

seismic data available at Wellington Field. This attribute highlights possible High Permeability Zones (HPZs) and baffle zones within the Arbuckle Group, which is being considered for CO_2 storage. A fracture-fill attribute named Gradient Anisotropy (GA) is also extracted. This attribute attempts to provide further insight into the fluid that fills Arbuckle fractures. Results of this study show that adopting a pre-stack approach using S-waves can provide high-resolution fracture characterization compared to traditional travel-time based methods.

4.3 Study Area and Data Set

Wellington Field is a sub-crop play involving Mississippian cherty, dolomitic reservoirs preserved in structural blocks bounded by NE and NW trending lineaments in Sumner County, Kansas (Figure 4.1). These lineaments have been widely identified on 3D seismic studies (Ohl and Raef, 2014) and Landsat images and are understood to be the extensions of Precambrian structures associated with the Nemaha Uplift (Merriam, 1963; Baars and Watney, 1991), which plays a crucial role in accumulating hydrocarbons throughout Kansas. The stratigraphic units that are of immediate interest to this study are the Lower Ordovician carbonates that are collectively called the Arbuckle Group. Arbuckle Group rocks are part of the North America craton-wide Sauk Sequence that consists of hundreds of meters of largely dolomitized inter-tidal to shallow sub-tidal cyclic carbonates overlain by a regional unconformity (Wilson et al., 1991). Franseen et al. (2003) described the Arbuckle Group as having three end-member reservoir types: a) reservoirs with abundant fractures in which litho-facies control porosity and fractures control overall permeability, b) reservoirs with karst overprinting on litho-facies and fractures, resulting in complex porosity and permeability, and c) reservoirs where litho-

facies control porosity and permeability. The lower Arbuckle is believed to be heavily dolomitized and fractured and is being considered for CO_2 storage (Watney and Rush, 2012). Most natural fractures in the Lower Arbuckle are either associated with karst (Franseen et al., 2003) or with reactivation of the Precambrian basement structures (Merriam, 1963; Baars and Watney, 1991). Fracture orientations interpreted from the micro-resistivity image logs acquired on wells, show widespread azimuths (Watney and Rush, 2012). However, dipole sonic measurements made in Wellington Field show 85°E orientation of fast S-wave polarization with an uncertainty of ±5%. This unimodal distribution might be linked to preferential closure of fractures in response to anisotropic subsurface stress. The orientation of maximum horizontal stress has been interpreted to be approximately 75°E using data from drilling induced fractures (Watney and Rush, 2012). Understanding fracture characteristics and their role in facilitating fluid flow is essential for optimal reservoir management in the Wellington Field.

4.3.1 Seismic data

To better understand the role of fractures and heterogeneities in the CO_2 injection interval and overlying sealing formations, a 9C-2D seismic survey was acquired across Wellington Field. This survey consisted of two 2D seismic lines, 7 miles (11 km) in length, with 9-component seismic data collected using 3-component geophones and vertical and horizontal vibrators. Line-1 and Line-2 were orientated at 55°E and 135°E, respectively (Figure 4.2). 2D stacking fold for both S and P-wave data is about 55, and total trace length of the data is 3 s for P-wave data and 4 s for S-wave data. Horizontal vibrators, which were the primary sources for S-waves, made six linear sweeps of 20 s with frequency ranging from 4 Hz to 50 Hz to make maximum utilization of the lower

end of the frequency spectrum. Vertical vibrators on the other hand, made two non-linear sweeps of 40 s ranging from frequencies 6 Hz to 150 Hz with a taper of 3 db/octave.

The 2D multicomponent seismic data were processed at a commercial data-processing shop where they were segregated into various wave modes including direct P (P-P) and direct S (S-S), converted P (SV-P) and converted S (P- SV). The SV-P wave data generated by the vertical vibrator sources were also processed. Theory describing the extraction of these wave modes has been widely discussed in Hardage et al. (2011) and Hardage and Wagner (2014 a, b). For work presented in this paper, only direct S-wave modes have been used. Radial and transverse S-wave data were rotated to the best known estimates of fast (90^{o}E) and slow (0^{o}) directions obtained from velocity analysis and dipole sonic measurements in the calibration wells. These fast and slow S-S wave modes were used in the AVO analysis. Some additional pre-stack seismic processing steps were applied to data to prepare trace gather for AVO analysis. These steps are discussed later in this paper.

4.3.2 Well data

In order to do a small-scale field test demonstrating CO_2 sequestration and EOR in the Arbuckle and Mississippian strata, extensive well data were collected by the Kansas Geological Survey (KGS) in Wellington Field. Two of the wells, KGS 1-28 and KGS 1-32 are located directly on the 9C-2D seismic survey lines and present an opportunity to calibrate our subsurface interpretations from seismic measurements. Well 1-28 lies on the intersection of line-1 and line-2 and well 1-32 lies on line-1 about 893 m SW of well 1-28. Both wells have a full suite of well logs including spectral gamma ray, neutron density, resistivity, cross-dipole sonic, Nuclear Magnetic Resonance (NMR) and micro-resistivity imaging. Some of the logs used in this study for rock physics modeling

and comparing results are shown in Figure 4.3. In addition to well logs, approximately 490 m of core were acquired in these wells to sample both Mississippian and Arbuckle reservoir rocks as well as their cap rocks. Multiple thin sections and photomicrographs have been prepared from the acquired core to understand textural details of rocks and pore-scale variability. Greater abundance of fractures and vugs in the Arbuckle Group has been reported at all scales based on dipole sonic logs and borehole micro-resistivity image logs and T2 relaxation times observed on NMR logs. These vugs and fractures have been found to govern overall permeability in the Lower Arbuckle (Gupta et al., 2014 and 2015; Ohl and Raef, 2014; Watney and Rush, 2012; Franseen et al., 2003; and Byrnes et al., 1999). Permeability estimates obtained from measurements on core plugs provided Kmax values up to 425 mD in the Lower Arbuckle. A step-rate test was also performed between well 1-32 (source well) and 1-28 (observation well), that are 3000 ft apart, in a 20 ft perforated zone in the Lower Arbuckle. Permeability of approximately 1 Darcy was estimated from the step-rate test. Geological data collected from these wells supports the idea that fractures control overall permeability in the lower Arbuckle. This suggests that identifying lateral distribution of open fractures in the Lower Arbuckle might help identify zones of higher permeability.

4.4 METHODS

I wish to study how fractures affect elastic properties of a rock, and which S-wave Amplitude Variation with Offset (AVO) attributes can be used to understand fracture density and fluid fill in fractures in a subsurface carbonate formation. To study these topics, I created a rock physics model using the information from well logs and cores acquired in well 1-28 and 1-32. This rock physics model effectively estimates fast and

slow P-wave and S-wave seismic velocities, and Thomsen-style anisotropic parameters. These elastic parameters are further used to predict AVO behaviors of SV and SH waves in directions parallel and perpendicular to fractures and to derive seismic based attributes for fracture density and fluid fill in fractures.

4.4.1 Rock physics modeling

Previous studies done on the Arbuckle (Watney and Rush, 2012; Franseen et al., 2003; Bliefnick, 1992; and Byrnes et al., 1999) show that this interval consists of complex stacks of reservoir and non-reservoir lithologies at various scales, which makes the Arbuckle highly heterogeneous. In Kansas, the Arbuckle has been demonstrated to have reservoir architectures representing fracture-, karst-, and matrix-dominated architectural systems. In some areas of Wellington Field, the Arbuckle is dominated by fractures, possibly related to karst or basement faults in structurally complex areas. Lithofacies control porosity and permeability within individual layers (beds), but fractures dominate overall permeability. Rock physics modeling of the Arbuckle attempts to account for mineralogical and textural variations observed in well log and core data, due to dolomitization and anisotropic subsurface stresses. Correct depiction of these facture-dominated architectural systems is the key goal of rock physics modeling.

In the first stage of rock physics modeling, I model an isotropic carbonate background that closely resembles the Arbuckle in terms of mineralogy, porosity distribution, and pore-shapes (Chapter 3; Gupta et al., 2014). Several thin sections and photomicrographs made from core samples in wells 1-28 and 1-32 are used to depict mineralogical and textural details. Model construction is done using the isotropic Differential Effective Medium (DEM) model (Norris, 1985). The DEM model predicts the elastic constants of an effective medium obtained by introducing inclusions

representing porosity into an isotropic and homogeneous background (Norris, 1985 and Berryman, 1992). This model assumes that the inclusions are dry ellipsoidal pores that are randomly oriented in an isotropic and homogeneous dolomitized carbonate background. The elastic constants obtained from the DEM model act as the input for the second stage of rock physics modeling, where a single set of aligned fractures are introduced into the isotropic and homogeneous carbonate background. This construction is done using both Hudson's (1981) penny-shaped crack model and the linear-slip model to address any biases in the results caused by a particular approach.

4.4.2 S-wave AVO attributes for fracture characterization

Angle-dependent reflectivity modeling of the S-S seismic mode is critical for understanding which rock or fracture properties govern direct S-wave seismic-amplitude responses. In this effort, AVO behavior of SV-SV and SH-SH wave modes were analyzed in both the isotropy plane (plane parallel to fractures) and the symmetry plane (plane orthogonal to fractures) in Chapter 3. In the symmetry plane, the SV wave can also be called the slow S-wave because its polarization direction is orthogonal to the fractures. Similarly, the SH wave in the symmetry plane also acts as the fast S-wave. Mathematical formulations proposed by Ruger (2001) for HTI media were used to model these wave modes. One thousand Monte-Carlo simulations were completed to model AVO responses for both SV and SH waves for varying input rock and fracture parameters. AVO intercept and gradient attributes for both reflectivity modes were calculated to understand their dependencies on different rock and fracture properties. Attributes sensitive to fracture density and fluid fill are derived in Appendix A (Section 4.8), from the AVO intercept and gradient responses of SV and SH waves and were interpreted based on information obtained from well logs.

In order to extract AVO attributes depicting fracture density and fluid fill from S-S seismic data acquired in Wellington Field, additional pre-stack gather conditioning steps were performed after routine S-wave seismic processing. Some of these steps were constructing super-gathers, band pass filtering, multiple attenuation, random noise attenuation, trim statics correction, and converting offset gathers to angle gathers using the S-wave velocity model. These steps ensured seismic amplitude fidelity and optimal S/N for AVO attribute extractions. After gather conditioning, well-to-seismic ties were performed. Gupta et al. (2015) show an 82% correlation between the synthetic and composite trace of the S-S wave mode at well 1-32. Geological horizons corresponding to top of Oread, Kansas City, Mississippian and Precambrian were interpreted on the fast and slow S-S seismic data to create a robust structural framework for subsurface characterization. AVO analysis was then performed for both S-wave modes at the 1-32 well location and results were compared to the AVO model generated at the well. After an acceptable match was obtained, AVO analysis was done for Line-1. S-wave AVO intercept and gradient sections were created for both fast and slow seismic wave modes. These intercept and gradient sections were registered in time using local seismic attributes (Fomel, 2007) to remove any time-shifts caused by anisotropy and were used to calculate the fracture-density and fracture-fill attributes as derived during the AVO modeling stage. These fracture attributes were interpreted for the Arbuckle Group to understand the lateral variation of fractures and their interconnectivity to assess the CO_2 injection potential of the Arbuckle.

4.5 RESULTS

4.5.1 Rock physics and AVO modeling of the Arbuckle Group

The rock physics model estimates the elastic properties for the Arbuckle Group using mineralogy, porosity, and pore fluids as inputs from well logs and side-wall cores. Calcite and dolomite were the primary minerals identified in the Arbuckle Group. An average porosity ranging from 5-8 percent was observed from routine core analysis performed on side-wall cores. Well log data also suggested that the Arbuckle in Wellington Field is fractured and saturated with brine. A range of crack-density (mean=0.05, standard deviation=0.015) and pore aspect ratios (mean=0.04, standard deviation=0.015) were used in the rock physics model to account for subsurface uncertainty. Figures 4.4a and 4.4b show fast and slow P-wave velocities, respectively, predicted from the rock physics model for dry (black) and brine (blue) saturated Upper Arbuckle. Scatter in these cross plots depicts uncertainty in prediction of elastic constants due to variability in model inputs, including mineralogy, porosity, pore shapes, and crack density. Also, note there is more data scatter in dry P-wave velocities, and scatter decreases as the rock is saturated with brine. This effect implies that the cracks become stiffer due to the presence of fluid, thereby reducing crack sensitivity to velocity. The modeled fast P-wave seismic velocity is calibrated against the P-wave velocity measurements made in the well logs for the brine-saturated Upper Arbuckle. Figures 4.4c and 4.4d show fast and slow S-wave velocities, respectively, predicted from the rock physics model for dry and brine saturated rock. As expected, little difference exists between dry and wet rock shear velocities. The green data points are S-wave velocity (Vs) measurements in the borehole for brine-saturated Upper Arbuckle in orthogonal directions, which were later rotated to the fast and slow directions. Modeled fast and slow S-wave velocities are in general agreement with borehole measurements. Some scatter

observed in the fast Vs measured in the well could be caused by variability in lithology with depth or inaccurate velocity measurements.

In addition to seismic velocities, the rock physics model also provides estimates of anisotropic parameters ε, δ and γ described by Thomsen (1986). Figure 4.5 shows the porosity-dependent Thomsen-style parameters (γ and $\Delta\delta^{(v)} - \Delta\varepsilon^{(v)}$) defined with respect to vertical direction in a HTI medium. These parameters are the direct input into the P- and S-wave AVO equations. Understanding their behavior with changing rock and fracture properties is important for quantitative fracture characterization. Figure 4.5a shows the variation of γ with total porosity and crack density parameter. Here, γ shows a direct relationship with the crack density, i.e., a higher value of γ corresponds to higher crack density and vice versa. Filled black circles shown on the γ plot are S-wave velocity anisotropy data from borehole measurements in the Upper Arbuckle and are in agreement with rock physics model predictions. I notice that $\delta^{(v)}$ is relatively insensitive to fluid fill in fractures in the Arbuckle, but $\varepsilon^{(v)}$ is higher for brine-saturated compared to dry rock. Similar dependence of $\varepsilon^{(v)}$ on fluid fill has also been discussed in Sava et al. (2001). The behavior of ($\Delta\delta^{(v)} - \Delta\varepsilon^{(v)}$) in Figure 4.5b shows a clear separation between two fracture fills, implying its application as a proxy for identifying fluid fill in fractures, which has also been suggested by Bakulin et al. (2000). However, in order to extract lateral variation in fracture density and fluid fill with more certainty, I require attributes that are sensitive to identified parameters like γ and $\Delta\delta^{(v)} - \Delta\varepsilon^{(v)}$, and which can be extracted from seismic data.

To understand the dependence of direct S-wave seismic amplitudes on different rock and fracture properties, AVO responses of both SV and SH waves were estimated in isotropy and symmetry planes. I observed a noticeable difference in AVO intercept and gradients between SV and SH waves in both principal directions. Figure 4.6a shows a

cross plot between modeled SV-SV and SH-SH AVO intercepts in the symmetry plane, color coded by the crack density parameter. Data points deviate away from the line $y=x$, as the crack density parameter increases in value. This behavior implies that in the presence of aligned fractures, the AVO intercepts of SV and SH waves would be different, and the difference between their AVO intercepts will be proportional to the fracture density. Qualitatively, amplitudes of SV and SH waves for near-normal incidence angles can be used to differentiate between zones of high and low intensity of fracturing. Figure 4.6b shows the cross plot between my simulated SV wave AVO gradient and the SH wave AVO gradient (after multiplying by 7) for dry fractures and brine- and CO_2 -filled fractures. The change in the observed gradient in the cross plot is a direct consequence of the dependence of the $\Delta\delta^{(v)} - \Delta\varepsilon^{(v)}$ parameter on fluid fill. The scatter in each of the fluid-fill groups represents the variability in Vp/Vs of fast seismic velocities and Thomsen style parameters $\Delta\delta^{(v)}$ and $\Delta\varepsilon^{(v)}$ that arises due to uncertainty in model input parameters. This figure shows that even with reasonable amounts of uncertainty in crack density and crack shapes, it might be possible to see fluid signals in the direct S-wave AVO gradients.

Using the information obtained from Figure 4.6, I devised Intercept Anisotropy (IA) and Gradient Anisotropy (GA) attributes to depict fracture density and fluid fill in fractures, respectively (Appendix A). Figure 4.7 shows the IA-GA crossplots for different fluid-fill types color-coded with crack density parameter (7a) and fluid type (7b). Figure 4.7a shows that irrespective of the fluid fill, the IA attribute can be used to understand variations in fracture density. Similarly, Figure 4.7b shows distinct separation in clusters of different fluid fill, underscoring the viability of the GA attribute for fracture-fluid discrimination.

4.5.2 Fracture characterization of Arbuckle Group in Wellington Field

To test the efficacy of the IA and GA attributes on the Wellington seismic dataset, a thorough post-stack and pre-stack seismic interpretation routine was followed. Five geological horizons were identified and interpreted on both the fast and slow S-wave seismic data. These horizons are the Top Oread, Top Kansas City, Top Mississippian, Top Arbuckle, and Top Precambrian. S-wave AVO attributes were calculated for both fast and slow seismic-wave modes. Figure 4.8 shows fast and slow S-wave AVO intercepts for Line-1 in Wellington Field. The northeast quarter section of Line-1 in these figures show low discontinuous amplitudes at all image times. This poor image in AVO intercept is consistent with what was observed during data processing and was attributed to S-wave statics-related issues. The AVO intercept section of the slow S-S wave mode (Figure 4.8a) generally shows laterally discontinuous amplitudes over the entire section as compared to the fast S-S wave mode (Figure 4.8b). In areas above the Top Oread horizon and within the Arbuckle, major differences in AVO intercepts can be seen, which as suggested by the AVO modeling (Figure 4.6a), might indicate seismic anisotropy related to the presence of fractures. Figure 4.9a shows the IA attribute calculated using the difference in the S-S AVO intercepts shown in Figure 4.8. High values of IA in Figure 4.9a are observed near well 1-32, above the Oread horizon and sporadically within the Arbuckle. Figure 4.9b shows the S-wave velocity anisotropy calculated from the difference in the fast and slow S-wave interval velocities. These velocities were obtained from the stacking velocities of respective S-S wave modes using Dix conversion, and applying lateral and vertical smoothing to remove any velocity picking artifacts. Anisotropy observed from the S-wave processing velocities (Figure 4.9b) has a lower vertical resolution, but is consistent with the anisotropy picture obtained from S-wave AVO intercepts (Figure 4.9a). Independent anisotropy measurements obtained from S-

wave amplitudes complements the anisotropy estimates obtained from stacking velocities, and provides a higher resolution characterization of subsurface fractures.

Figure 4.10 shows the cross plot of fast and slow S-S AVO intercepts on Line 1, color coded with IA. Data points on or near the $y=x$ line as shown in Figure 4.10 correspond to intervals with low values of seismic anisotropy and hence indicate low fracture density. Data points that depart away from the line $y=x$ come from areas where seismic anisotropy is relatively high, indicating high fracture density as modeled in Figure 4.6a. The data points indicating high fracture densities also have high values of IA. Figure 4.11 shows the S-S IA attribute depicting lateral and depth variation in fracture densities in the Arbuckle Group. The high fracture-induced seismic anisotropy in the Arbuckle Group is consistent with the low-frequency anisotropy measurements made using the seismic velocities in Figure 4.9b and also with high-frequency seismic anisotropy measurements made using cross dipole sonic logs and borehole image logs in well 1-32.

Figure 4.12 shows S-wave AVO gradients for Line-1 in Wellington Field. The AVO gradient section of the slow S-S wave mode (Figure 4.12a) generally shows low and laterally discontinuous amplitudes all over the section compared to the fast S-S wave mode (Figure 4.12b). This difference is exemplified in the regions of high-fracture density in the Arbuckle. Modeling suggests that the difference in AVO gradients of the fast and slow S-waves on Line-1 are due to two factors. First, the fast S-wave also happens to be dominated by SV wave motion, which has a higher AVO gradient than the SH wave motion. Second, SV waves propagating in a direction oblique to fractures tend to be more sensitive to fluid fill compared to the corresponding SH waves. To decouple these effects and extract the effects of fluid fill, the GA attribute was derived. This result was achieved by calculating a weighted difference in the fast and slow AVO gradients

and retaining the fluid-sensitive term dominated by density reflectivity, velocity ratio, and $\Delta\delta^{(v)} - \Delta\varepsilon^{(v)}$ as explained in Appendix A.

For applications on a 3D seismic dataset where data are available in all azimuths, the GA can be calculated in the direction perpendicular to the local fracture orientation (symmetry plane). However, for the Wellington 2D seismic dataset, azimuths were restricted to the strike of the 2D lines. Figure 4.13 shows the GA attribute calculated for Line-1. The higher magnitudes of the GA that coincide with high IA values might indicate the presence of a stiffer fluid, which in most cases is brine. In the Arbuckle, most of the GA anomalies coincide with IA anomalies indicating that fluid fill in high fracture zones is brine. Because injection of CO_2 in the Arbuckle injection zones had not started at the time these data were acquired, it is not possible to see signatures of CO_2 in place. The Mississippian interval, which is a depleted oil reservoir, shows lower values of GA the near well 1-32 consistent with the what modeling suggests (Figure 4.7b).

4.6 DISCUSSION

Results from AVO modeling and analysis suggest that the IA attribute, which is the difference between AVO intercepts of different polarizations of S-wave, is directly linked to the crack density parameter (Figure 4.6). This implies that the IA attribute can act as a proxy to estimate relative changes in fracture density from surface seismic measurements. IA attributes extracted on Line 1 show high seismic anisotropy in areas close to well 1-32, which is consistent with seismic anisotropy estimates obtained from processing S-wave velocities. This anisotropy is probably caused by swarms of aligned fractures that formed in response to reactivation of regional faults. The presence of such faults within Mississippian and Arbuckle strata has also been reported by other scientists

working in this area (Baars and Watney, 1991; Ohl and Raef, 2014; Franseen et al., 2003). Within the Arbuckle Group, IA also helps delineate mechanical stratification linked with variations in seismic anisotropy and possibly areas of high fracture density in the Upper and Lower Arbuckle. Zones of high IA anomalies at well 1-32 coincide with high anisotropy observed on dipole sonic logs, validating my results. These zones also show poor core recovery attributed to abundant fractures in recovered core, as described in reports produced by the Kansas Geological Survey (Watney and Rush, 2012).

Fracture density could be used as a proxy for reservoir permeability, given the fractures are open and connected. In the Lower Arbuckle, T2 relaxation time measurements obtained from NMR logs indicate presence of abundant open fractures and large vugs. This conclusion is further supported by multiple permeability measurements varying from 100's of mD up to 1 Darcy made at scales ranging from few centimeters (using core plugs) to 100's of meters (using step-rate tests between wells) in these otherwise tight carbonate rocks. These observations suggest that high fracture density intervals in the Lower Arbuckle have a greater likelihood to act as High Permeability Zones (HPZ). This logic implies that intervals of high fracture density identified from IA attributes can act as potential targets for CO_2 injection. IA analysis also shows that these HPZs are often capped by intervals of low fracture density interpreted in the Middle Arbuckle. Other studies (Gupta et al., 2015; Watney and Rush, 2012) performed on Middle Arbuckle strata show high P-impedance and Vp/Vs suggesting the presence of muddy, crystalline, dolomitic facies that create a baffle zone. This observation implies that the Middle Arbuckle can act as a barrier to vertical flow of CO_2 from lower layers. This interpretation is also supported by hydro-stratigraphy studies that concluded there is lack of communication between the Lower and Middle Arbuckle (Watney and Rush,

2012). Presence of high fracture density zones in the Lower Arbuckle that are capped by tight Middle Arbuckle rocks, make it a good candidate for CO_2 sequestration.

Rock physics modeling also shows that the GA attribute derived from S-wave AVO gradients normal to fracture orientation can act as a potential seismic attribute for discriminating fluid fill in fractures. High GA anomalies seen on Line 1 might be suggestive of brine as the primary fluid fill in the fractures identified in the Arbuckle. However, other factors such as presence of mineralized deposits in these fractures could also lead to similar GA anomalies. Inadequate geological information about fracture fill in these anomalous areas make it difficult to corroborate these results. Moreover, because multicomponent seismic data were acquired prior to CO_2 injection and no monitor seismic survey has been acquired since injection started, application of GA to discern movement of CO_2 in Arbuckle reservoirs could not be tested.

Overall in this study, I have tried to achieve a seismic-based fracture characterization using S-wave AVO attributes. I feel that it is important to highlight some of the limitations that a seismic-based fracture characterization entails. Interpretation of fracture properties using seismic attributes relies on assumptions about shapes, openness, sizes, and spatial arrangement of fractures. Moreover, results of such a study can be difficult to verify independently due to model limitations, data quality and constraints on spatial sampling of well data. To deal with these limitations, it is crucial to realize the importance of multi-disciplinary data and multi-scale measurements. This study attempts to integrate seismic observations with other geological information like core, well logs, and dynamic pressure measurements. The methodology and results could have been further strengthened if independent estimates of elastic constants were available to create an anisotropic rock physics model and time-lapse seismic data were available to see subsurface fluid movement.

4.7 CONCLUSIONS

This study explored the dependence of shear-wave seismic amplitudes on fracture properties. It demonstrates using modeling and surface seismic data that fracture properties can be obtained using S-wave seismic data given good quality pre-stack seismic data and supporting geological information is available. This study presents viable fracture attributes to characterize tight reservoirs, now that more economic S-wave data acquisition methods are becoming available through the use of P-wave sources. Fracture analysis of the Arbuckle Group in Wellington Field demonstrates that S-wave AVO methods can delineate HPZs and baffle zones at resolution higher than possible with travel-time based methods. This analysis helps identify lateral heterogeneities and fractures present in the Arbuckle interval, potentially affecting the injection and movement of CO_2 in the subsurface. In addition to lateral variation of fracture density, S-waves methods have the potential to monitor fluid movements through fractures, which could have significant implications for applying time-lapse seismic technology to tight formations.

4.8 APPENDIX A

4.8.1 S-wave AVO intercept gradient attributes

Using the S-wave AVO approximations described in section 3.7.1, AVO intercepts and gradients of an S_H wave ($I_{S_H} and\ G_{S_H}^{sym}$) and an S_V wave ($I_{S_V} and\ G_{S_V}^{sym}$) can be calculated as follows:

$$I_{S_H} = -\frac{1}{2}\frac{\Delta Z^s}{\overline{Z^s}} \qquad (A-1)$$

$$G_{S_H}^{sym} = \frac{1}{2}\left(\frac{\Delta\beta}{\overline{\beta}} - \Delta\gamma\right) \qquad (A-2)$$

$$I_{S_V} = -\frac{1}{2}\left(\frac{\Delta Z^s}{\overline{Z^s}} - \Delta\gamma\right) \qquad (A-3)$$

$$G_{S_V}^{sym} = \frac{7}{2}\left(\frac{\Delta\beta}{\overline{\beta}} - \Delta\gamma\right) + 2\frac{\Delta\rho}{\overline{\rho}} + \frac{1}{2}\left(\frac{\overline{\alpha}}{\overline{\beta}}\right)^2 . \left(\Delta\varepsilon^{(v)} - \Delta\delta^{(v)}\right) \qquad (A-4)$$

$$G_{S_V}^{iso} = \frac{7}{2}\frac{\Delta\beta}{\overline{\beta}} + 2\frac{\Delta\rho}{\overline{\rho}} \qquad (A-5)$$

AVO intercepts and gradients are used to calculate an Intercept Anisotropy attribute (IA) as:

$$IA = 2(I_{S_V} - I_{S_H}) \qquad (A-6)$$

Gradient Anisotropy attribute (GA) for 2D and 3D seismic application can be calculated as:

$$GA = G_{S_V}^{sym} - 7G_{S_H}^{sym} \qquad (A-7)$$

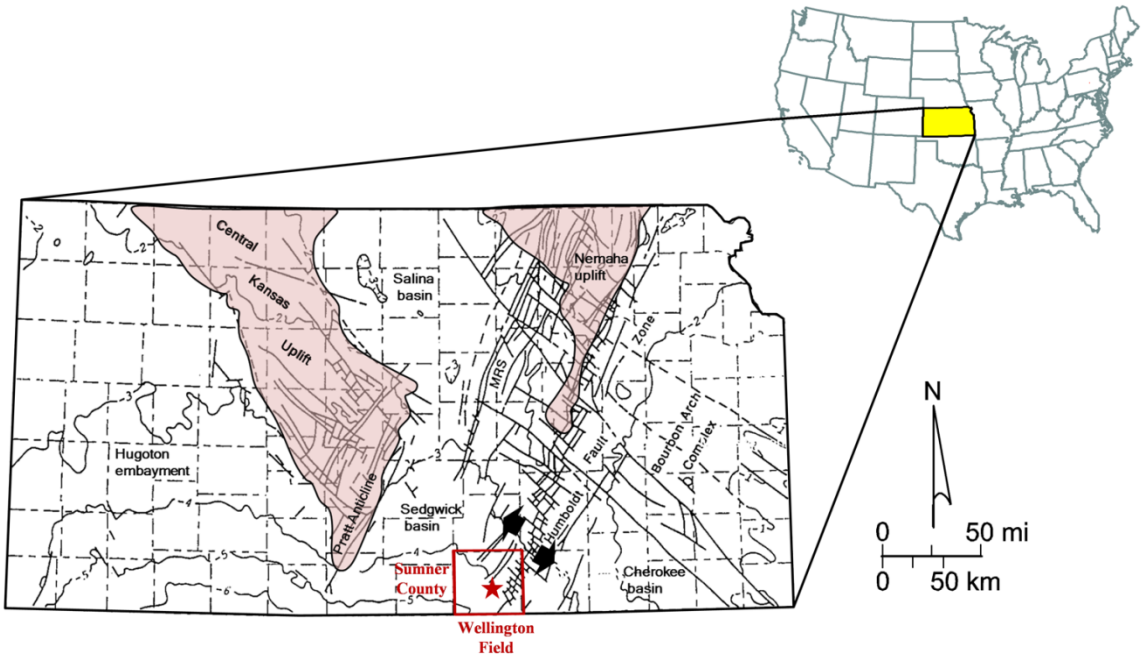

Figure 4.1: Wellington field (red star) is located in Sumner County (red square), Kansas. It is a sub-crop play of Mississippian age carbonate reservoirs within the Sedgwick Basin, a Precambrian structure formed by the Nemaha uplift, The Nemaha ridge separates the Sedgwick Basin from the Cherokee Basin to the east. Black arrows show the direction of crustal extension resulting from the Nemaha uplift, and contours represent the regional Precambrian basement. The Sedgwick Basin is bounded by the Central Kansas Uplift to the west, the Salina Basin to the north, and the Anadarko Basin to the south (not shown). Figure modified after Merriam (1963) and Baars and Watney (1991)

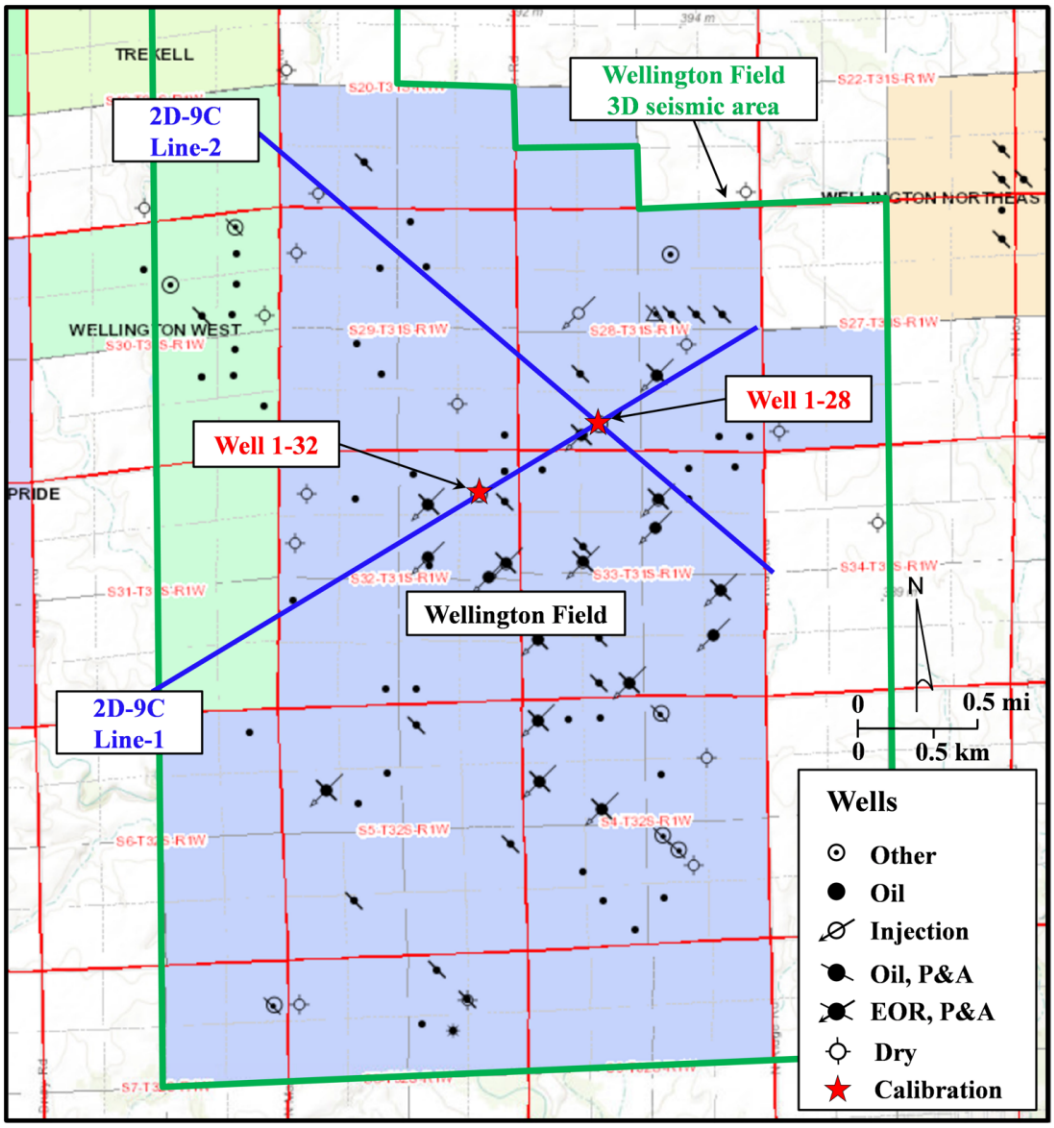

Figure 4.2: Base map of Wellington Field (shaded blue area) showing the 9C-2D seismic data (blue lines), 3D P-wave seismic data (green area) and different wells with at least some log data available. 2D-9C Line-1 was used for the S-wave AVO analysis presented in this paper. Wells 1-32 and 1-28 had a full suite of well logs and cores acquired and are used as calibration wells.

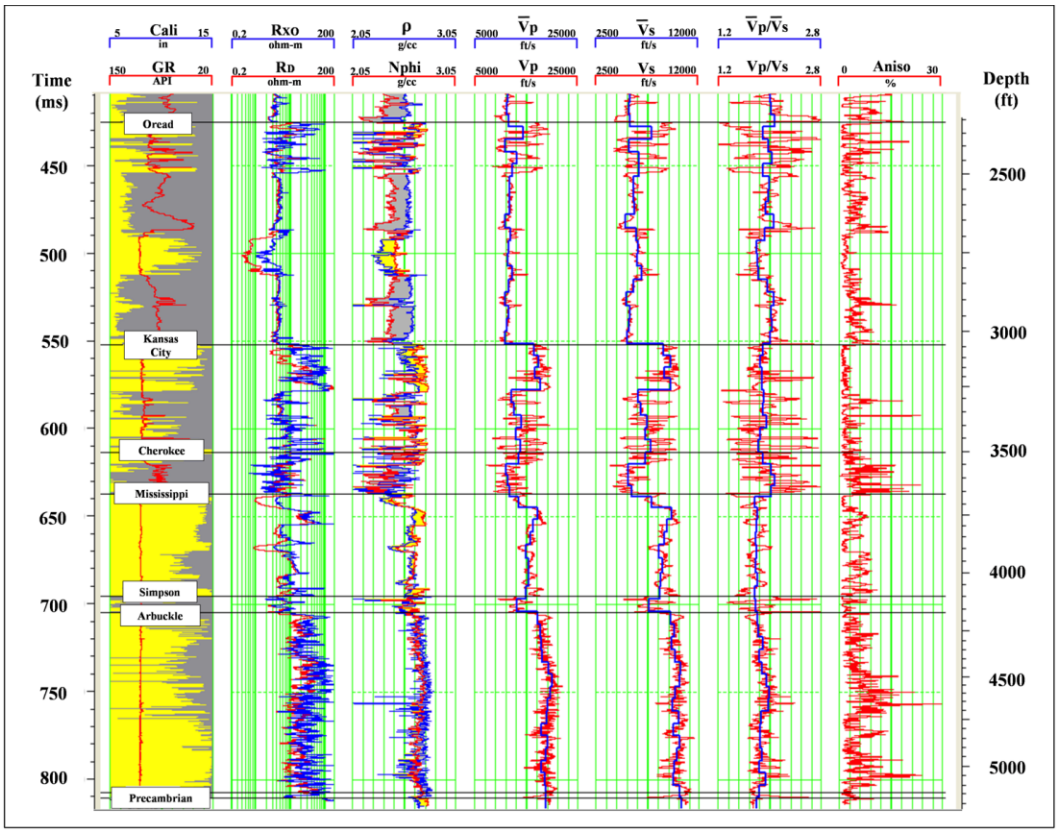

Figure 4.3: Well log suite acquired in well 1-32. The area shaded yellow in the GR track corresponds to the carbonate intervals in the well. Shaly intervals are shaded gray. Wellington Field produces from the Mississippian interval, and the Arbuckle Group is being considered for CO_2 storage. Seismic velocity measurements (Vp and Vs curves in red) were made in the wells. Backus averages of seismic velocities ($\bar{V}p$ and $\bar{V}s$ curves in blue) were used to calibrate the rock physics model. Dipole sonic measurements were taken in this well to estimate the percentage of S-wave anisotropy, which is shown in the Aniso track.

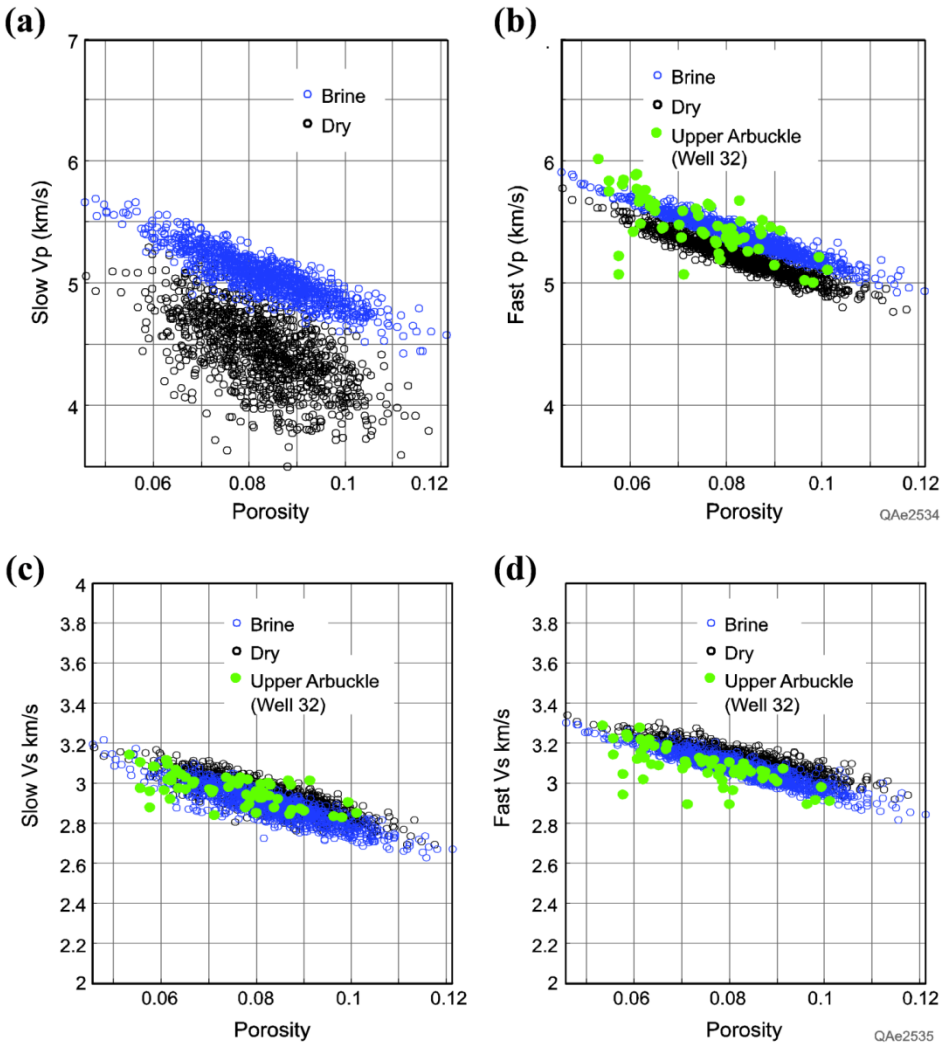

Figure 4.4: Slow and fast P-wave velocities (a and b) and S-wave velocities (c and d) obtained from rock physics model plotted against total porosity. Black and blue open circles correspond to modeled seismic velocities for the Upper Arbuckle with dry and brine-saturated fractures, respectively. Green points are seismic velocities obtained from the well logs in well 1-32. Note that the modeled S-waves and fast P-wave velocities are consistent with borehole measurements.

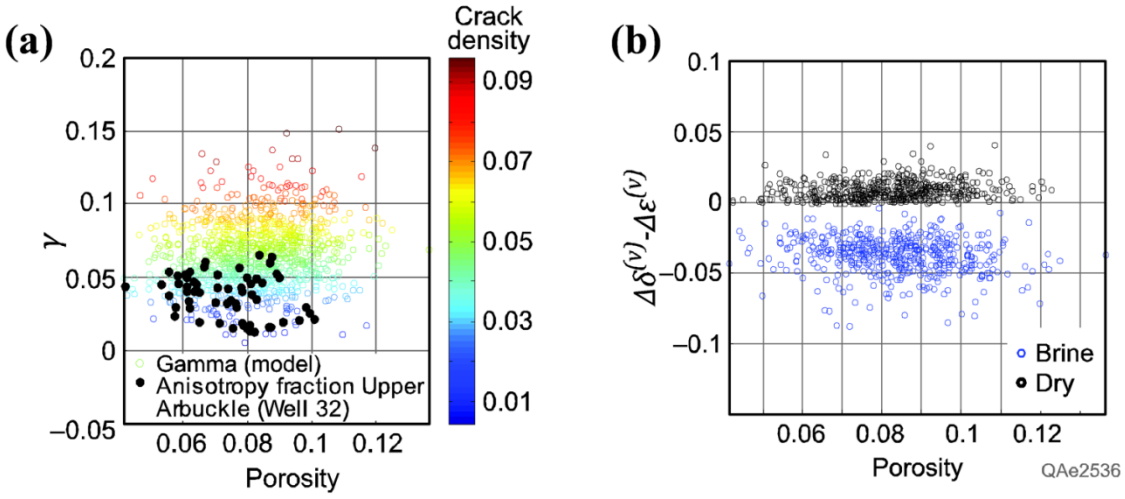

Figure 4.5: Porosity dependence of Thomsen style anisotropic parameters derived from the rock physics model. (a) Variation of γ with total porosity, color coded with crack density parameter. Modeled γ (open circles) is consistent with the well measurements (filled black circles). Also note that gamma is directly correlated to the crack density parameter. (b) Variation of $\Delta\delta^{(v)} - \Delta\varepsilon^{(v)}$ with total porosity, color coded with fluid fill, respectively. $\Delta\delta^{(v)} - \Delta\varepsilon^{(v)}$is sensitive to the fluid fill and is able to discriminate between dry (black) and brine (blue) filled fractures.

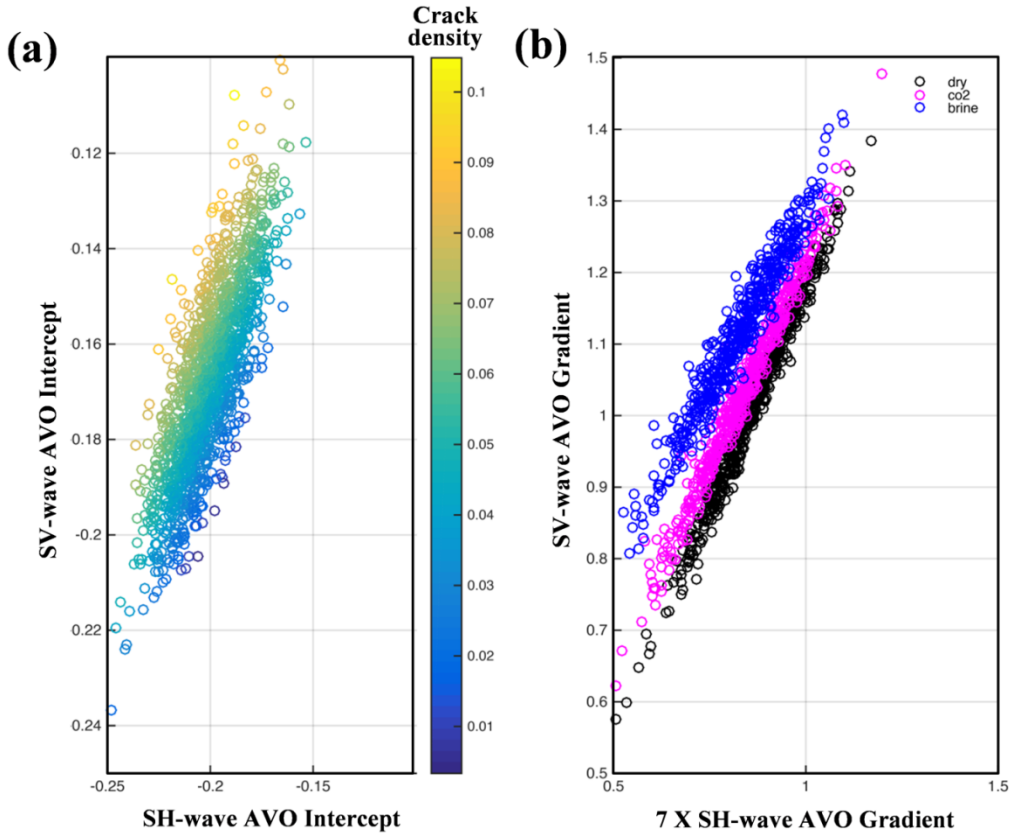

Figure 4.6: (a) Modeled SV and SH wave AVO intercept cross plots for dry, brine and CO_2 filled fractures in symmetry plane, color-coded with crack density parameter. Since fluid fill does not affect AVO intercepts, no separation is seen between different fluid fills. Increasing offset between SV and SH AVO intercepts suggests increase in fracture density, as indicated by the color shift towards yellow end of the spectrum. (b) Modeled SV and SH wave AVO gradient cross plot in symmetry plane for different fluid fill in fractures. Black open circles are modeled gradients for dry fractures. Blue and magenta open circles represent AVO gradients for brine and CO_2 filled fractures, respectively. Note that S-wave AVO gradients can be used to discriminate between different fracture fluids.

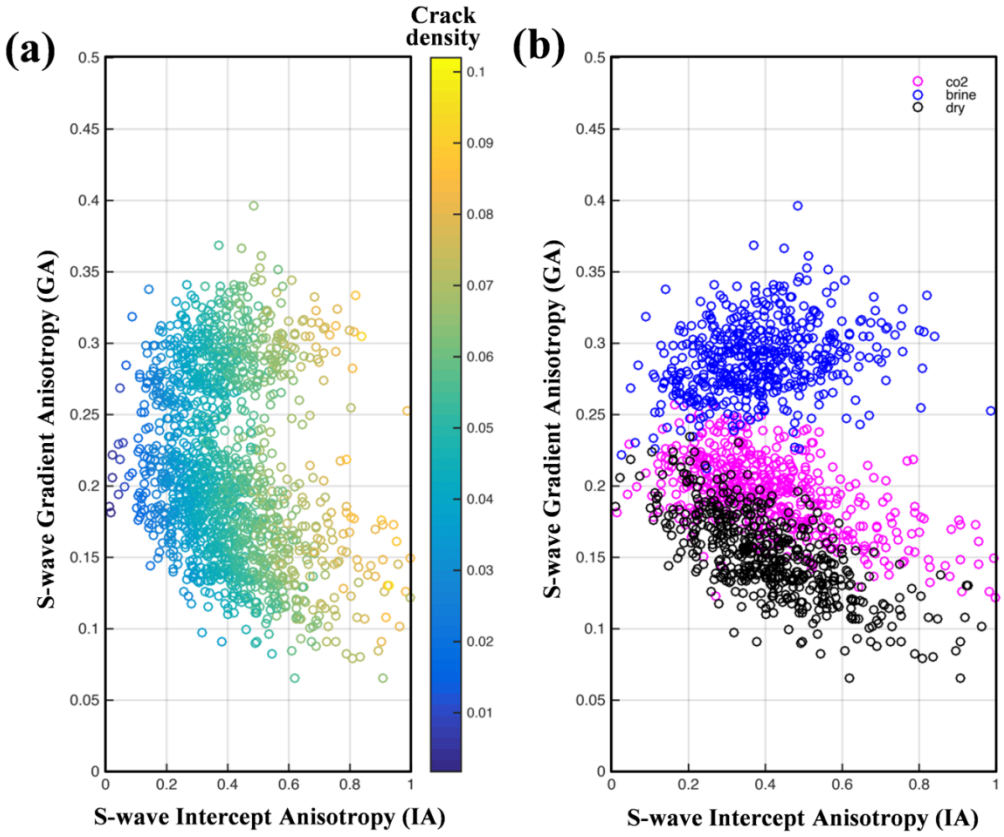

Figure 4.7: Crossplots between Gradient Anisotropy (GA) and Intercept Anisotropy (IA) attributes modeled in the symmetry plane. (a) IA-GA cross plot for dry, brine-filled and CO_2-filled fractures, color-coded with crack density parameter. Each cluster in the cross plot corresponds to a different fracture-fill. These clusters can be identified using Figure 4.7b. Irrespective of the fluid fill, the IA increases with increasing crack density, demonstrating its viability as a fracture density attribute. (b) IA-GA crossplot for dry (black), brine-filled (blue), and CO_2-filled (magenta) fractures. Separation between clusters of different fluids along y-axis indicate applicability of GA as a proxy for fluid fill in fractures. Note that the separation between different fluid fill increases with increasing fracture density, as depicted by IA.

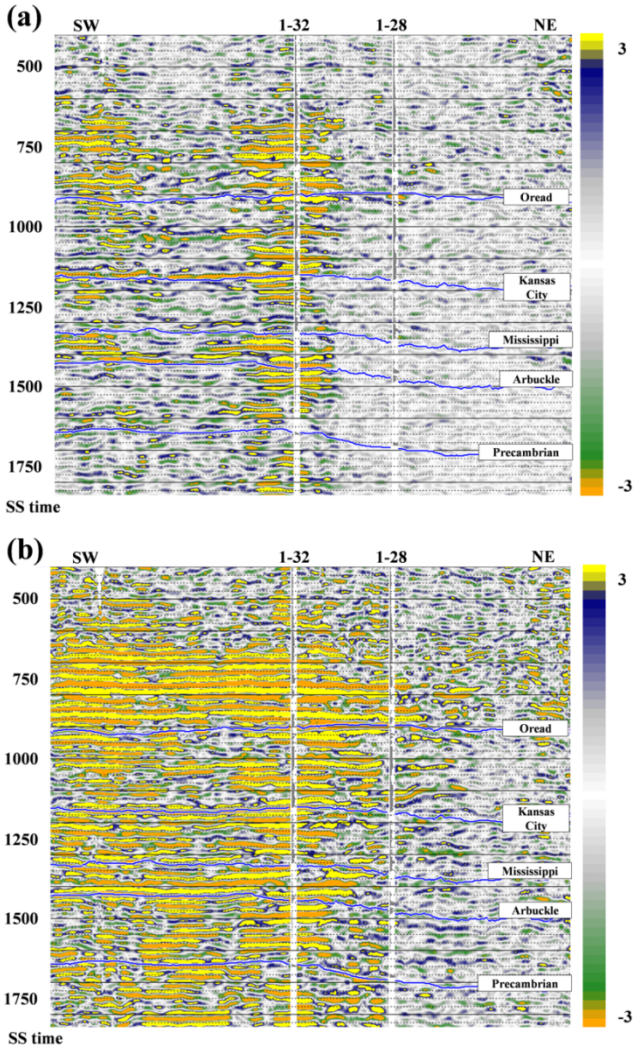

Figure 4.8: AVO intercepts for different S-S wave modes acquired on Line-1 in Wellington field. For this study, CDPs on the SW half of Line-1 are interpreted because they show reliable amplitudes. The NE part of the seismic line shows low discontinuous seismic amplitudes, which is probably due to S-static issues and poor seismic illumination of targets. (a) Slow S-S AVO intercepts on Line-1. Bright colors showing the AVO intercept anomalies are primarily located at Well 1-32 and towards the SW end of the line. (b) Fast S-S AVO intercepts on Line-1. Bright colors showing the AVO intercept anomalies are primarily located above the Oread reflector, at Well 1-32 and towards the SW end of the line. Difference in AVO intercepts of slow and fast S-waves is an indicator of fracture-induced seismic anisotropy.

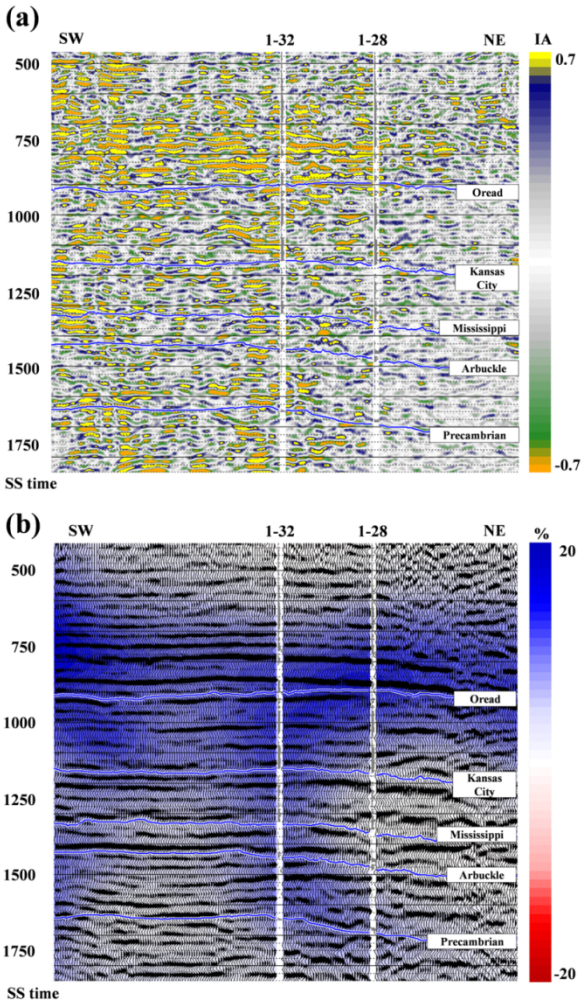

Figure 4.9: (a) IA attribute calculated using the difference between the AVO intercepts of fast and slow S-wave modes for Line-1 in Wellington field depicting fracture-induced seismic anisotropy. (b) Seismic velocity anisotropy estimated from the percentage difference in S-wave interval velocities obtained from stacking velocities after Dix conversion and lateral and vertical smoothing. Note that the high-frequency estimates of fracture density obtained from S-S AVO qualitatively agree with the low-frequency anisotropy estimates obtained from seismic velocities. High fracture density is observed above the Oread reflector, near the location of well 1-32 and towards SW end of the Line 1. Higher fracture density near well 1-32 is due to presence of fracture swarms associated with a regional fault, which runs sub-parallel to the strike of the seismic line. High anisotropy observed above the Oread towards the NE on seismic velocities are not present on the IA attribute. This difference is caused by the poor S/N ratio in this area.

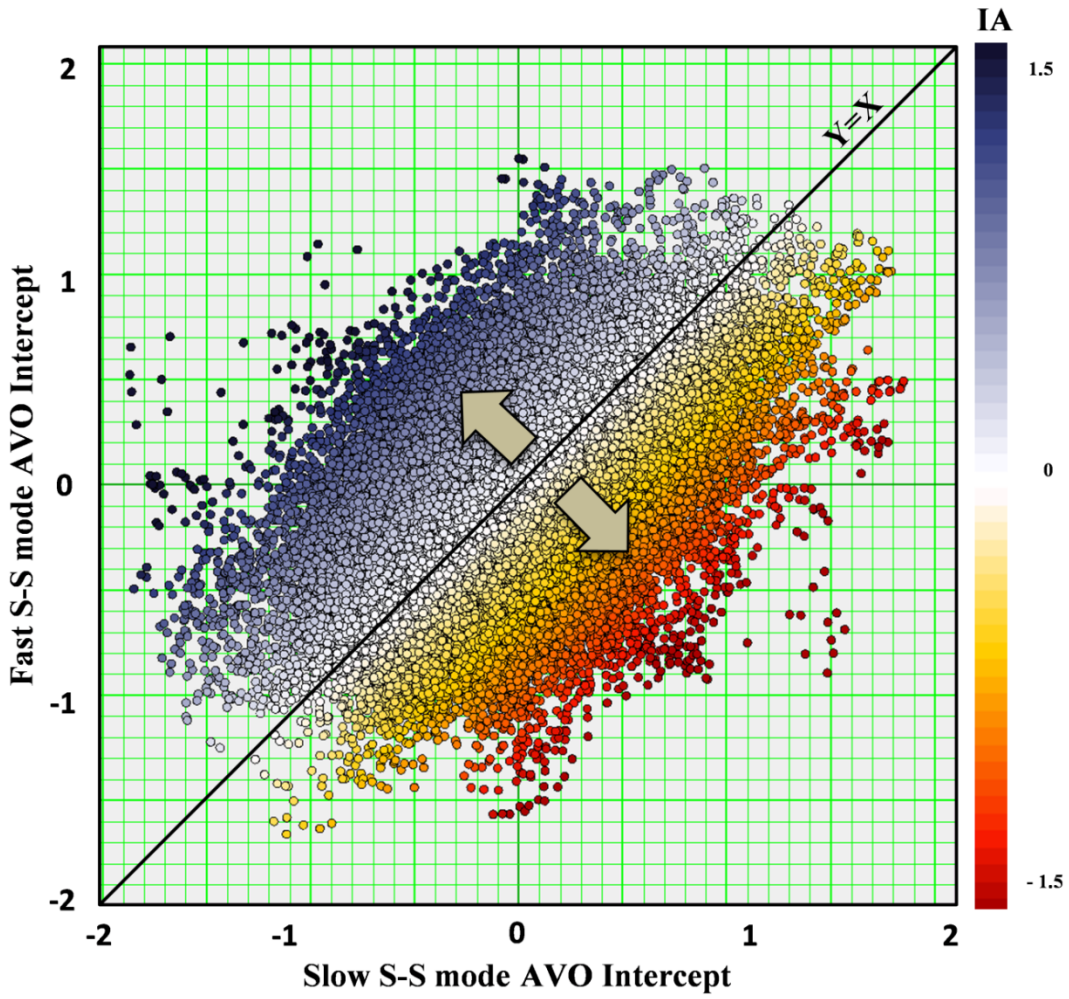

Figure 4.10: S-S AVO Intercepts crossplot for slow and fast S-waves color coded by the Intercept Anisotropy (IA) attribute for Line-1. Data points on and near the Y=X line correspond to low values of the IA attribute and indicate low fracture density. Departure from the Y=X line corresponds to increasing value of the IA attribute and higher fracture density.

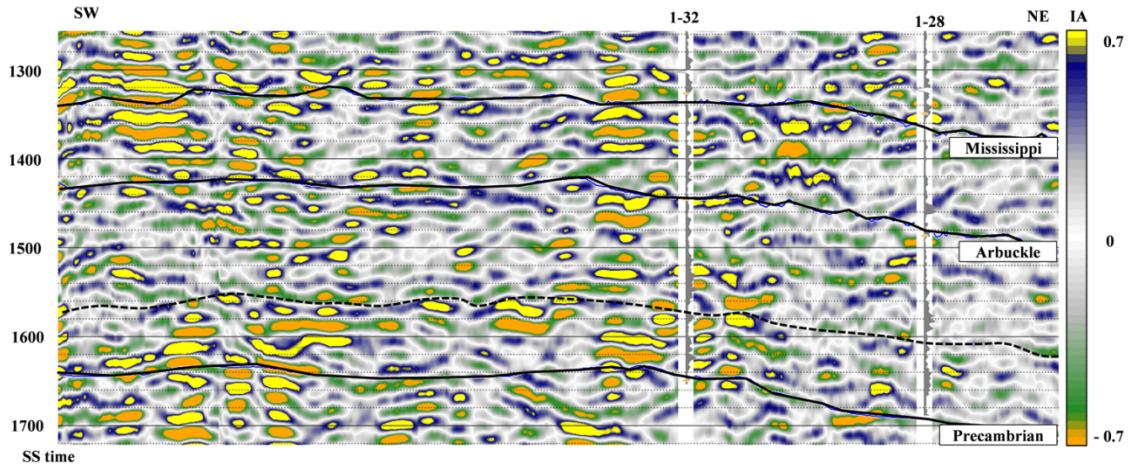

Figure 4.11: S-S Intercept Anisotropy (IA) attribute depicting lateral and depth variation in fracture density in the Arbuckle Group. Well log information inserted at the well locations is anisotropy measured from dipole sonic logs, which is in qualitative agreement with the high magnitude of the IA attribute as seen near well 1-32. Attribute quality at and east of well 1-28 is sub-optimal due to poor data quality. The dotted horizon describes the interpreted top of the High Permeability Zone (HPZ) in the Arbuckle Group. Fracture density seems to vary laterally within the HPZ with higher values near Well 1-32 possibly due to the presence of a fault. Above the HPZ, a low fracture-density zone can be seen that thickens SW of the well. This zone might be responsible for reduced vertical hydraulic connectivity between the Upper and Lower Arbuckle and may act as a baffle zone.

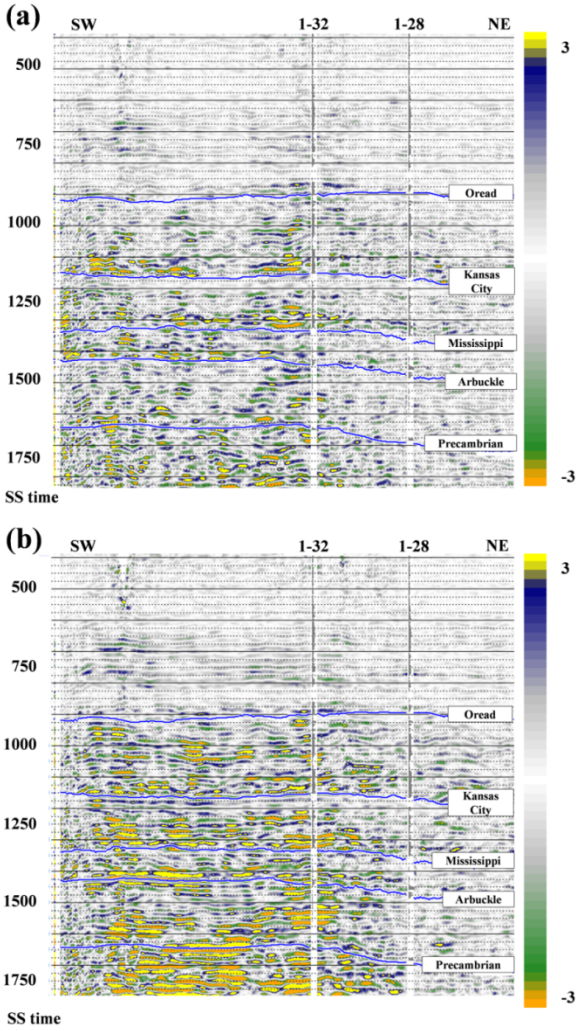

Figure 4.12: AVO gradients for different S-S wave modes acquired on Line-1 in Wellington field. The NE part of the seismic line is excluded from the interpretation because of its poor image quality. (a) Slow S-S AVO gradients on Line-1. Bright colors showing the AVO gradient anomalies are primarily located above the Kansas City, Mississippi, and Arbuckle reflectors. Within the Arbuckle such anomalies are near well 1-32 and towards the SW end of the line. (b) Fast S-S AVO gradients on Line-1. AVO gradient anomalies for fast S-wave mode are higher than for the slow S-waves. These anomalies are primarily located above the Kansas City, Mississippi, and Arbuckle reflector. Within the Arbuckle such anomalies are seen near well 1-32 and in the Middle and Lower Arbuckle. AVO gradients of slow and fast S-waves are further used to understand fluid fill in fractures.

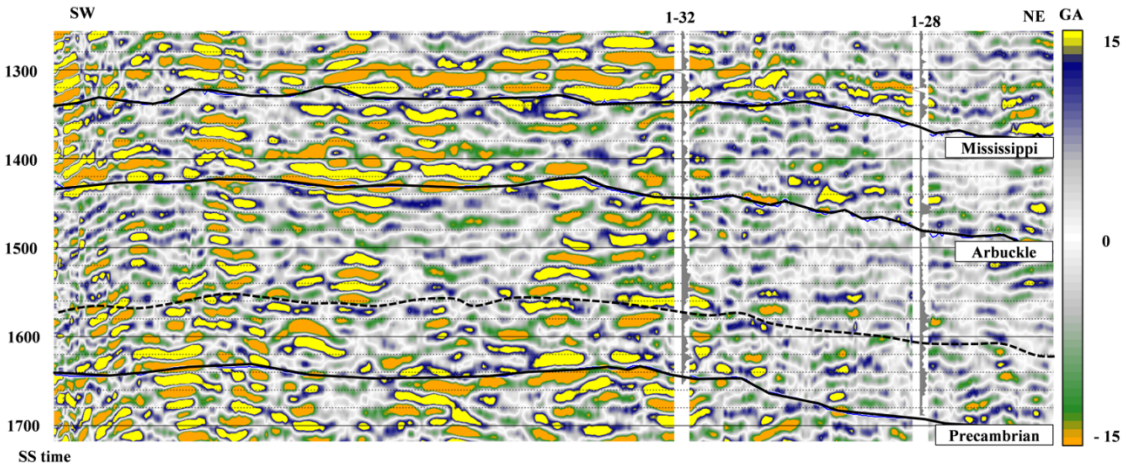

Figure 4.13: GA attribute calculated using S-wave AVO gradients on Line 1 in Wellington field. Most of the GA anomalies in the Arbuckle either lie in the HPZ or close to well 1-32 where fracture swarms associated with the regional faults have been identified. High values of GA that coincide with high values of IA suggest that these fractures are predominantly brine filled, except for the oil producing Mississippian interval that shows lower values of GA in the upper interval. Data were acquired prior to CO_2 injection in the Lower Arbuckle, so all fractures were assumed to be brine saturated. A time-lapse version of the GA attribute might help in monitoring the movement of CO_2 in the Arbuckle Group.

Chapter 5: SV-P: A Viable Alternative to Mode-converted P-SV Seismic Data for Reservoir Characterization[4]

5.1 ABSTRACT

P-SV (converted-SV) seismic acquisition requires special receiver equipment (3C geophones) and thus more cost than does the acquisition of conventional P-wave seismic data. However, some companies justify this added cost because P-SV data provide an independent set of shear-wave seismic measurements, which might increase the reliability of estimates of subsurface properties. This study investigates SV-P (converted-P) data generated by P-wave sources (e.g. a vertical vibrator) and recorded by vertical geophones, not 3C geophones, as a cost-effective alternative to traditional P-SV data. To evaluate the efficacy of the SV-P mode relative to P-P and P-SV modes, a detailed multi-component seismic interpretation was done in Wellington Field, Kansas. P-P AVO trace gathers and stacked SV-P seismic data were jointly inverted to estimate subsurface elastic properties. Resulting P- and S-impedances were compared with the estimates obtained from joint-inversion of P-P AVO trace gathers and stacked P-SV seismic data, and inversion of P-P AVO trace gathers data. All inversions provide identical P-impedance characteristics. However, a significant improvement in S-impedance estimates is observed when P-P AVO trace gathers and stacked converted wave data (either SV-P or P-SV) are inverted jointly, compared to inversion results of P-P data alone. In the Arbuckle interval, which is being considered for CO_2 injection, use of converted-wave data clearly brings out the distinction between the Middle Arbuckle baffle zone and the

[4] This chapter has been accepted to be published in Journal Interpretation. M. Gupta conceptualized and performed the research. M. Gupta wrote the manuscript. B. Hardage contributed in discussions and revisions.

Lower Arbuckle injection zone, with the latter having low P- and S-impedances. This observation, while absent on P-P only inversion results, is consistent with the absence of chert and siliceous cement, and with the presence of a weak and fractured rock in the Lower Arbuckle injection zone. No major difference in the inversion results is seen when SV-P data are used instead of P-SV data, in conjunction with the P-P seismic mode. Moreover, comparing the SV-P seismic image obtained from vertical-vibrator data and the SV-P image obtained from horizontal-vibrator data establishes that both images are essentially equivalent, except for the important distinction that the former contains valuable higher frequencies than the latter. Because legacy P-wave data can be reprocessed to extract the SV-P mode, the use of SV-P data can revolutionize the way we acquire multi-component seismic data and provide a cost-effective way of obtaining the same subsurface information provided by more expensive P-SV data.

5.2 INTRODUCTION

Use of multi-component seismic data has been rising due to continuous advances in seismic acquisition and processing technology. Of all possible shear wave modes, mode-converted P-SV data have been the most popular data choice among proponents of multi-component seismic technology. Reasons for this popularity are that P-SV data: (1) provide an independent set of shear-wave measurements, (2) can be generated by a conventional vertical-force source, and (3) are more practical in terms of data volume and acquisition cost, compared to S-S mode data. A typical setup to acquire P-SV seismic data requires a P-wave source like a vertical vibrator, which is used to generate illuminating seismic waves, and 3-component geophones that record the seismic response. P-SV seismic amplitudes strongly depend on rock density and shear-wave

reflectivities, and rock density effects can be measured at much shorter source-receiver offsets compared to P-P data (Gray, 2003). These attributes make P-SV data a viable candidate for estimating subsurface density from surface seismic data. Also, because the S-wave leg of P-SV data is less perturbed by transmission through overlying gas-sands than are P-wave data, the P-SV mode produces a better seismic image in gas charged strata. Where P-SV data really stand apart is their application in understanding seismic anisotropy. Multiple studies have successfully demonstrated use of P-SV data for subsurface fracture characterization (Shen et. al, 2002; Perez et. al, 1999; Liu and Martinez, 2013; Lynn et. al, 1995).

Despite all these proven advantages, there is still reluctance in the geophysical community towards incorporating P-SV mode into routine interpretation projects. Reasons are: (1) algorithms developed for common-mode seismic processing do not apply to mode-converted waves, (2) acquiring P-SV data requires 3-component receivers which adds to cost and complexity of data acquisition, (3) P-SV seismic data are sometimes noisy, because of the geophone-coupling noise-sensitivity issues, and (4) complex processing algorithms when considering anisotropy, making the upfront investment in seismic acquisition compared to the value of information obtained, less justified. Recent advancements in Common Conversion Point (CCP) processing algorithms have somewhat helped offset challenges related to mode-converted seismic processing. However, problems associated with data acquisition complexity, and investment risk still remain with P-SV data. Recent advances made in extracting the SV-P mode generated by P-wave sources (Gaiser and Verm, 2012; and Hardage and Wagner, 2014a, b, and Li and Hardage 2015) offer a unique and effective solution to this dilemma.

SV-P data generated from vertical-force sources makes use of the down-going shear wave-field generated directly at the source (Miller and Pursey, 1954; Hardage and

Wagner, 2014; Alkan and Hardage, 2013) which then is mode-converted into up-going P-waves that are recorded on vertical geophones. This wave physics eliminates the need for using a 3-component receiver to record an up-going wave-field, in contrast to what happens in the case of P-SV data. Principles and algorithms of CCP processing originally developed for processing P-SV data can be easily applied to the processing SV-P data. Moreover, SV-P data provide a unique opportunity to reprocess legacy P-P data that have sufficient record length and optimal low-frequency content, and extract the SV-P mode, eliminating the need of a large investment to acquire multi-component seismic data.

SV-P data are also observed to have a higher S/N compared to P-SV mode data (Fraiser and Winterstein, 1990; Li and Hardage 2015). These benefits have encouraged the geophysical community to extract SV-P data from vertical-force sources. Alkan and Hardage (2013) showed similarities between down-going direct S-waves produced by vertical and horizontal vibrators on a vertical array of 3-comoponent geophones. Hardage et al (2014) created a SV-P image using vertical-force sources and discussed the governing principles. Soon after, Li and Hardage (2015) demonstrated successfully that an SV-P image can be generated from offset VSP data and that the SV-P image was significantly better than images produced by P-P and P-SV modes. These latter studies also focused on processing field data generated by P-wave sources to create an SV-P image. None of these studies compared the SV-P image produced by a P-wave source with an SV-P image generated by a horizontal vibrator. Moreover, there is not any study that investigates if an SV-P image created from a P-wave source can be used as an alternative to a P-SV image for estimating subsurface rock properties. In this study, I address these gaps by comparing various mode-converted waves (SV-P and P-SV) generated by a vertical vibrator and a horizontal vibrator and exploit the potential of SV-

P data for reservoir characterization. I do these comparisons using 2D 9-component seismic data acquired across Wellington Field, Kansas.

In this study, I evaluate the efficacy of the SV-P mode to understand subsurface properties and compare this estimate with the estimates of properties obtained from P-P data alone, and from a combination of P-P and P-SV data. Results show that P-P data provide excellent P-impedance (IP) information, but that it is essential to use high-quality well log data and P-wave AVO gradients to obtain S-impedance (IS). Use of converted-wave data offsets this problem because these data provide an independent S-wave measurement and more reliable information about IS behavior. Results also show that SV-P data generated with a vertical-vibrator source contain equivalent, and occasionally better, information compared to P-SV data, and SV-P data generated by horizontal vibrator.

5.3 DATA SET

The Wellington Field is located in Sumner County, Kansas and has been producing from cherty, dolomitic reservoirs of Mississippian age. This study focuses on the Lower Ordovician-aged carbonates that are collectively called the Arbuckle Group. The Lower Arbuckle is believed to be heavily dolomitized and fractured and is being considered for CO_2 storage (Watney and Rush, 2012 and Gupta et al., 2017). Most natural fractures in the Lower Arbuckle are either associated with karst (Franseen et al., 2003) or with reactivation of the Precambrian basement structures (Merriam, 1963; Baars and Watney, 1991). Such fractures have been interpreted with well-logs, such as micro-resistivity and dipole sonic logs (Watney and Rush, 2012), and with multi-component

seismic data (Gupta et. al, 2017) acquired in Wellington Field. Seismic-scale fractures are assumed to facilitate fluid flow in the Lower Arbuckle.

5.3.1 Seismic data

To better understand the role of fractures and heterogeneities in the Lower Arbuckle injection interval and overlying sealing formations, a 9C-2D seismic survey was acquired across the Wellington Field. This survey consisted of two 2D seismic lines, each 7 miles (11 km) in length, with 9-component seismic data collected using 3-component geophones and vertical and horizontal vibrators. Line-1 and Line-2 were orientated at 55^{o}E and 135^{o}E, respectively (Figure 4.2). 2D stacking fold for both S and P-wave data is about 55, and total trace length of the data is 3s for P-wave data and 4s for S-wave data. Horizontal vibrators made six linear sweeps (20 s long) with frequency ranging from 4Hz to 50Hz to make maximum utilization of the lower end of the frequency spectrum. Vertical vibrators on the other hand, made two non-linear sweeps (40 s long) ranging from frequencies 6Hz to 150Hz with a taper of 3db/octave. Unfortunately, non-linear sweeps are not ideal for generating optimal quality illuminating SV wave-fields because SV wave-fields need to have robust low-frequency energy.

The 2D multicomponent seismic data were processed at a commercial data-processing shop where they were segregated into various direct and converted seismic wave modes. This study utilizes direct P (P-P), converted-P (SV-P), and converted-S (P-SV) to characterize Arbuckle reservoirs. The SV-P wave mode generated by both vertical and horizontal vibrator sources were processed. Theory describing the extraction of SV-P wave mode from vertical force source data has been widely discussed in Hardage et al. (2011) and Hardage and Wagner (2014 a, b). Some additional pre-stack seismic

processing steps were applied to the data to prepare trace gathers for AVO inversion. These steps are discussed later in this paper.

5.3.2 Well data

Kansas Geological Survey (KGS) acquired extensive well data in the Wellington field to conduct a small-scale field test demonstrating CO_2 sequestration and EOR in the Arbuckle and Mississippian strata. Two calibration wells, KGS 1-28 and KGS 1-32, that are located directly on the 9C-2D seismic survey lines are used for this study. Well 1-28 lies on the intersection of Line-1 and Line-2, and well 1-32 lies on Line-1 about 893 m SW of well 1-28. Both wells have a full suite of well-logs including spectral gamma ray, neutron density, resistivity, cross-dipole sonic, nuclear magnetic resonance (NMR) and micro-resistivity imaging. In addition to well-logs, lithology data from cuttings and information about rate of drill bit penetration (ROP) are also available as shown in Figure 5.1. Approximately 490 m of core were acquired in well 1-32 to sample Mississippian and Arbuckle reservoir rocks as well as their cap rocks. Greater abundance of fractures and vugs in the Arbuckle Group has been reported at all scales based on dipole sonic logs, borehole micro-resistivity image logs, and T2 relaxation times observed on NMR logs. These vugs and fractures have been found to govern overall permeability in the Lower Arbuckle (Gupta et al., 2014 and 2015; Ohl and Raef, 2014; Watney and Rush, 2012; Franseen et al., 2003; and Byrnes et al., 1999). Permeability estimates obtained from measurements on core plugs provided Kmax values up to 425 mD in the Lower Arbuckle. A step-rate test was also performed on well 1-32 (source well) and 1-28 (observation well), that are 3000 ft apart, in a 20 ft perforated zone in the Lower Arbuckle. Permeability of approximately 1 Darcy was estimated from the step-rate test.

Geological data collected from these wells support the idea that fractures are abundant in the Lower Arbuckle and control overall permeability.

5.4 METHODS

5.4.1 Pre-stack conditioning of multi-component seismic data

In order to interpret pre-stack converted-wave data (P-SV and SV-P) and perform inversion on P-P angle gathers, additional gather-conditioning steps were performed after routine seismic processing. The aim of this conditioning was to increase the signal-to-noise ratio (S/N) of gathers and to suppress multiples and random noise for P-P, P-SV and SV-P seismic modes. The first step in the gather-conditioning workflow was to apply an offset mute to remove low-frequency noise caused by NMO stretching. Random noise attenuation techniques were implemented including super-gathers, band-pass filtering and Radon filtering. Multiples and contamination from other wave modes were addressed using a separate Radon filter. To remove any residual misalignment of reflections in the gathers, trim statics corrections were applied. Gathers generated from this workflow were used for depth registration and interpretation. An additional step of converting offset gathers to angle gathers was performed for the P-P mode using the P-wave velocity model. These gather-conditioning steps ensured seismic amplitude fidelity and optimal S/N for multi-component seismic interpretation.

5.4.2 Post-stack interpretation of P-P, P-SV and SV-P wave modes

Interpretation of multi-component seismic data requires an understanding of P- and S-wave velocities of the subsurface so that seismic reflections corresponding to known geological boundaries can be interpreted and correlated on different wave modes. A seismic velocity model developed using P-P and S-S wave event registration (Gupta

et.al, 2015) was used to identify depth-equivalent seismic events between P-P, P-SV and SV-P data. This initial velocity model was updated using seismic events correlated in P-P, P-SV and SV-P seismic sections in their respective time domains away from the wells. Regional seismic events that were interpreted on all wave modes correspond to top of Oread, Kansas City, Mississippian, Arbuckle and Precambrian. Updated P- and S-wave velocity models were then used for seamless conversion of all data into the P-P time domain. In addition to these regional events, key reflectors within the Arbuckle Group, where this study primarily focuses, were also picked. These events were the top of Middle Arbuckle (Horizon A), Top of Lower Arbuckle (Horizon B), and base Arbuckle. These reflectors form important geological boundaries (Figure 5.1) where significant changes in elastic properties are observed on well-logs.

5.4.3 Seismic inversion for subsurface elastic properties

Seismic inversion helps eliminate some seismic wavelet effects and estimates subsurface elastic properties from seismic reflections to aid geological interpretation. To understand the efficacy of SV-P data generated by a vertical vibrator in determining sub-surface elastic properties, three sets of inversions (P-P AVO inversion, P-P gathers and stacked P-SV joint inversion, and P-P gathers and stacked SV-P joint inversion) were performed using CGG GeoSoftware and results compared. The first inversion used P-P angle gathers and was used as a baseline for all the comparisons. AVO inversion of P-P data is a widely-accepted practice to estimate subsurface elastic properties from conventional P-wave seismic data. However, such an inversion relies solely on AVO gradients for subsurface shear wave information, in absence of any direct S-wave measurement. To perform such an inversion, a low-frequency model was generated using a seismic velocity model created from the event registration process and available well-

logs. A statistical estimation of the embedded wavelet was done for the inversion, and P-P angle gathers were inverted for elastic properties such as P-impedance (IP) and S-impedance (IS).

The second inversion that was performed was a joint inversion that used an independent S-wave measurement made from P-SV stacked seismic data, in addition to the P-P angle gathers, to constrain inversion results. All other aspects of the inversion, such as inversion parameters, number of iterations, low-frequency models and well-log constraints, were kept the same as the first inversion to illustrate the value added because of the addition of the P-SV seismic data. Similar to the first case, statistical estimations of P-P and P-S wavelets were done, and IP and IS were estimated by inverting P-P angle gathers and P-SV stacked data.

The third inversion used stacked SV-P seismic data generated by a vertical vibrator in addition to P-P angle gathers as opposed to stacked P-SV data used in the second inversion. This inversion was performed to test if SV-P data obtained from vertical vibrator can be used as an alternative to conventionally acquired P-SV data. All other aspects of inversion (inversion parameters, number of iterations, low-frequency models and well-log constraints) were kept the same. This inversion was also performed with CGG GeoSoftware, which inverts P-P and P-SV data jointly. Ideally, for such an inversion SV-P reflectivity equations should be used for forward modelling. However, the SV-P reflectivity curve tends to track the P-SV reflectivity curve but with a modestly smaller magnitude. Because the ratio of seismic reflectivity of SV-P and P-SV remains practically constant for small incident angles, post-stack SV-P reflectivity can be estimated by post-stack P-SV reflectivity, and an appropriate scalar can be calculated and applied to the SV-P wavelet to account for the difference. Equation 5.1 shows the approximate relation between SV-P reflectivity and P-SV reflectivity at an interface

between two elastic media with similar petrophysical properties as described by Aki and Richards (1980).

$$R_{SvP} = \frac{\cos j}{\alpha} \quad \frac{\beta}{\cos i} \; R_{PSv} \tag{5.1}$$

$$R_{SvP} = \left(\frac{3 + cos^2 i}{4 \cos i} \right) R_{PSv} \tag{5.2}$$

Where, R_{SvP} is SV-P reflectivity, R_{PSv} is P-SV reflectivity, i is incident angle, j is the reflection angle, β is S-wave velocity and α is P-wave velocity. Equation 5.1 can be simplified into Equation 5.2 by assuming a background Vp/Vs of 2. The multiplication scalar in Equation 5.2 changes less than 8% for i < 25 degrees, enabling me to perform a P-P and SV-P joint inversion using the reflectivity equations of P-SV. After calculating the scalar, statistical estimation of P-P and P-S wavelets was done, and IP and IS were estimated from the joint inversion.

5.5 RESULTS

5.5.1 P-P and P-SV data analyses

To compare and interpret P-P and P-SV wave modes, pre-stack gather conditioning was applied on corrected gathers obtained from the data-processing contractor (FairfieldNodal). Figure 5.2a shows the P-P gathers obtained after gather-conditioning processing. Similar processing was done for P-SV gathers to create conditioned P-SV gathers shown in Figure 5.2b. Both P-P and P-SV gathers shown in Figure 5.2 have been depth registered and converted to P-P time. Seismic horizons corresponding to key geological boundaries like Kansas City, Mississippian, Arbuckle and Precambrian have been interpreted on both sets of seismic trace gathers. The

Arbuckle Group, which is the primary zone of interest, stretches from the Arbuckle horizon (at 710 ms) to base Arbuckle horizon (at 810 ms) in P-P time. The onset of the baffle zone in the Middle Arbuckle is marked by a high amplitude seismic reflection marked as horizon A (at 740 ms), which can be seen on both P-P and P-SV images. Also, seismic reflectors corresponding to the Lower Arbuckle stretch from horizon B (at 775 ms) to base Arbuckle, with the proposed CO_2 injection zone highlighted in green. These gathers were used to create final stacked seismic images of P-P and P-SV modes as shown in Figure 5.3. Figure 5.3a shows the final P-P stacked image, which has a better S/N compared to the P-SV image in Figure 5.3b. However, event correspondence between these two wave modes is still apparent. High amplitude reflectors between Kansas City and Mississippi horizons can be seen on both seismic sections. Also reflectors associated with Middle and Lower Arbuckle can be correlated on both images. The CO_2 injection zone highlighted in green can also be correlated on both seismic images. The image quality of P-SV section deteriorates NE of well 1-28 due to poor S-wave static corrections.

After the structural interpretation of P-P and P-SV data is completed, a quantitative analysis of both data sets is warranted to understand the value that mode-converted data bring to subsurface property estimation. This analysis required inverting P-P data first, and then comparing those results with a joint-inversion of P-P AVO trace gathers and stacked P-SV data. Figure 5.4 shows the pre-stack inversion results for the P-P AVO trace gather data. CDP gathers shown in Figure 5.2a were converted to angle gathers, which were then inverted to estimate IP and IS for Line 1. IP results in Figure 5.4a shows good agreement with the IP observed on the well logs, which are shown as a narrow-colored strip below each well label. Results show high IP below the Kansas City reflector, where there is an onset of thick limestone units. Similarly, the high-impedance

zone just below the Mississippi reflector coincides with the onset of dolomite. The Middle Arbuckle shows high IP, which indicates a possible change in litho-facies from the Upper Arbuckle. Also, low IP values can be seen in the Lower Arbuckle. Figure 5.4b shows the IS estimated from pre-stack P-P trace gathers. Within the Kansas City, Mississippian and Arbuckle intervals, IS seems to be in general agreement with measurements made on well-logs (vertical colored strips below well labels). The Middle Arbuckle (A to B) shows high IS values. A smaller change is observed in IS from Middle to Lower Arbuckle compared to the inverted IP. Additionally, the proposed injection zone is not well defined in Figure 5.4b.

Figure 5.5 shows the subsurface elastic properties obtained from inverting P-P gathers and P-SV stacked seismic data jointly. Figure 5.5a shows IP which provides the same details in the Kansas City, Mississippian and Arbuckle group depicted by P-P AVO inversion results in Figure 5.4a, including the Lower Arbuckle injection zone. Figure 5.5b shows the S-wave impedance obtained from the joint inversion. This inverted IS shows good agreement with the IS calculated at well locations in the Kansas City and Mississippi intervals. Within the Arbuckle, inversion results are consistent with well-log observations in the Middle Arbuckle. IS obtained from the joint inversion does not agree with well-logs in the Lower Arbuckle injection zone (below horizon B). However, inverted IS in the injection zone coincides remarkably with the zones of fast ROP and low GR values (refer to Figure 5.1), suggesting mechanically weaker rock. Moreover, these low IS zones also coincide with the low IP zone seen on inverted IP results. Such variation of IS in the injection zone was not evident on IS obtained from P-P AVO inversion shown in Figure 5.4b. Thus, an independent set of subsurface measurements made using P-SV data captures more information about subsurface properties and

increases the reliability of interpretation compared to results achieved with P-P trace gather data only.

5.5.2 Analyses of SV-P seismic data

After ascertaining that using P-P and P-SV modes together improves subsurface rock property estimation, I wanted to see if SV-P data could be used in place of P-SV data. Figure 5.6 shows a comparison between P-SV and SV-P wave modes obtained on Line-1. The P-SV mode shown here is same as the data shown in Figure 5.3b, except that a bandpass filter has been applied to match the frequency spectrum of the SV-P image. The corner frequencies of the bandpass filter are 10, 15, 65, and 90 Hz. The SV-P data shown in Figure 5.6b are derived with a vertical-vibrator source and vertical geophone. As a result, this image is generated from the same source-receiver setup that is used to acquire conventional P-wave seismic data. Seismic reflections corresponding to Kansas City, Mississippi, Arbuckle and Precambrian can be seen on both converted-wave modes. In the Arbuckle group, the top of Middle Arbuckle (horizon A) and the injection zone in the Lower Arbuckle (green highlight) can be correlated on both images SW of well 1-32. In areas NE of well 1-32, image quality is relatively poor in the P-SV image but is better in the SV-P image. Some of the differences in P-SV and SV-P images are thought to be caused by the fact that horizontal geophones (P-SV data) do not couple to the Earth as well as do vertical geophones (SV-P data).

To ascertain the fidelity of SV-P data generated by a vertical vibrator, I compared vertical-vibrator SV-P data to a SV-P data generated by a horizontal-vibrator, the source that is considered to be the gold standard for generating down-going illuminating S-waves. Figure 5.7 shows such a comparison. Figure 5.7a and 5.7b show SV-P images generated by a horizontal and vertical vibrator, respectively. Key seismic horizons have

been identified and interpreted on both SV-P data panels. Within the Arbuckle, the top of Middle Arbuckle (horizon A) and the top of Lower Arbuckle (horizon B) can be clearly correlated. The Lower Arbuckle injection zone is highlighted in green. In addition to a reasonable correspondence between the two images, SV-P data generated by a vertical vibrator also provide higher resolution compared to SV-P mode generated from a horizontal vibrator, particularly close to the two calibration wells. This improved resolution happens because the sweep frequencies of the vertical vibrator (6-150 Hz) are higher compared to the sweep frequencies of horizontal vibrator (4-50 Hz). Thus the SV-P image from the vertical vibrator should have higher frequencies as can be seen in Figure 5.8. However, the vertical vibrator sweep parameters were not optimal for low frequencies (non-linear sweep with a slope of +3 db/octave and starting frequency 6 Hz). If the data were acquired using a lower starting frequency and a linear sweep, the SV-P mode would have more valuable low-frequency energy needed for broad-band applications. Nonetheless, Figures 5.6 through 5.8 demonstrate that SV-P data generated from a conventional P-wave source can be a viable alternative to both the P-SV mode produced by a P-wave source and SV-P seismic mode generated by S-wave sources.

The next step is to invert P-P and SV-P data jointly to see if using SV-P data instead of P-SV data makes any difference in subsurface property estimation. Figure 5.9 shows the results from joint inversion of P-P gathers and SV-P stacks (from vertical vibrator) for Line-1. Figure 5.9a is the inverted IP with color-fill inserted at the well locations being the IP computed from well-logs. High IP in the Middle Arbuckle (between horizons A and B), and low IP in the Lower Arbuckle injection zone are consistent with the observations made on IP obtained from P-P AVO inversion, and P-P and P-SV joint inversion in Figures 5.4a and 5.5a, respectively. Figure 5.9b shows IS for Line-1 compared to IS computed from well-logs. IS is consistent with the IS estimated

from P-P and P-SV joint inversion as shown in Figure 5.5b and contains almost identical S-wave information. Moreover, IS estimated from P-P and SV-P joint inversion better resolves lithology variations associated with Kansas City and Mississippi horizons, and within the Arbuckle Group, compared to IS estimated from P-P inversion (Figure 5.4b). The Lower Arbuckle injection zone (below B) shows low values of IS, suggesting variation in rock properties as has been seen on IP. These variations are not as evident on IS obtained from P-P AVO inversion results (Figure 5.4b). Thus use of an independent shear-wave measurement obtained from SV-P data in conjunction with P-P gathers helps constrain the inversion result of IS, making IS estimate more reliable compare to IS obtained from P-P data alone.

5.6 DISCUSSION

Results from structural and quantitative interpretation of P-P, P-SV and SV-P surface seismic data from Wellington Field suggests that P-SV and SV-P wave modes provide equivalent information about the subsurface and can be used interchangeably. Similar observations have been reported by studies performed in the Appalachian Basin that focus on Marcellus Shale and Tully Limestone. Modeling seismic reflectivities of PS-V and SV-P modes from the Marcellus and Tully (Hardage et al, 2014), and comparing an SV-P image made from vertical seismic profile (VSP) data with a surface seismic based P-SV image (Li and Hardage, 2015), also suggest P-SV and SV-P images and attributes are equivalent. We also saw that SV-P data produced a better image NE of well 1-28, where P-SV data fell short. Frasier and Winterstein (1990) also reported an unexpectedly higher S/N ratio on SV-P images compared to P-SV images. Moreover, comparison of SV-P data generated by horizontal and vertical vibrators suggest, that SV-

P data generated by vertical vibrator contain higher frequencies, making the SV-P mode more useful converted-wave mode for reservoir characterization.

Joint inversion of P-P and SV-P data provided valuable insight into the Lower Arbuckle injection zone, which AVO inversion of P-P data alone failed to provide. In the Lower Arbuckle, IP and IS obtained from joint inversion show low values, suggesting the presence of mechanically weaker litho-facies compared to the Middle Arbuckle. Zones of low IS also coincide with high rates of drill bit penetration, low values of gamma ray recorded on well-logs (Figure 5.1), lack of cherty facies reported in core analysis and zones of higher permeability (Figure 5.10), and fracture density (Gupta et al, 2017), validating my results. These results are further supported by multiple permeability measurements varying from 100's of mD up to 1 Darcy made at scales ranging from a few centimeters (using core plugs) to 100's of meters (using step-rate tests between wells) in these otherwise tight carbonate rocks. This behavior and high T2 relaxation time as shown in Figure 5.10 suggests the presence of fractures and vugs (Watney and Rush, 2012) that could cause low values of IS. Similarly, high values of IP and IS observed in the Middle Arbuckle rocks are corroborated by well-log and core observations that indicate the presence of muddy, crystalline, dolomitic facies with lower fracture density that create a baffle zone (Watney and Rush, 2012; Gupta et al, 2017).

Overall this study shows the effectiveness of SV-P seismic data produced by P-wave sources and recorded by only vertical geophones as a viable alternative to P-SV seismic data for reservoir characterization. This conclusion is reached through comparison of seismic images and inversion results produced by P-SV and SV-P stacked seismic data when inverted jointly with P-P gathers. AVO inversion of SV-P gathers was not attempted because that would require a more accurate calculation of SV-P reflectivities with incident angle than were used in this study. Because this study used

commercial software (CGG GeoSoftware) originally designed to invert P-P and P-SV data, post-stack SV-P reflectivity was approximated by a scalar multiplication of P-SV reflectivity. Use of exact reflection coefficients suggested by Ruger (2001) can be done to update existing commercial inversion software to enable precise SV-P AVO inversion. This approach could enable determination of subsurface density and anisotropic parameters from conventional seismic data acquired using P-wave sources and a vertical receiver via the SV-P mode. Also, it should be noted that a modest amount of azimuthal anisotropy is present in the propagation medium across Wellington Field (Aniso track, Figure 5.1). However, I made no attempt to segregate either P-SV or SV-P data into fast-S and slow-S modes. Thus, each example of converted-mode data shown in this chapter, whether a trace gather or a stacked image, is a weighted mixture of fast-S and slow-S modes. No effort was made to determine that fast/slow weighting factors that are involved in the P-SV and SV-P data that I used. Instead. I assumed that because the length of the SV leg is the same for both P-SV and SV-P reflections in the laterally uniform, layered medium at Wellington Field, that anisotropy effects would be identical for both P-SV and SV-P modes. Thus, comparisons of P-SV and SV-P stacked images and trace gathers or of elastic properties derived through inversion of P-SV and SV-P data would still be valid for determining image equivalences and for illustrating the value of attributes derived from each converted-wave mode.

5.7 CONCLUSIONS

This study investigates the ability of SV-P data generated by available P-wave sources and recorded by vertical geophones to substitute for P-SV data recorded by 3C geophones and to increase the value of conventional P-wave data for subsurface

characterization. I demonstrate through comparison of P-P, P-SV and SV-P seismic data and inverted elastic properties that vertical-vibrator SV-P data from vertical geophones works as good as P-SV seismic data from horizontal geophones to understand reservoir properties, and provide a better resolution compared to SV-P data generated by horizontal vibrator. This study shows that the use of SV-P data from a vertical vibrator, along with P-P data, significantly improves S-impedance estimates in the Arbuckle injection zone. Such improved S-impedance characterization helps to delineate weak and fractured injection zones in the Lower Arbuckle from tight and siliceous baffle-zones present in the Middle Arbuckle. Independent shear-wave measurements made with the SV-P mode utilizes low-cost, conventional P-wave seismic data acquisition setups, Converted-wave studies can now be performed on available legacy P-wave seismic data, which will revolutionize the way that multi-component reflection seismology is done.

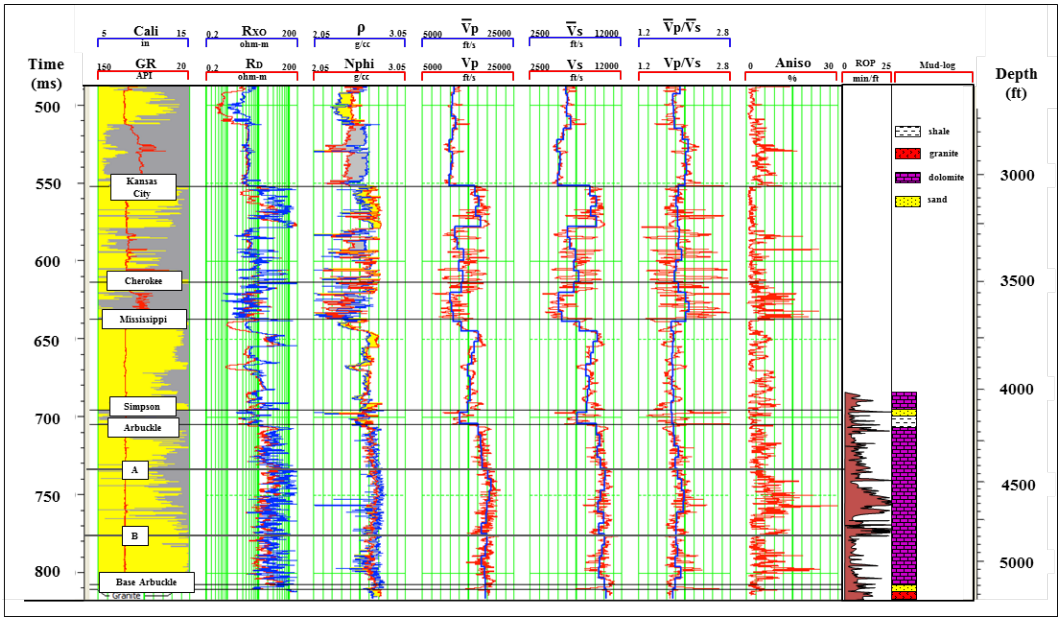

Figure 5.1: Well log suite acquired in well 1-32. The area shaded yellow in the Gamma Ray (GR) track corresponds to the carbonate intervals in the well. Shaly intervals are shaded gray. Wellington Field produces from the Mississippian interval, and the Arbuckle Group is being considered for CO_2 storage. Seismic velocity measurements (Vp and Vs curves in red) were made in the wells. Backus averages of seismic velocities (Vp and Vs) are overlain in blue. Dipole sonic measurements were taken in this well to estimate the percentage of S-wave anisotropy, which is shown in the Aniso track. Rate of Penetration (ROP) and lithology estimates for the Arbuckle group are digitized from the mud-log of well 1-32. Middle Arbuckle (between markers A and B) shows a higher GR and slower ROP compared to the Lower Arbuckle (below marker B), suggesting the Middle Arbuckle is a tighter formation. This variation is not captured by the seismic velocities measurements made at well-log scale.

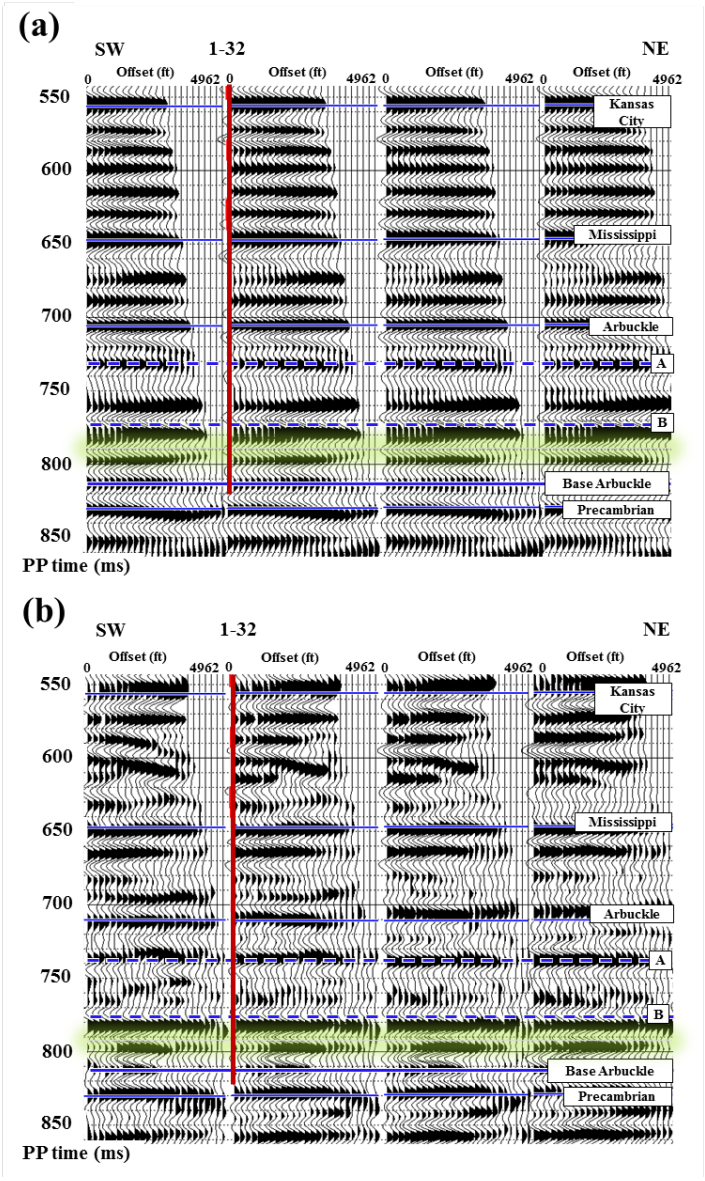

Figure 5.2: Conditioned P-P (a) and P-SV gathers (b) for CDPs near well 1-32 on Line-1. Original gathers for both P-P and P-SV modes underwent a series of gather-conditioning steps to suppress noise and enhance signal. P-P and P-SV conditioned gathers have been depth registered and polarity matched, and are shown in P-P time. The zone of interest is the Arbuckle group between 710 ms and 810 ms. High positive amplitude at 740 ms in both P-P and P-SV gathers marks the top of Middle Arbuckle (horizon A) that has been interpreted as the baffle zone. High negative amplitude at 775 ms marks the top of Lower Arbuckle (horizon B), which is being considered for CO_2 injection. The proposed injection zone has been highlighted in green.

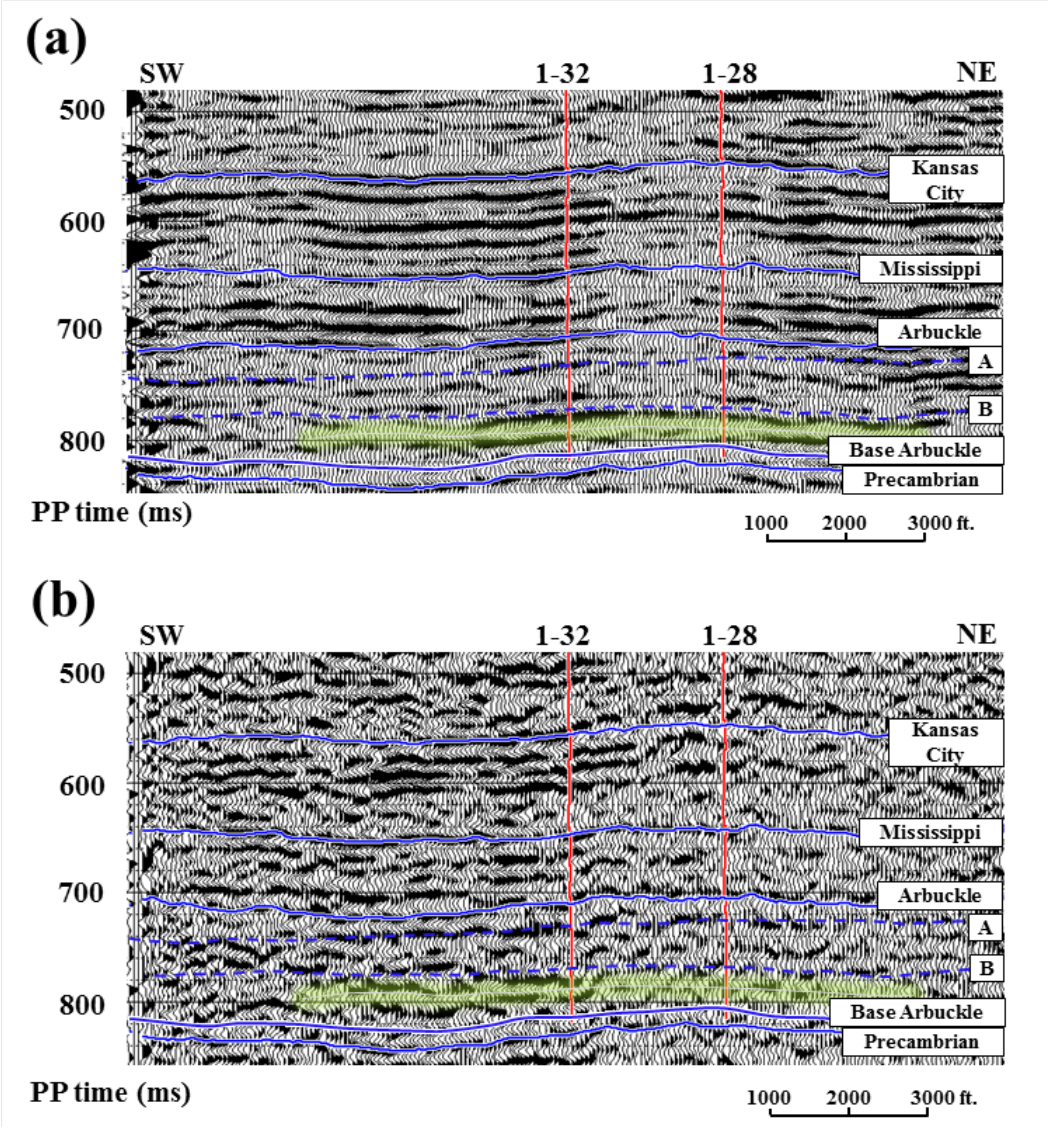

Figure 5.3: P-P (a) and P-SV (b) stacked seismic section showing the key interpreted seismic horizons on Line-1. P-P seismic has better signal-to-noise ratio compared to the P-SV seismic section. Both P-P and P-SV images have been depth registered and are shown in P-P time. Polarity on the P-SV seismic section has been matched to the P-P seismic data to see event correspondence. Within the Arbuckle Group, high amplitude reflectors in the Lower Arbuckle injection zone (green highlighted zone) are observed on both seismic sections. Image quality of the P-SV mode towards NE side of well 1-32 is sub-standard due to S-wave static related issues.

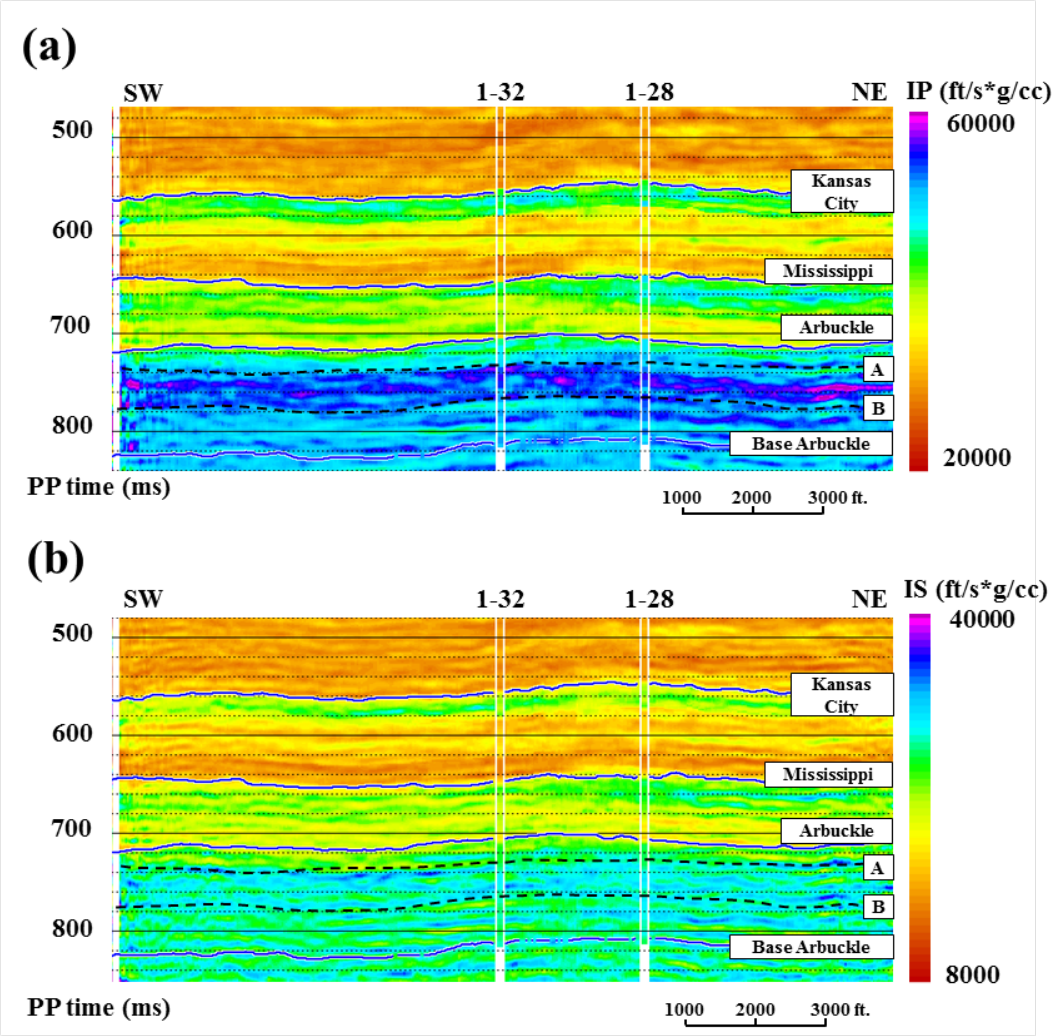

Figure 5.4: (a) P-impedance (IP) obtained from AVO inversion of P-P gathers for Line-1 compared to IP computed from well-logs (vertical colored strips below well labels). Middle Arbuckle interval (between A and B) shows high IP values, suggesting a possible lithology change, consistent with presence of muddy crystalline dolomite observed in core. This high impedance layer coincides with the baffle zone known to be present in the Middle Arbuckle (Watney and Rush, 2012). Lower Arbuckle injection zone (below horizon B) shows lower values of IP which coincides with the presence of fractured dolomitic limestone. (b) S-impedance (IS) obtained from AVO inversion of P-P gathers compared to IS computed from well-logs. Middle Arbuckle interval (between A and B) shows high values of IS. Change in IS values from Middle to Lower Arbuckle is considerably less compared to what was observed on IP section. Lower Arbuckle injection zone is not clearly visible on IS image.

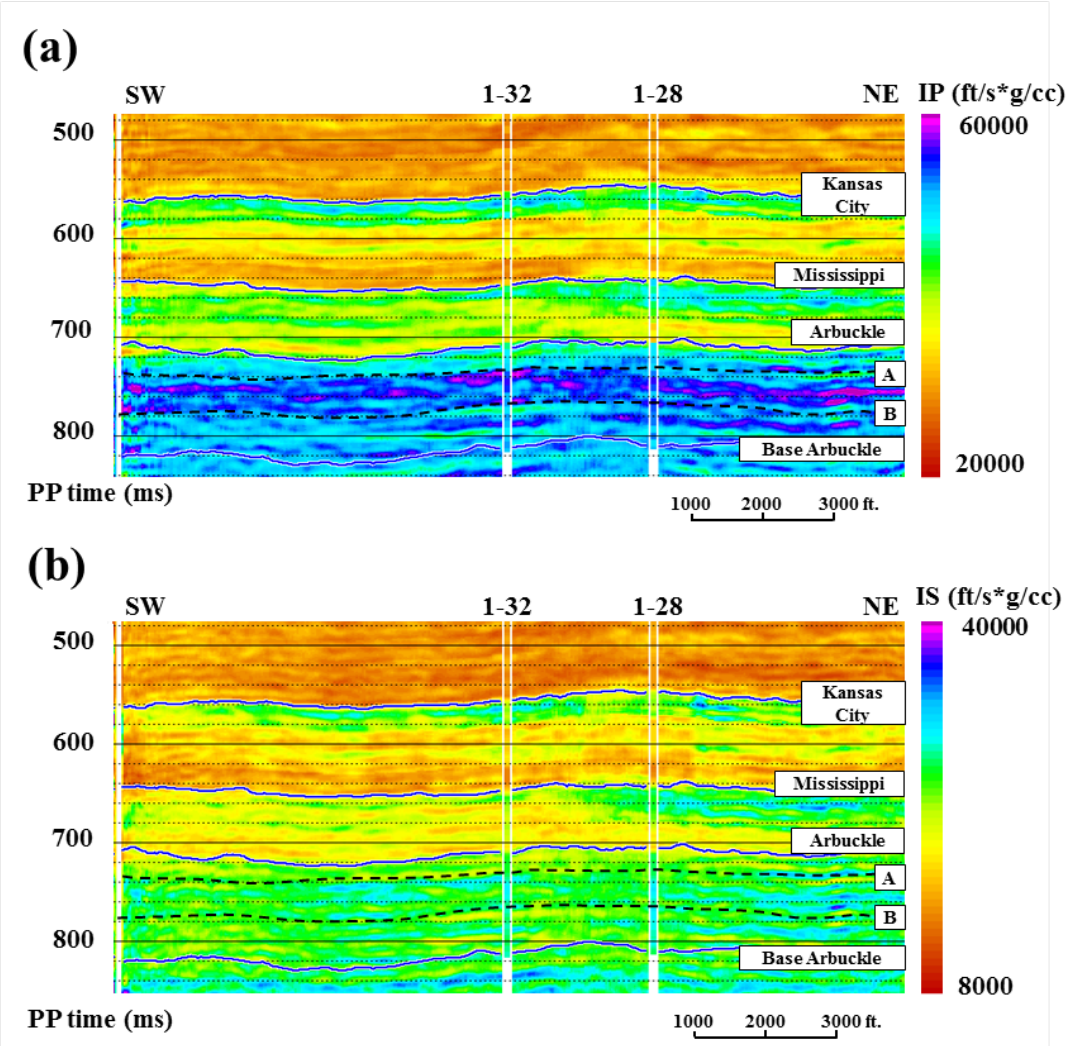

Figure 5.5: (a) P-impedance (IP) obtained from a joint-inversion performed on P-P gathers and P-SV stacked seismic section for Line-1 compared to IP computed from well-logs (vertical colored strips below well labels). This IP image is consistent with IP obtained from P-P AVO inversion, capturing all the detained in Arbuckle Group. (b) S-impedance (IS) obtained from P-P and P-SV joint inversion compared to IS computed from well-logs. Middle Arbuckle interval shows IS (between A and B) indicating a change in lithology. Lower Arbuckle injection zone (below B) show low values of IS, suggesting some variation in lithology and possibly presence of fractures, which are not observed on well-logs. Low IS values in the injection zone are consistent with the observations made on IP images. Use of an independent shear-wave measurement (P-SV seismic) helps constrain the inversion result of IS, making it more reliable compare to IS obtained from P-P data alone.

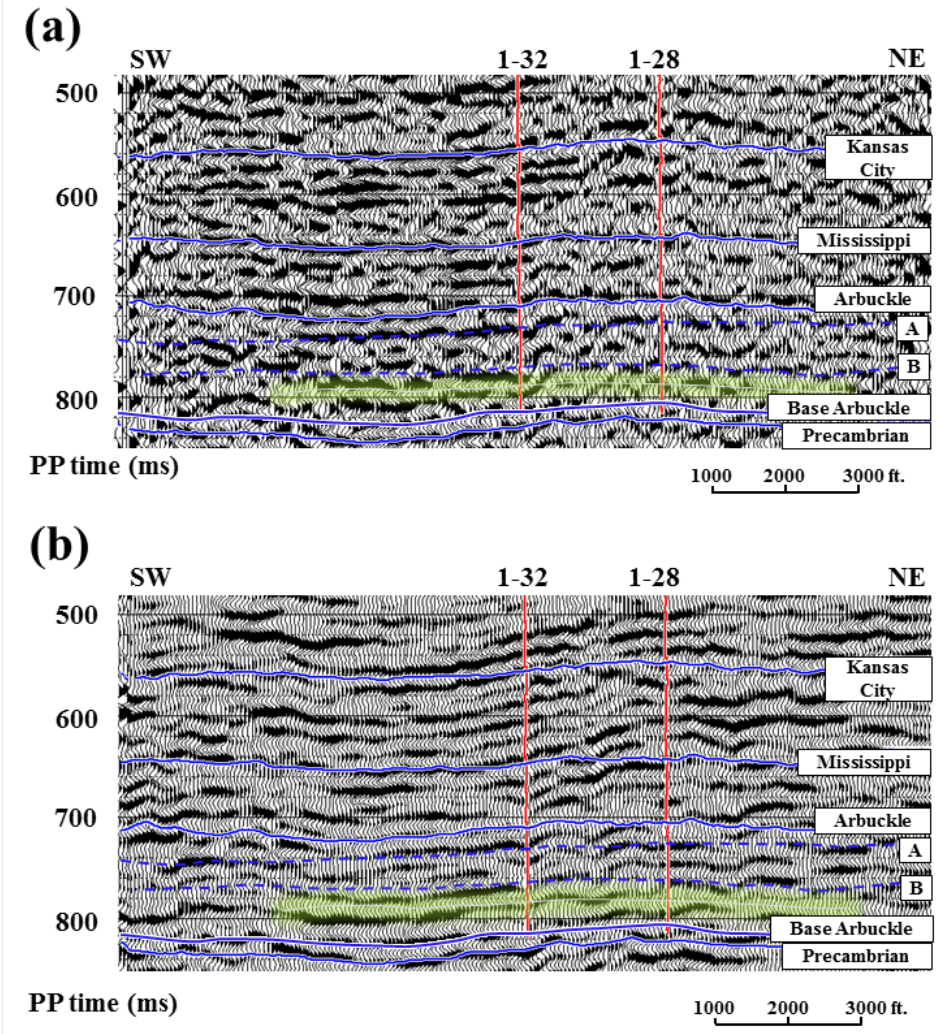

Figure 5.6: (a) P-SV seismic section along Line-1 showing the key interpreted seismic horizons. A bandpass filter with corner frequencies (10, 15, 65, 90) has been applied to the P-SV image to match its frequency spectrum with the SV-P image. (b) SV-P seismic section generated from a vertical vibrator on Line-1 with the P-SV horizons overlain. This SV-P image generated from a conventional P-wave source provides a low-cost alternative to a P-SV seismic image. Seismic reflections corresponding to Kansas City, Mississippi, Arbuckle and Precambrian can be seen on both converted-wave modes. In the Arbuckle group, geological events like top of Middle Arbuckle (A) and top of Lower Arbuckle (B) are also visible on both images. Lower Arbuckle injection zone is highlighted in green on both images. Seismic image quality NE of well 1-32 is sub-standard on the P-SV image. Degradation of the SV-P image NE of well 1-32 is less obvious.

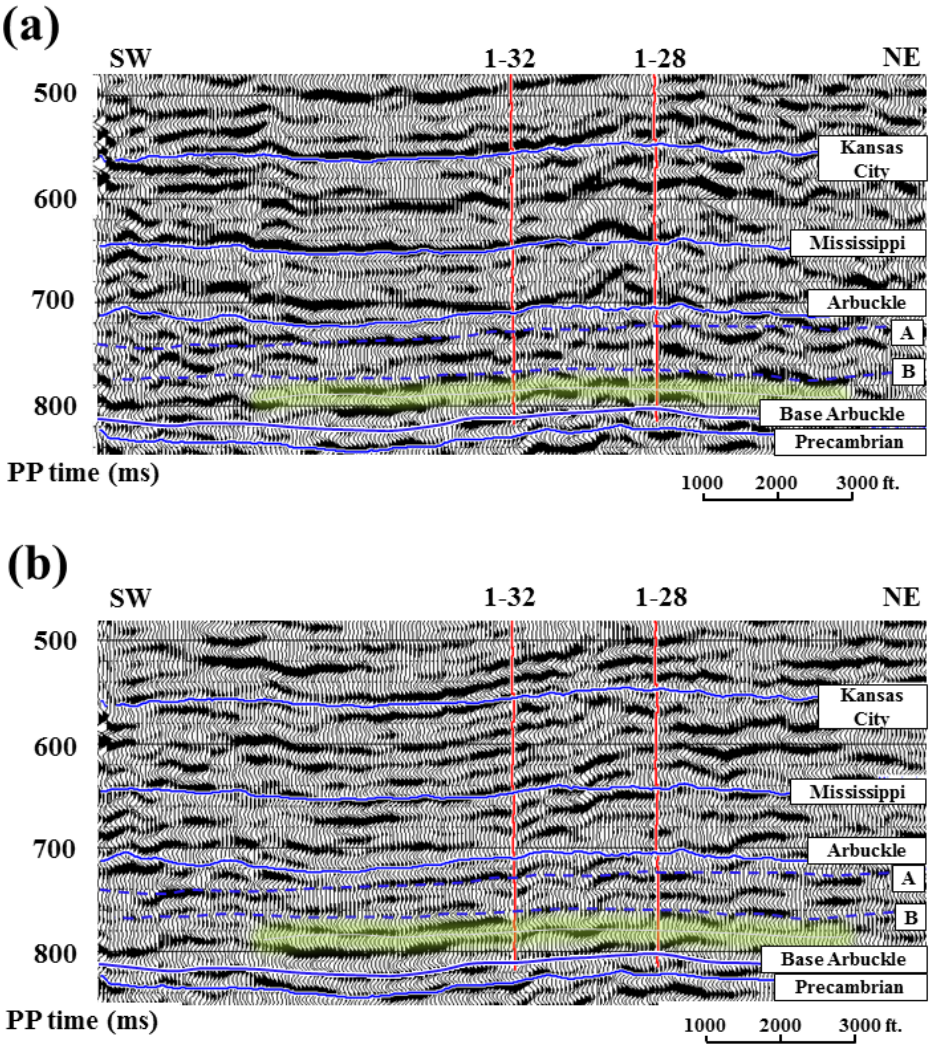

Figure 5.7: A comparison of the SV-P image obtained from a horizontal vibrator (a) with the SV-P image obtained from a vertical vibrator (b). Seismic reflections corresponding to Kansas City, Mississippi, Arbuckle and Precambrian are shown on both converted-wave modes. Within the Arbuckle Group, top of the Middle Arbuckle reflection (A) and top of the Lower Arbuckle injection zone (highlighted in green) are consistent in both seismic sections, demonstrating the efficacy of using a vertical vibrator to generate down-going S-waves. However, seismic image quality NE of well 1-32 is sub-standard due on both images due to S-wave static-related issues.

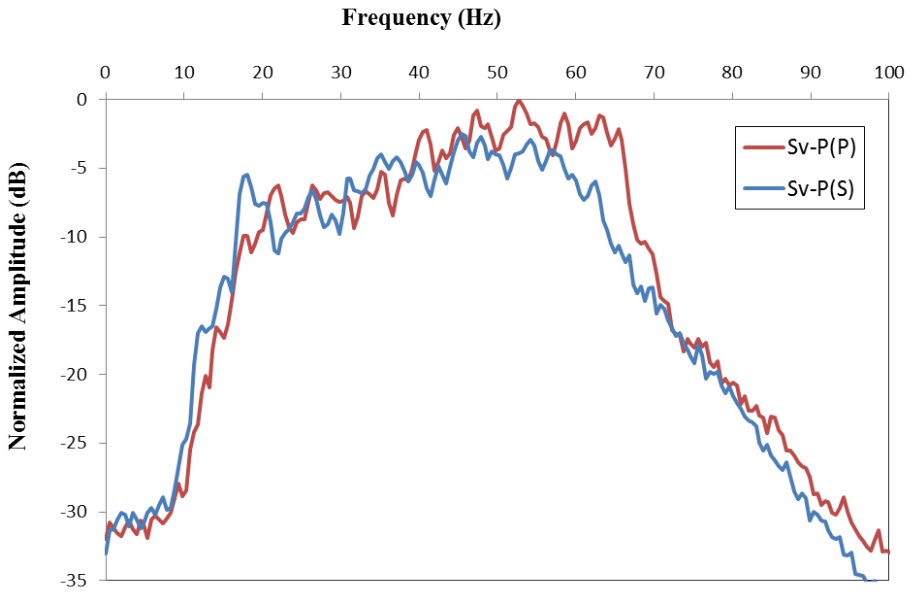

Figure 5.8: A comparison of the frequency spectra of SV-P seismic mode generated by P-wave source (red) and S-wave source (blue). A window from 0-900 ms in P-P time was used to calculate these spectra. The SV-P mode generated by a vertical vibrator contains more high frequency energy from 57 Hz to approximately 67 Hz. This increase in frequency content is a result of using a P-wave source which generates sweeps with broader frequency spectrum compared to an S-wave source. These additional high frequencies help generate higher resolution image of the subsurface enabling more reliable interpretation. The vertical vibrator sweep parameters were not optimal for low frequencies (non-linear sweep with a slope of +3 db/octave and starting frequency 6 Hz). If the data were acquired using a lower starting frequency and linear sweep, SV-P mode could also provide the valuable low-frequency energy needed for broad-band applications.

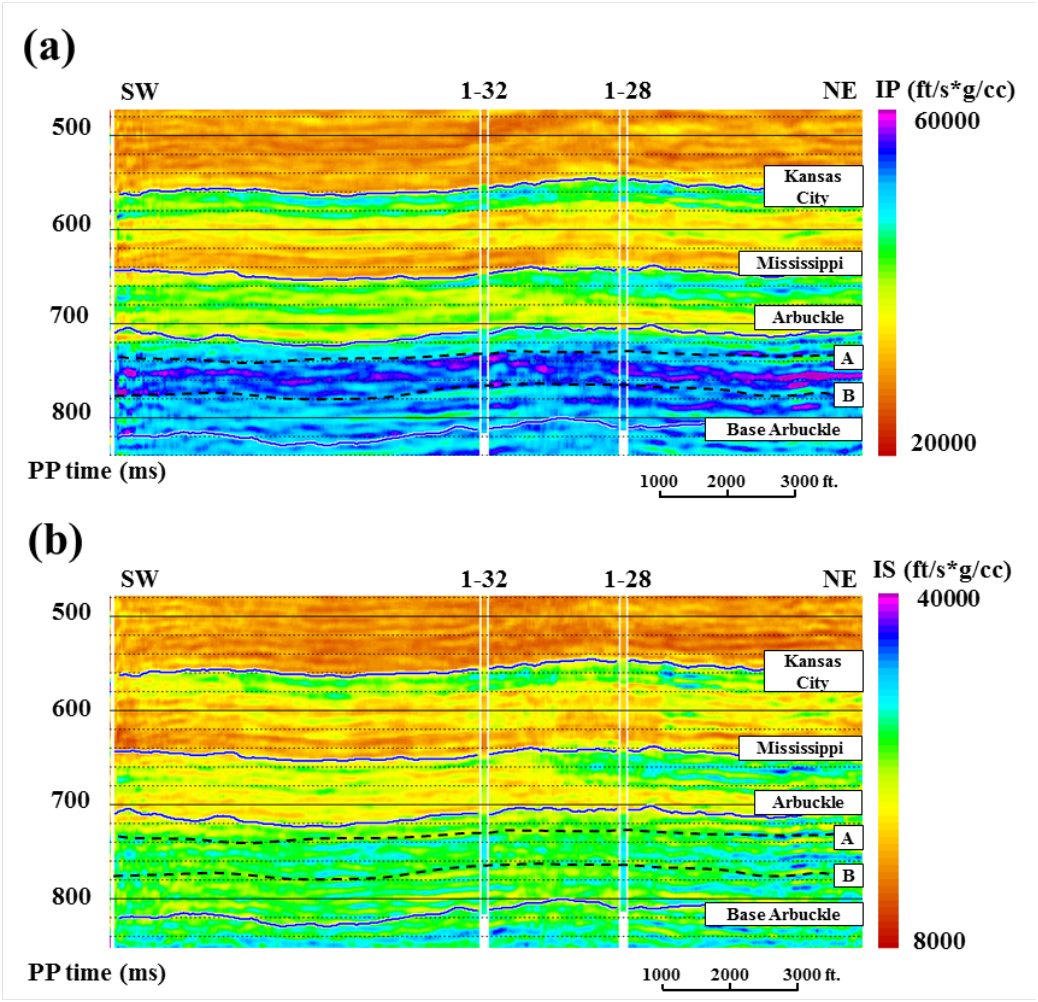

Figure 5.9: (a) P-impedance (IP) obtained from joint-inversion of P-P gathers and SV-P stacks (from vertical vibrator) for Line-1 compared to IP computed from well-logs (vertical colored strips below well labels). High IP in Middle Arbuckle (between A and B), and low IP in Lower Arbuckle injection zone are consistent with the observations made on IP obtained from P-P AVO inversion, and P-P and P-SV joint inversion in Figures 5.4a and 5.5a. (b) S-impedance (IS) obtained from joint-inversion of P-P gathers and SV-P stacks (from vertical vibrator) for Line-1 compared to IS computed from well-logs. This IS is consistent with the IS estimated from P-P and P-SV joint inversion as shown in Figure 5.5b. Moreover, IS estimated from P-P and SV-P joint inversion better resolves lithology variation in Kansas City and Mississippi horizons, and within Arbuckle Group, compared to IS estimated from P-P inversion (Figure 5.4b). Lower Arbuckle injection zone (below B) shows low values of IS, suggesting lithology variation not as evident on P-P inversion results.

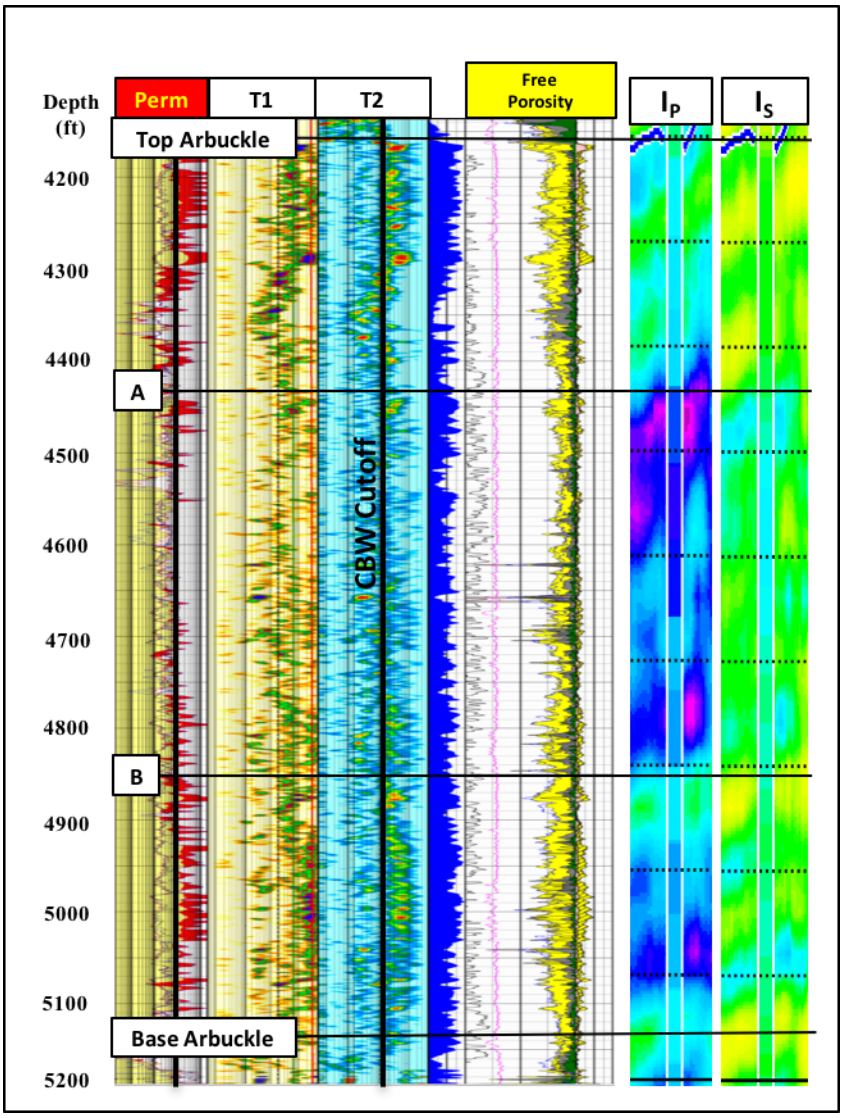

Figure 5.10: Well log panel showing permeability (track 1) and T_2 relaxation times (track 3) in Arbuckle interval, alongside I_P and I_S obtained from Sv-P and P-P joint inversion. Upper Arbuckle (zone between Top Arbuckle and marker A) and Lower Arbuckle injection zone (below marker B) show low I_P and I_S values, indicating presence of larger vugs and fractures. This interpretation is corroborated by higher permeability and T_2 relaxation times calculated from NMR measurements. Similarly, Middle Arbuckle (zone between marker A and B) shows smaller T_2 relaxation times, low permeability and higher I_P and I_S values, suggesting presence of a baffle zone.

Chapter 6: Conclusions and Future Work

6.1 CONCLUSIONS

This dissertation explored the possibility of utilizing direct S-waves for reservoir delineation and fracture characterization. I found that direct S-wave data (generated by P- or S-wave sources), when used in conjunction with P-P seismic data, vastly improves understanding of lithofacies and fracture properties such as spatial-density and fluid-fill of fractures.

Measurements made using various aspects of seismic data such as seismic velocity, travel time, and seismic amplitudes samples the subsurface at different scales, providing a robust framework for geological interpretation. This interpretation was calibrated and corroborated with well-log data, core data, and dynamic pressure data acquired at two wells. Vp/Vs estimates obtained from depth registration of P-P and S-S data (Chapter 2) provided a low-frequency framework suggesting a tight /baffle zone in the Middle Arbuckle and high permeability zones in the Lower Arbuckle. Inversion of P-P and SV-P data (Chapter 5) filled in the high frequency details of lithofacies variation within the Middle and Lower Arbuckle, highlighting the CO_2 injection zones and mapping lateral heterogeneities present in the Arbuckle interval, potentially affecting the injection and movement of CO_2 in the subsurface.

Rock physics modeling (Chapter 3) suggests that S-waves are relatively more sensitive to fractures compared to P-waves. For the P-P mode, magnitudes of azimuthal variations in AVO intercepts and gradients are often masked by the variations due to uncertainty in lithology and fracture-density and hence are not an optimal choice of data analysis to determine fracture properties. Time-shift analysis of fast and slow S-S data

(Chapter 2) along with the processing velocities (Chapter 4), indicates presence of seismic anisotropy, which can be linked to the presence of fractures that remained open in response to anisotropic subsurface stress. S-S AVO attributes such as IA and GA (Chapter 4) provided reservoir-scale details and unraveled high fracture-density zones and fluid-fill within the Lower Arbuckle injection zone. These high fracture-density zones coincided with dolomitic lithofacies suggested by the Vp/Vs analysis. In addition to lateral variation of fracture density, S-S AVO attributes also have the potential to monitor fluid movements through fractures, which could have significant implications for applying time-lapse seismic technology to tight formations. Use of amplitude-based analysis in conjunction with travel-time-based analysis for seismic anisotropy helps reduce ambiguity in interpretation and provides a high-resolution fracture characterization. Moreover, using S-wave AVO attributes for fracture property estimation offers a fast and effective solution to interpreting large volumes of surface seismic data for sweet-spots.

This dissertation also shows that direct S-wave data generated by conventional P-wave sources are equally competent for reservoir characterization compared to data generated by more expensive S-wave sources. A series of comparisons between the inversion results of P-P, P-SV and SV-P seismic data show that vertical-vibrator SV-P data from vertical geophones works as good as P-SV seismic data from horizontal geophones to understand reservoir properties and provide better resolution compared to SV-P data generated by horizontal vibrator. This demonstration of low-cost but highly-effective direct S-wave data presents a tremendous opportunity to the geophysical community to incorporate S-waves in reservoir characterization workflows. Converted-wave studies can now also be performed on available legacy P-wave seismic data, which will revolutionize the way that multi-component reflection seismology is done.

6.2 FUTURE WORK

S-S data used for fracture characterization in this dissertation was generated by a horizontal vibrator. Due to delays in seismic processing, 2D S-S data generated by vertical vibrators were not made available and feasibility of using a vertical vibrator generated S-S data for determining fracture properties could not be assessed. It would be worthwhile investigating how do fracture-density and fracture-fluid estimated from S-S data generated by vertical vibrator compare with the results shown in Chapter 4. Additionally, this dissertation used 2D S-S data as a proof-of-concept, to derive AVO attributes for spatial-density and fluid-fill of fractures. To map the reservoir-wide variations in fracture properties, this workflow needs to be extended to 3D S-S data. Such 3D S-S data could be extracted from the 3D3C survey (green box in Figure 2.3) acquired in Wellington Field generated by vertical vibrators as a seismic source.

There is substantial supporting information available from well-logs, cores, and pressure measurements made between the wells to corroborate fracture-density results (obtained via IA attribute) in Chapter 4. However, due to lack of supporting data on subsurface CO_2 movement, claims that the GA attribute can map the fluid-fill in fractures, could not be substantiated. In the near future, availability of multicomponent time-lapse seismic data or production logs in the two calibration wells, can present an opportunity to evaluate the GA attribute as a viable proxy to identify changes in fracture fluid in the CO_2 injection intervals.

In Chapter 5, while inverting P-P and mode-converted P-wave data (SV-P), exact reflection coefficients of SV-P mode were not used. Instead, SV-P reflection coefficients were approximated by P-SV reflection coefficients and a scaled wavelet, to make use of

existing inversion software. To perform a more precise joint inversion, exact reflection coefficients proposed by Ruger (2001) can be used. Additionally, converted-wave study used post-stack SV-P data for the inversion. A pre-stack joint inversion of P-P and SV-P AVO gathers can be attempted for improved characterization. However, such an inversion would require caution because mode-converted P-wave (SV-P) approaches critical angle close to incidence angle of 30 degrees and reflection amplitudes show anomalous highs.

References

Aki, K., and Richards, P. G. (1980) Quantitative seismology: Theory and methods (Eds.), W. H. Freeman and Co., New York.

Alford, R. M., 1986, Shear data in the presence of azimuthal anisotropy: 56th Annual International Meeting, SEG, Expanded Abstracts, 476–479.

Alkan, E. and B., Hardage, B., 2013. Direct-S wave modes produced by vertical and horizontal vibrators:. Journal of Seismic Exploration, 22(2), pp.147-168.

Alkan, E., 2012, Exploring hydrocarbon-bearing shale formations with multicomponent seismic technology and evaluating direct shear modes produced by vertical-force sources, PhD Dissertation, The University of Texas at Austin.

Anselmetti, F. S., and G. P. Eberli, 1993, Controls on sonic velocity in carbonates: Pure and Applied Geophysics, 141, 287–323.

Assefa, S., C. McCann, and J. Sothcott, 2003, Velocities of compressional and shear waves in limestones: Geophysical Prospecting, 51, 11–13.

Baars, D. L., and W. L., Watney, 1991, Paleotectonic control of reservoir facies: Kansas Geological Survey, Bulletin, 233, pp.253-262.

Bakulin, A., I., Tsvankin, I., and V., Grechka, V., 2000, Estimation of fracture parameters from reflection seismic data-Part I: HTI model due to a single fracture set: Geophysics, 65, 1788–1802.

Bansal, R. and J., Gaiser, J., 2013. An introduction to this special section: Applications and challenges in shear-wave exploration:. The Leading Edge, 32(1), pp.12-12.

Beckham, W.E., 1996. Seismic anisotropy and natural fractures from VSP and borehole sonic tools-A field study. Geophysics, 61(2), pp.456-466.

Berryman, J. G., 1992, Single-scattering approximations for coefficients in Biot's equations of poroelasticity: The Journal of the Acoustical Society of America, 91, 551–571.

Bliefnick, D. M., 1992, Karst-related diagenesis and reservoir development in the Arbuckle Group, Paschall #2 core, Wilburton field, Oklahoma; in, Permian Basin Section: Society of Economic Paleontologists and Mineralogists, Publication No. 92-33, p.137-152.

Boness, N.L. and M.D., Zoback, M.D., 2004. Stress-induced seismic velocity anisotropy and physical properties in the SAFOD pilot hole in Parkfield, CA:. Geophysical Research Letters, 31(15).

Brown, R. J., and J. Korringa, 1975, On the dependence of the elastic properties of a porous rock on the compressibility of the pore fluid: Geophysics, 40, no.4, 608-616.

Byrnes, A. P., E. K., Franseen, and D. M., Steinhauff, 1999, Integrating plug to well-scale petrophysics with detailed sedimentology to quantify fracture, vug, and matrix properties in carbonate reservoirs—An example from the Arbuckle Group, Kansas: Kansas Geological Survey, Open-file Report 99-47.

Carr, T.R., D.F. Merriam, and J.D. Bartley, 2005, Use of relational databases to evaluate regional petroleum accumulation, groundwater flow, and CO_2 sequestration in Kansas: AAPG Bulletin, v. 89/12, p. 1607-1627.

Corrigan D, R., Withers, R, J., Darnall, J., and T., Skopinski, T., 1996, Fracture mapping from azimuthal velocity analysis using 3-D surface seismic data 66th Int. Ann. Meeting Soc. Expl. Geophys. Expanded Abstracts pp 1834-7

DeAngelo, M. V., M. Backus, B. A. Hardage, P. Murray, and S. Knapp, 2003, Depth registration of P-wave and C-wave seismic data for shallow marine sediment characterization, Gulf of Mexico: The Leading Edge, 22, no. 2, p. 96-105.

DeVault, B., T. L. Davis, I. Tsvankin, R. Verm, and F. Hilterman, 2002, Multicomponent AVO analysis, Vacuum field, New Mexico: Geophysics, 67, 701-710.

Fertig, J., 1984. Shear waves by an explosive point-source: the earth surface as a generator of converted PS waves:. Geophysical Prospecting, 32(1), pp.1-17.

Fomel, S., 2007. Local seismic attributes. Geophysics, 72(3), pp. A29-A33.

Franseen, E. K., A. P. Byrnes, J. R. Cansler, D. M. Steinhauff, T. R. Carr, and M. K. Dubois, 2003, Geologic controls on variable character of Arbuckle reservoirs in Kansas—An emerging picture: Kansas Geological Survey, Open-file Report 59, 30.

Frasier, C. and D., Winterstein, D., 1990. Analysis of conventional and converted mode reflections at Putah sink, California using three-component data. Geophysics, 55(6), pp.646-659.

James E. Gaiser J. E., (1996). "Multicomponent VP/VS correlation analysis." Geophysics, 61(4), 1137-1149.

Gaiser, J., and R. Verm, 2012, SS-wave reflections from P-wave sources in azimuthally anisotropic media: 82nd Annual International Meeting, SEG, Expanded Abstracts

Gale, J. F., R. H., Lander, R. M., Reed, and S. E., Laubach, 2010, Modeling fracture porosity evolution in dolostone. Journal of Structural Geology, v. 32, no. 9, p. 1201-1211. doi:10.1016/j.jsg.2009.04.018

Gray, D., 2003. PS converted-wave AVO. CSEG Technical Abstracts.

Grossman, P. J., G. Popov, and C. Steinhoff, 2013, Integration of multicomponent time-lapse processing and interpretation: Focus on shear wave splitting analysis: The Leading Edge, 32, no.1, 32–38.

Gupta, M., K., Spikes, and B., Hardage, 2017. Characterization of naturally fractured Arbuckle Group in the Wellington Field, Kansas, using S-wave amplitude variation with offset. Interpretation, 5(1), pp.T49-T63.

Gupta, M., K., Spikes, M. E., Far, D., Sava, and B., Hardage, 2014, October. Statistical AVO intercept-gradient analysis of direct S-waves: A methodology for quantitative fracture characterization:. In 2014 SEG Annual Meeting. Society of Exploration Geophysicists.

Gupta, M., M.V. DeAngelo, and B., Hardage, 2015, December. PP and SS Wave Interpretation of a Carbonate Formation: A Case Study from the Arbuckle Interval in the Wellington Field, Kansas. In 2015 SEG Annual Meeting. Society of Exploration Geophysicists.

Hall, S. A., and J. M. Kendall, 2000, Constraining the interpretation of AVOA for fracture characterization: Anisotropy 2000: Fractures, converted waves, and case studies, 107–144.

Hardage, B.A., D., Sava, and D., Wagner, 2014, SV-P: An ignored seismic mode that has great value for interpreters: Interpretation, 2(2), pp.SE17-SE27.

Hardage, B. A., and D. E. Wagner, 2014a, S-S imaging with vertical force sources: Interpretation, 2, no. 2, SE29–SE38.

Hardage, B. A., and D. E. Wagner, 2014b, Generating direct-S modes with simple, low-cost, widely available seismic sources: Interpretation, 2, no. 2, SE17 –SE27.

Hardage, B. A., M. V. DeAngelo, P. E. Murray, and D. Sava, 2011, Multicomponent seismic technology: Tulsa, Society of Exploration Geophysicists, Geophysical References Series No. 18, 318 p.

Hardage, B. A., M. V. DeAngelo, P. E. Murray, and D. Sava, 2011, Multicomponent seismic technology: Geophysical References Series No. 18, SEG.

Hudson, J. A., 1981, Wave speeds and attenuation of elastic waves in material containing cracks: Geophysical Journal of the Royal Astronomical Society, 64, no.1, 133–150.

Jenner, E., 2001, Azimuthal anisotropy of 3-D compressional wave seismic data, Weyburn field, Saskatchewan, Canada: Ph.D. thesis, Colorado School of Mines.

Kendall, R. R., and J. M. Kendall, 1996, Shear-wave amplitude anomalies in south-central Wyoming: Leading Edge, 15, 913–920.

Laubach, S. E., 2003, Practical approaches to identifying sealed and open fractures, AAPG Bulletin, v. 87, No. 4, (April 2003) 561-579.

Li X-Y, 1997, Fractured reservoir delineation using multicomponent seismic data: Geophysical Prospecting, 45, 39–64.

Li, Y. and B.A., Hardage, B.A., 2015. SV-P extraction and imaging for far-offset vertical seismic profile data. Interpretation, 3(3), pp.SW27-SW35.

Liu, E., and A. Martinez, 2013,. "Seismic fracture characterization: Concepts and practical applications: EAGE." (2013).

Lynn H. B., and L., Thomsen L., 1990, Reflection shear wave data collected near the principal axes of azimuthal anisotropy: Geophysics 55 147-156

Lynn, H. B., K. M. Simon, C. R. Bates, M. Layman, R. Schneider, and M. Jones, 1995, Use of anisotropy in P-wave and S-wave data for fracture characterization in a naturally fractured gas reservoir: The Leading Edge, 14, no. 8, 887–893.

Lynn, W., 2007, Uncertainty implications in azimuthal velocity analysis: 77th Int. Annu. Meeting Soc. Expl. Geophys. Expanded Abstracts pp 84-7

Mallick, S., K., Craft, L., K., Meister, L., and Chambers, R., 1996, Determination of the principal directions of azimuthal anisotropy from P-wave seismic data: 58th EAGE Conf. and Exhibition Extended Abstracts, C023.

Martin, M. A., and T. L. Davis, 1987, Shear-wave birefringence: A new tool for evaluating fractured reservoirs: The Leading Edge, 6, no. 10, 22–28.

Merriam, D. F., 1963, The Geologic History of Kansas. Lawrence, Kansas: University of Kansas Publications.

Miller, G., and H. Pursey, 1954, The field and radiation impedance of mechanical vibrators on the free surface of a semi-infinite isotropic solid: Proceedings of the Rroyal Society of London, Series A, 223, 521 –541.

Mueller, M.C., 1991, Prediction of lateral variability in fracture intensity using multicomponent shear wave surface seismic as a precursor to horizontal drilling in the Austin chalk: Geophysical Journal International, 107, 409–415.

Norris, A., 1985, A differential scheme for the effective moduli of composites: Mechanics of Materials, **4**, 1–16.

Ohl, D. and A., Raef, A., 2014,. Rock formation characterization for carbon dioxide geosequestration: 3D seismic amplitude and coherency anomalies, and seismic petrophysical facies classification, Wellington and Anson-Bates Fields, Kansas, USA. Journal of Applied Geophysics, 103, pp.221-231.

Pérez, M. A., R. L. Gibson, and M. N. Toksöz, 1999, Detection of fracture orientation using azimuthal variation of P-wave AVO responses: Geophysics, 64, no. 4, 1253–1265.

Queen, J.H. and W.D., Rizer, W.D., 1990. An integrated study of seismic anisotropy and the natural fracture system at the Conoco Borehole Test Facility, Kay County, Oklahoma. Journal of Geophysical Research: Solid Earth, 95(B7), pp.11255-11273.

Roche, S. L., M., Wagaman, M., and H. J., Watt, 2005, Analysis of P-wave and converted-wave 3D seismic data, Anadarko Basin, Oklahoma, USA 75th Int. Annu. Meeting Soc. Expl. Geophys. Expanded Abstracts pp 979-82

Ruger, A., 2001, Reflection Coefficients coefficients and aAzimuthal AVO aAnalysis in aAnisotropic mMedia:, Geophysical Monograph Series No. 10,: Society of Exploration Geophysics, Tulsa, OK.

Rusmanugroho, H. and G. A. McMechan, 2010, Modeling sensitivity of 3D, 9-C wide azimuth data to changes in fluid content and crack density in cracked reservoirs: Geophysics, 75, no. 5, T155–T165.

Sava, D. C., T. Mukerji, J. M. Florez, and G. Mavko, 2001, Rock physics analysis and fracture modeling of the San Andres reservoir, Yates field: 71st Annual International Meeting, SEG, Expanded Abstracts, 1748–1751.

Sava, D.C. and G., Mavko, 2004, Azimuthal analysis of reflectivity for fracture characterization: Rock physics modeling and field example. in 2004 SEG Annual Meeting. Society of Exploration Geophysicists.

Schoenberg, M., and C., Sayers, C., 1995, Seismic anisotropy of fractured rock: Geophysics, 60, 204–211.

Shen, F., J. Sierra, D. R. Burns, and M. N. Toksöz, 2002, Azimuthal offset-dependent attributes applied to fracture detection in a carbonate reservoir: Geophysics, 67, no. 2, 355–364.

Sinha, S., S. Abaseyev, and E. Chesnokov, 2012, Radiation pattern in homogeneous and transversely isotropic attenuating media, Geohorizons, 38–45.

Tatham, R.H. and M.D., McCormack, M.D., 1991. Multicomponent seismology in petroleum exploration.

Tatham, R.H., 1982, Vp/Vs & lithology: Geophysics, 47, 336–344

Thomsen, L., 1986, Weak elastic anisotropy: Geophysics, 51, no. 10, 1954–1966.

Tsvankin I., J. Gaiser, V. Grechka, M. Van der Baan, and L. Thomsen, 2010, Seismic anisotropy in exploration and reservoir characterization: An overview: Geophysics, 75, 15–29.

Watney, W.L. and J. Rush, 2012, Small scale field test demonstrating CO_2 sequestration in Arbuckle Saline Aquifer and by CO_2-EOR at Wellington Field, Sumner County, Kansas: DOE Project Report Number DE-FE0006821, 28 p.

Wilson, J.L., R.D., Fritz, and P.L., Medlock, 1991, The Arbuckle Group--relationship of core and outcrop analyses to cyclic stratigraphy and correlation: Oklahoma Geological Survey Special Publication 91-3, p. 133-145.

Yardley, G.S., G. Graham, and S. Crampin, 1991, Viability of shear-wave amplitude versus offset studies in anisotropic media: Geophysical Journal International, 107, 493–503.